

Electronic Theses and Dissertations, 2004-2019

2013

Suction Detection And Feedback Control For The Rotary Left Ventricular Assist Device

Yu Wang
University of Central Florida

 Part of the [Electrical and Electronics Commons](#)
Find similar works at: <https://stars.library.ucf.edu/etd>
University of Central Florida Libraries <http://library.ucf.edu>

This Doctoral Dissertation (Open Access) is brought to you for free and open access by STARS. It has been accepted for inclusion in Electronic Theses and Dissertations, 2004-2019 by an authorized administrator of STARS. For more information, please contact STARS@ucf.edu.

STARS Citation

Wang, Yu, "Suction Detection And Feedback Control For The Rotary Left Ventricular Assist Device" (2013). *Electronic Theses and Dissertations, 2004-2019*. 2795.
<https://stars.library.ucf.edu/etd/2795>

SUCTION DETECTION AND FEEDBACK CONTROL FOR THE ROTARY
LEFT VENTRICULAR ASSIST DEVICE

by

YU WANG

B.S. Dalian University of Technology, 2004

M.S. Southern Polytechnic State University, 2007

M.S. University of Central Florida, 2010

A dissertation submitted in partial fulfillment of the requirements
for the degree of Doctor of Philosophy
in the Department of Electrical Engineering and Computer Science
in the College of Engineering and Computer Science
at the University of Central Florida
Orlando, Florida

Fall Term
2013

Major Professor: Marwan A. Simaan

© 2013 Yu Wang

ABSTRACT

The Left Ventricular Assist Device (LVAD) is a rotary mechanical pump that is implanted in patients with congestive heart failure to help the left ventricle in pumping blood in the circulatory system. The rotary type pumps are controlled by varying the pump motor current to adjust the amount of blood flowing through the LVAD. One important challenge in using such a device is the desire to provide the patient with as close to a normal lifestyle as possible until a donor heart becomes available. The development of an appropriate feedback controller that is capable of automatically adjusting the pump current is therefore a crucial step in meeting this challenge. In addition to being able to adapt to changes in the patient's daily activities, the controller must be able to prevent the occurrence of excessive pumping of blood from the left ventricle (a phenomenon known as ventricular suction) that may cause collapse of the left ventricle and damage to the heart muscle and tissues.

In this dissertation, we present a new suction detection system that can precisely classify pump flow patterns, based on a Lagrangian Support Vector Machine (LSVM) model that combines six suction indices extracted from the pump flow signal to make a decision about whether the pump is not in suction, approaching suction, or in suction. The proposed method has been tested using in vivo experimental data based on two different LVAD pumps. The results show that the system can produce superior performance in terms of classification accuracy, stability, learning speed,

and good robustness compared to three other existing suction detection methods and the original SVM-based algorithm. The ability of the proposed algorithm to detect suction provides a reliable platform for the development of a feedback control system to control the current of the pump (input variable) while at the same time ensuring that suction is avoided.

Based on the proposed suction detector, a new control system for the rotary LVAD was developed to automatically regulate the pump current of the device to avoid ventricular suction. The control system consists of an LSVM suction detector and a feedback controller. The LSVM suction detector is activated first so as to correctly classify the pump status as No Suction (NS) or Suction (S). When the detection is “No Suction”, the feedback controller is activated so as to automatically adjust the pump current in order that the blood flow requirements of the patient’s body at different physiological states are met according to the patient’s activity level. When the detection is “Suction”, the pump current is immediately decreased in order to drive the pump back to a normal No Suction operating condition. The performance of the control system was tested in simulations over a wide range of physiological conditions.

ACKNOWLEDGMENTS

I would like to thank Dr. Marwan A. Simaan, my advisor, for his constant support and numerous suggestions on my study and research. I am also thankful to Dr. Eduardo Divo for his guidance through my early periods of confusion on my work.

I would also like to give thanks to Dr. Zhihua Qu, Dr. Michael Haralambous, and Dr. Alain Kassab as my other committee members, especially my research teammate, George Faragallah, who gave me much great help for my research.

I specially thank to my parents, for their patience and love, and my wife Cui Jin, who is by my side to give me spiritual support and encouragement all the time.

This work was supported in part by NSF under grant ECCS-0852440. I would like to express my gratitude to them for their financial support.

TABLE OF CONTENTS

LIST OF FIGURES	ix
LIST OF TABLES	xii
CHAPTER 1: INTRODUCTION.....	1
CHAPTER 2: CARDIOVASCULAR PHYSIOLOGY	8
2.1 Heart and Circulatory System.....	8
2.1.1 Heart.....	8
2.1.2 Circulatory System.....	10
2.2 Cardiac Cycle.....	12
2.2.1 Review of Some Basic Concepts	12
2.2.2 Heart Cycle.....	14
CHAPTER 3: THE COMBINED CARDIOVASCULAR-LVAD MODEL	19
3.1 Cardiovascular Model.....	19
3.1.1 Cardiovascular Circuit Model	20
3.1.2 State Equations.....	24
3.1.3 Simulation Results	28
3.2 The Combined Cardiovascular-Pump Model	30
3.2.1 Cardiovascular-LVAD Model.....	30
3.2.2 State Equations.....	36

3.2.3 Open Loop Simulations	40
CHAPTER 4: SUCTION PHENOMENON AND INDICES	43
4.1 Data Acquisition	46
4.2 Feature Extraction of Pump Flow	47
4.3 Definition of Pump States	48
4.4 The Window Length Issue	52
4.5 Time Domain Based Suction Indices	53
4.6 Frequency Domain Based Suction Indices	54
4.7 Time-Frequency Domain Based Suction Index	55
CHAPTER 5: SUCTION DETECTION FOR THE ROTARY LVADS	58
5.1 Support Vector Machine	58
5.2 Lagrangian Support Vector Machine	65
5.3 Classification Performance Evaluation Criteria	69
5.4 In Vivo Data Analysis	70
5.5 Two-State Classification Task for the MedQuest Pump	78
5.6 Three-State Classification Task for the MedQuest Pump	79
5.7 Two-State Classification Task for the Nimbus Pump	81
5.8 Three-State Classification Task for the Nimbus Pump	82
5.9 Comparison with Other Classifiers	84

5.10 Robustness Analysis	92
5.11 Statistical Significance Test.....	92
CHAPTER 6: FEEDBACK CONTROL SYSTEM OF A ROTARY LVAD.....	96
6.1 Feedback Control Design	97
6.2 Simulation Studies	102
6.3 Discussion.....	113
CHAPTER 7: CONCLUSION	115
LIST OF REFERENCES.....	119

LIST OF FIGURES

Figure 2.1 Anterior and Posterior Aspects of the Heart [21] [22]	9
Figure 2.2 Basic Structure of the Heart [23].....	10
Figure 2.3 Block Diagram of Human Circulation Process	11
Figure 2.4 Ventricular Systole (Left) and Diastole (Right) [24]	13
Figure 2.5 Events of the Cardiac Cycle for Left Ventricular Function [25].....	15
Figure 3.1 Cardiovascular Circuit Model	20
Figure 3.2 Elastance Function $E(t)$	23
Figure 3.3 Isovolumic Phase for a Cardiovascular Circuit Model.....	25
Figure 3.4 Ejection Phase for a Cardiovascular Circuit Model	26
Figure 3.5 Ejection Phase for a Cardiovascular Circuit Model	27
Figure 3.6 Simulation of Main Hemodynamic Parameters for a Normal Heart.....	29
Figure 3.7 Schematic of a Rotary LVAD [19].....	30
Figure 3.8 Combined Cardiovascular-LVAD Circuit Model	31
Figure 3.9 Isovolumic Phase for a Combined Cardiovascular-LVAD Circuit Model	37
Figure 3.10 Ejection Phase for a Combined Cardiovascular-LVAD Circuit Model	38
Figure 3.11 Filling Phase for a Combined Cardiovascular-LVAD Circuit Model.....	39
Figure 3.12 Simulations of Ramp PC, LVP, AoP, Q_T , and PF.....	41
Figure 3.13 PS as a Function of Time When PC is Increased Linearly.....	42

Figure 4.1 The Mock Loop Experiment of Normal and Suction Cases [6].....	43
Figure 4.2 Flow Chart of the Proposed Suction Detection Algorithm	45
Figure 4.3 Example of In Vivo Data Based on MedQuest Pump. (a) PS. (b) LVP, PIP. (c) PF. (d) Zoomed PF for NS Case. (e) Zoomed PF for S Case	49
Figure 4.4 Example of In Vivo Data Based on Nimbus Pump. (a) PS. (b) LVP, PIP. (c) PF. (d) Zoomed PF for NS Case. (e) Zoomed PF for S Case	51
Figure 5.1 The Structure of a Simple SVM	59
Figure 5.2 The Schematic Diagram of SVM	65
Figure 5.3 Suction Indices Extracted from PF Based on MedQuest pump. (a) PF. (b) SI ₁ . (c) SI ₂ . (d) SI ₃ . (e) SI ₄ . (f) SI ₅ . (g) SI ₆	72
Figure 5.4 Box Plots of the Features per Pump State for MedQuest Pump. (a) SI ₁ . (b) SI ₂ . (c) SI ₃ . (d) SI ₄ . (e) SI ₅ . (f) SI ₆	75
Figure 5.5 Comparison of Classification Accuracy for 2-State Task (The Brackets Indicate the Standard Deviations)	85
Figure 5.6 Comparison of ROC Curves for 2-State Problem	86
Figure 5.7 Comparison of Classification Accuracy for 3-State Problem for MedQuest Pump. (a) NS. (b) AS. (c) S. (The Brackets Indicate the Standard Deviations).....	88
Figure 5.8 Comparison of Classification Accuracy for 3-State Problem for Nimbus Pump. (a) NS (b) AS (c) S (The Brackets Indicate the Standard Deviations)	89

Figure 5.9 Comparison of ROC Curves for 3-State Problem	90
Figure 6.1 Block Diagram of the Proposed Control System	98
Figure 6.2 Relationships among PC, PF, and PS Described by Circle Symbols. Solid Circle Symbols Indicate PS When Suction Occurred	101
Figure 6.3 Changing R_S from 1.0 to 0.5 mmHg·s/ml	103
Figure 6.4 Simulation Results Generated by the Feedback Controller with Varying R_S from 1.0 to 0.5 without Suction Detector	105
Figure 6.5 Simulation Results Generated by the Feedback Controller with Varying R_S from 1.0 to 0.5 with Suction Detector	106
Figure 6.6 Changing R_S from 1.0 to 0.6 mmHg·s/ml	107
Figure 6.7 Simulation Results Generated by the Feedback Controller with Varying R_S from 1.0 to 0.6 without Suction Detector	108
Figure 6.8 Simulation Results Generated by the Feedback Controller with Varying R_S from 1.0 to 0.6 with Suction Detector	109
Figure 6.9 Changing R_S from 1.0 to 0.7 mmHg·s/ml	110
Figure 6.10 Simulation Results Generated by the Feedback Controller with Varying R_S from 1.0 to 0.7 without Suction Detector	111
Figure 6.11 Simulation Results Generated by the Feedback Controller with Varying R_S from 1.0 to 0.7 with Suction Detector	112

LIST OF TABLES

Table 3.1 State Variables of the Cardiovascular Model	21
Table 3.2 Parameters of the Cardiovascular Model.....	22
Table 3.3 Phases of the Cardiac Cycle.....	24
Table 3.4 State Variables of the Combined Model.....	31
Table 3.5 Parameters of the LVAD Model.....	32
Table 4.1 Description of the Study on In-vivo Data for Two Pumps	47
Table 5.1 In-Vivo Data Statistics for the MedQuest Pump	73
Table 5.2 In-Vivo Data Statistics for the Nimbus Pump	74
Table 5.3 Correlation Coefficients from Six Indices for MedQuest Pump	76
Table 5.4 Correlation Coefficients from Six Indices for Nimbus Pump	77
Table 5.5 Classification Results of the LSVM Classifier on the Test Set for 2-State Problem Based on MedQuest Pump ^a	78
Table 5.6 Performance Analysis of the LSVM Classifier on the Test Set for 2-State Problem Based on MedQuest Pump (Numbers Inside the Parenthesis is SD in %)	79
Table 5.7 Classification Results of the LSVM Classifier on the Test Set for 3-State Problem Based on MedQuest Pump ^a	80
Table 5.8 Performance Analysis of the LSVM Classifier on the Test Set for 3-State Problem Based on MedQuest Pump (Numbers Inside the Parenthesis is SD in %)	80

Table 5.9 Classification Results of the LSVM Classifier on the Test Set for 2-State Problem	
Based on Nimbus Pump ^a	81
Table 5.10 Performance Analysis of the LSVM Classifier on the Test Set for 2-State Problem	
Based on Nimbus Pump (Numbers Inside the Parenthesis is SD in %)	82
Table 5.11 Classification Results of the LSVM Classifier on the Test Set for 3-State Problem	
Based on Nimbus Pump ^a	83
Table 5.12 Performance Analysis of the LSVM Classifier on the Test Set for 3-State Problem	
Based on Nimbus Pump (Numbers Inside the Parenthesis is SD in %)	83
Table 5.13 Comparison of Training/Test Time for 2-State Problem	87
Table 5.14 Comparison of Training/Test Time for 3-State Problem	91
Table 5.15 P-Value of T-Test for 2-State Problem for the MedQuest Pump	93
Table 5.16 P-Value of T-Test for 2-State Problem for the Nimbus Pump	94
Table 5.17 P-Value of T-Test for 3-State Problem for the MedQuest Pump	94
Table 5.18 P-Value of T-Test for 3-State Problem for the Nimbus Pump	95

CHAPTER 1: INTRODUCTION

According to a survey from World Health Organization, recently cardiovascular disease is a major problem in the United States and it occupies around one third of all types of diseases. Many cardiovascular diseases could affect the left ventricle of the heart [1] and then lead to congestive heart failure in which the heart cannot pump enough blood to support the body's other organs. Although drug treatments have positive effects to ensure that the patients are able to live normally, a high mortality is still inevitable since this pharmacological therapy often fails in long-term use. Hence, heart transplantation has been an acceptable method to treat serious cases of congestive heart failure.

However, such potential recipients often need to wait a long time (300 days or more on average) until a donor heart becomes available. During this waiting period, the patients' sick hearts may get worse and 20% - 30% of the patients will die. Therefore, one alternative is to use a mechanical support device (a blood pump) that can assist the natural weak heart in performing its functions. A Left Ventricular Assist Device (LVAD) is such a device as a bridge for transplantation to help a weak heart and "buy time" for the patients.

Based on the patterns of the blood flow pumped by the device, LVADs can be classified into two types: positive displacement (pulsatile) and turbo-dynamic (rotary) LVADs. The first generation

LVADs are built using pulsatile pumps that work in a beat-like style to create natural heart flow. The latest generation of the LVADs is built with rotary pumps, which generate continuous blood flow. Furthermore, the LVAD can be either used in the in vitro placement, which is percutaneously connected to the patient's heart and artery through the drainage catheter, or implanted in the patient's body (usually in the peritoneal cavity or extra-peritoneal space) [1]. In recently years, congestive heart failure patients have enjoyed many benefits from the rotary LVAD, which has been widely applied in clinical practice due to its smaller size, lighter weight, better durability [2], and higher efficiency compared to the conventional pulsatile LVAD.

The rotary LVAD is a mechanical pump surgically implanted in the patient as a bridge from the left ventricle to the aorta to help maintain the flow of blood from the patient's heart, which cannot effectively work on its own. In general, the most important objective of a LVAD is to assist the native weak heart in providing required blood flow for the patient until a donor heart becomes available. Therefore, in order to meet the circulatory demand of the patient, developing an appropriate pump control mechanism to adjust the blood flow through the pump by controlling the pump motor current is an important challenge facing the increased use of such devices [3]-[5].

Such a controller, in addition to being robust and reliable, must satisfy two important criteria. First, in order to meet the circulatory requirement of the patient, it must be able to adapt to the

different levels of activity and physiological changes of the patient by adjusting the pump current. Second, an important constraint that should be taken into consideration is to ensure that the pump current should stay below a value beyond which the pump will attempt to draw more blood from the left ventricle than available causing an event called ventricular suction. This event could cause ventricular collapse which could easily damage the heart muscles. It therefore needs to be detected and corrected quickly by lowering the pump current.

The detection of ventricular suction has been a hot topic in recent studies by a number of research groups worldwide. The common way of solving this problem is to extract several features from the pump variables, which are the only easily measureable signals. These features are called Suction Indices (SI). The differences among these studies are (1) the types of pump signals used such as pump speed, pump flow, or pump current, (2) the definition of pump states (no suction, or suction, etc.), and (3) the number of suction indices derived based on time or frequency domain. Based on several derived indices from the pump signals, an appropriate classification method is typically adopted to identify different pump states that may vary from threshold comparisons [6]-[9], to methods such as Classification and Regression Tree (CART) [10], Discriminant Analysis (DA) [11], and Neural Networks (NN) [12] implemented with in vitro, in vivo, or human data. While each of these methods has produced satisfactory results, each also has limitations in its practical application. Examples of these limitations include the

weakness at capturing strong linear structure in the CART-based algorithm, poor performance with complicated data structure and non-Gaussian distributed data in the DA-based method, slow learning speed in the NN-based approach, and unstable performance caused by local minima in both the CART and NN-based algorithms.

To achieve avoidance of suction, in this dissertation, we introduce and test a new suction detection and classification method for the LVAD based on the Lagrangian Support Vector Machine (LSVM) approach in pattern recognition [13]-[15]. The LSVM is a modified standard Support Vector Machine (SVM) and has high accuracy, stable performance, and fast learning speed (training time). This is the first time that an LSVM-based algorithm for suction detection is proposed and systemically and quantitatively compared to other existing pattern recognition-based suction detection algorithms for their performance (including training/test time) under the same conditions. The ability of the proposed algorithm to detect and classify suction will provide an alternative approach for treating the problem of suction detection and more importantly will facilitate an important step in the development of a feedback control system for the pump that has the capability of safeguarding against the occurrence of suction.

Furthermore, different control strategies for rotary LVADs have been developed. These approaches adopt varying pump signals and different principles. For instance, Giridharan et al. [16] developed an effective way to control LVADs by maintaining an average pressure

difference between the left heart and aorta. However, keeping a constant pressure difference does not guarantee required cardiac output in some cases and the suction detector is needed for this method as well.

A combined model of the cardiovascular-LVAD system and the baroreflex mechanism was proposed in [17]. Although the combined model could reproduce human responses and respond to change in the physiological states of congestive heart failure patients, it is acknowledged that in order to avoid the adverse suction phenomenon, a suction detector should be incorporated into the controller as a safeguard.

A rule-based controller for the rotary LVAD was developed to automatically regulate the pump speed without introducing suction [18]. The suction detector in the system was based on DA-based algorithm and generated two discriminant scores as the outputs of the suction detector, which were also used as the inputs of the Fuzzy Logic Controller (FLC). The performance of this control system was tested in the simulations, showing that the control system can automatically regulate the pump speed to avoid suction and demonstrate its feasibility. However, the suction detector does not provide a very high accuracy when compared to the other existing suction detection algorithms. In addition, the author mentioned that the inclusion of a baroreflex in the system would better represent the behavior of such a controller.

Simaan et al. [19] proposed a feedback controller using an extremum tracking method to adjust the pump speed based on the slope of the envelope of the minimum pump flow signal within every cardiac cycle. With the onset of suction, the slope of the minimum pump flow envelope was near zero. However, there was no embedded suction detector in the proposed system as the safeguard.

In this dissertation, a new patient-adaptive feedback controller based on a current-based control of the LVAD is presented, which extends the results of the LVAD model reported in [20]. The controller could automatically regulate the pump current in order to guarantee the physiological demand of the patient under different levels of the patient's activity when suction is absent ensured by the suction detection subsystem at the same time. When suction occurs, the suction case can be quickly detected by the suction detection subsystem and the controller can decrease the pump current immediately to avoid the occurrence of suction.

This dissertation is organized as follows. Chapter 2 reviews the basic concepts of cardiovascular physiology. Chapter 3 introduces the cardiovascular circuit model and presents a new current-based control model of the combined cardiovascular and rotary LVAD system. Chapter 4 introduces suction phenomenon and describes suction indices. In Chapter 5, an effective LSVM-based suction detection algorithm is proposed. Chapter 6 presents a new feedback

controller of the rotary LVAD supporting a failing cardiovascular system. Conclusion and future work is discussed in Chapter 7.

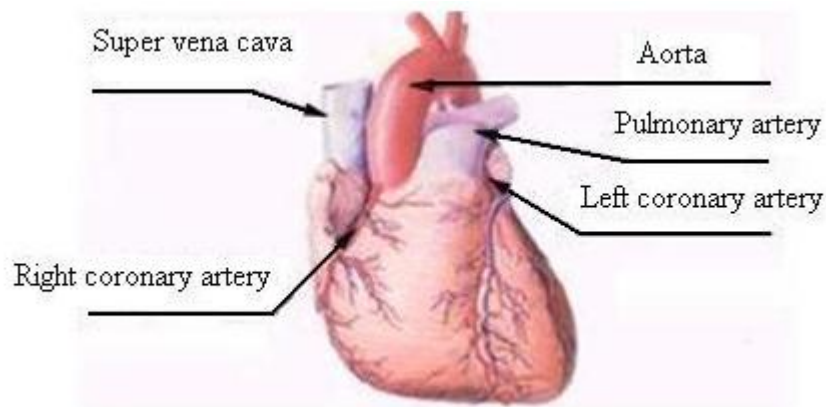
CHAPTER 2: CARDIOVASCULAR PHYSIOLOGY

In this chapter, the basic concepts regarding the heart and cardiovascular physiology that are important to further understand the model of the combined cardiovascular and rotary LVAD are reviewed. This chapter is organized as follows. Heart and circulatory system are introduced in Section 2.1. Section 2.2 describes the cardiac cycle in details.

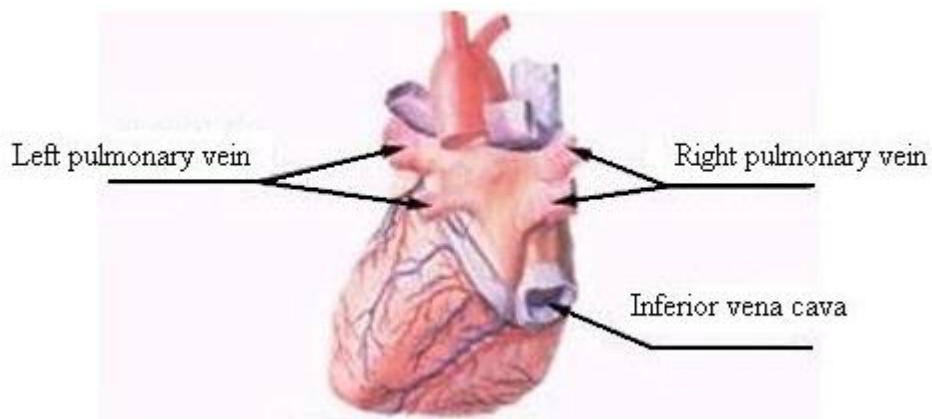
2.1 Heart and Circulatory System

2.1.1 Heart

The heart is an important organ in the circulatory system. It is in the thoracic cavity between left and right lungs. While contracting its size is close to that of the personal fist. The breastbone and costal cartilage are adjacent to the anterior-superior surface of the heart; the esophagus and the thoracic aorta are on the posterior surface of the heart; the inferior surface of the heart is close to the diaphragm muscle; the superior vena cava, aorta, and pulmonary artery are on the superior surface of the heart. Three sulci are on the surface of the heart. The coronary sulcus is the surface demarcation between atria and ventricles; the anterior-posterior longitudinal sulci are surface demarcations between left and right ventricles. Figure 2.1 shows the anterior and posterior aspects of the heart.



(a)



(b)

Figure 2.1 Anterior and Posterior Aspects of the Heart [21] [22]

The heart is a hollow organ, which is divided into four chambers: the upper two chambers are atria separated by the atrial septum as left and right atria, respectively; the lower two chambers are ventricles separated by the inter-ventricular septum as left and right ventricles, respectively.

Figure 2.2 illustrates the basic structure of the heart.

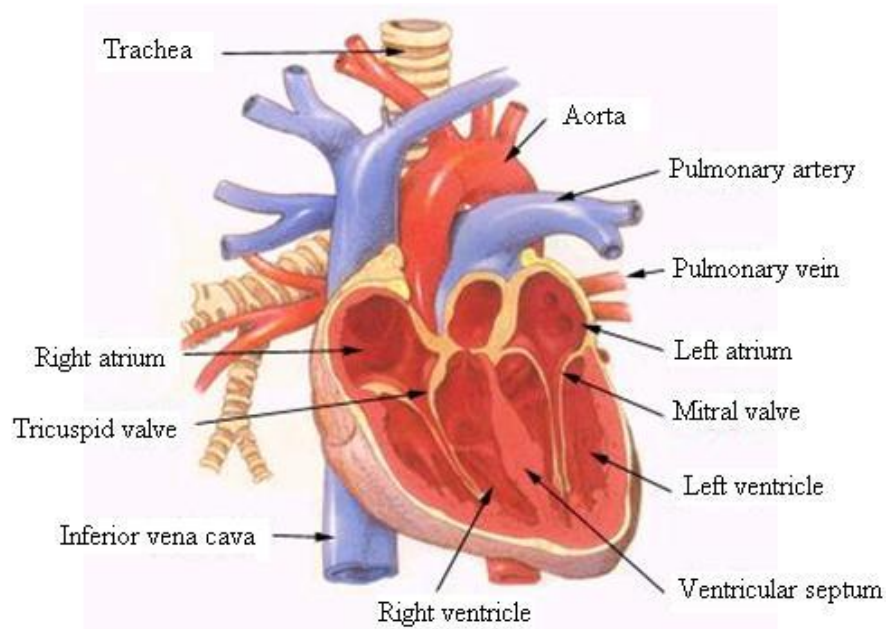


Figure 2.2 Basic Structure of the Heart [23]

2.1.2 Circulatory System

The circulatory system consists of the heart and blood vessels (arteries, arterioles, and blood), whose function is to provide the oxygen and nutrient products to tissues in the body and carry away the byproducts of metabolism. Figure 2.3 describes the block diagram of the circulation process in human's body that is made up of two circulations: systemic circulation and pulmonary circulation.

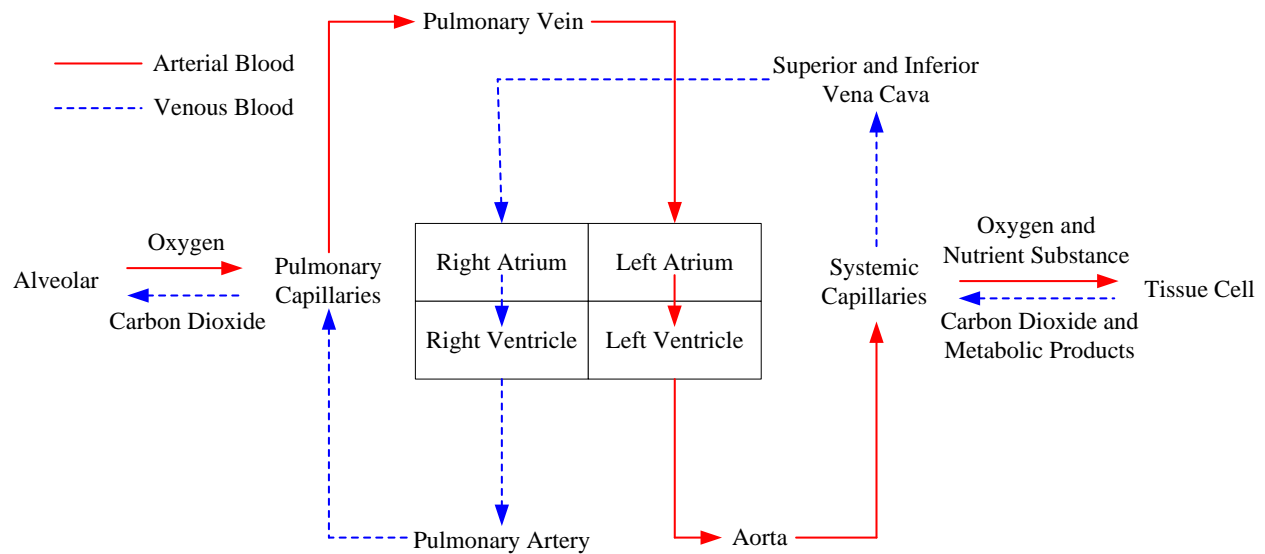


Figure 2.3 Block Diagram of Human Circulation Process

Systemic circulation, known as the major cycle, starts at the left ventricle. When the left ventricle contracts, the arterial blood, including oxygen and nutrient substance, is pumped into the aorta then enters the capillaries via various artery branches. The arterial blood changes into the venous blood that contains carbon dioxide and metabolic products by means of gas and substance exchange in the capillaries with tissues and cells. The venous blood enters the venules through the capillaries and flows into the superior-inferior vena cava and coronary sinus via different-level venous return then goes into the right atrium. After the venous blood flows into the right ventricle from the right atrium, pulmonary circulation begins.

Pulmonary circulation, known as the minor cycle, starts at the right ventricle. With the contraction of the right ventricle, the venous blood is pumped into the pulmonary artery and

flows into the capillaries in the alveolar wall with all branches of pulmonary arteries, and then the venous blood becomes the arterial blood with oxygen saturation by gas exchange between the blood vessels and alveolar. The arterial blood then enters the venules through the capillaries and flows into left and right pulmonary veins through venous return at various levels then goes into the left atrium. Finally the arterial blood flows into the left ventricle from the left atrium, another systemic circulation will start.

2.2 Cardiac Cycle

2.2.1 Review of Some Basic Concepts

In this section, before introducing the cardiac cycle, some important concepts related to the cardiac cycle are introduced first.

Heart Rate (HR): heart rate is the number of heartbeats per unit of time, typically expressed as beats per minute (bpm) that varies depending on the human's age, gender, or body's other physiological demand.

Systole: systole is a phase of the cardiac cycle when the heart is contracting, during which the pressure is generated within the atria and ventricles of the heart pumping blood flow.

Diastole: diastole is a phase of the cardiac cycle when the heart is filled with blood after systole.

Figure 2.4 shows the ventricular systole and diastole, respectively.

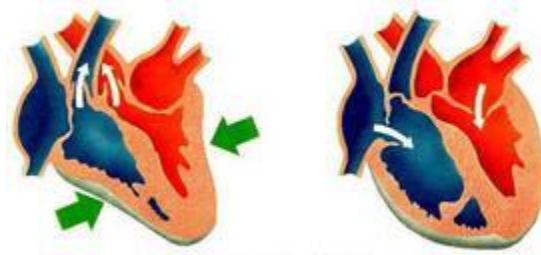


Figure 2.4 Ventricular Systole (Left) and Diastole (Right) [24]

Stroke Volume (SV): stroke volume is the volume of blood pumped from one ventricle of the heart with each beat. It is equally available for both the left and right ventricles of the heart. The expression is as follows:

$$SV = EDV - ESV \quad (2.1)$$

where EDV is the end-diastolic volume, the volume of blood in the ventricle prior to a beat and ESV is the end-systolic volume, the volume of blood at the end of a beat.

Cardiac Output (CO): cardiac output is the volume of blood pumped by the ventricle in a minute, it is the product of stroke volume and heart rate such that

$$CO = SV \cdot HR \quad (2.2)$$

Preload: known as the volume load, is thought of as the “load” before the cardiac muscle starts contracting.

Afterload: known as the pressure load, is defined as the "resistance" that the heart begins to contract and eject blood against.

2.2.2 Heart Cycle

The cardiac cycle is a period of time between two consecutive heart beats. For example, for a normal heart, if the heart rate is 75 bpm, the heart cycle would be 0.8 s. One cardiac cycle contains two main phases: systole (contraction) and diastole (relaxation) for both atrium and ventricle. However, during the cardiac pumping, the ventricle can play a major role compared to the atrium. Therefore, the cardiac cycle often means the activity cycle for the ventricle.

Figure 2.5 illustrates the changes of several important hemodynamic variables: Left Ventricular Pressure (LVP), Aortic Pressure (AoP), Left Atrial Pressure (LAP), and Left Ventricular Volume (LVV) during one cardiac cycle and takes into account the left ventricle as an example. In order to discuss a complete cardiac cycle in details, one cardiac cycle can be divided into 8 phases (see Figure 2.5):

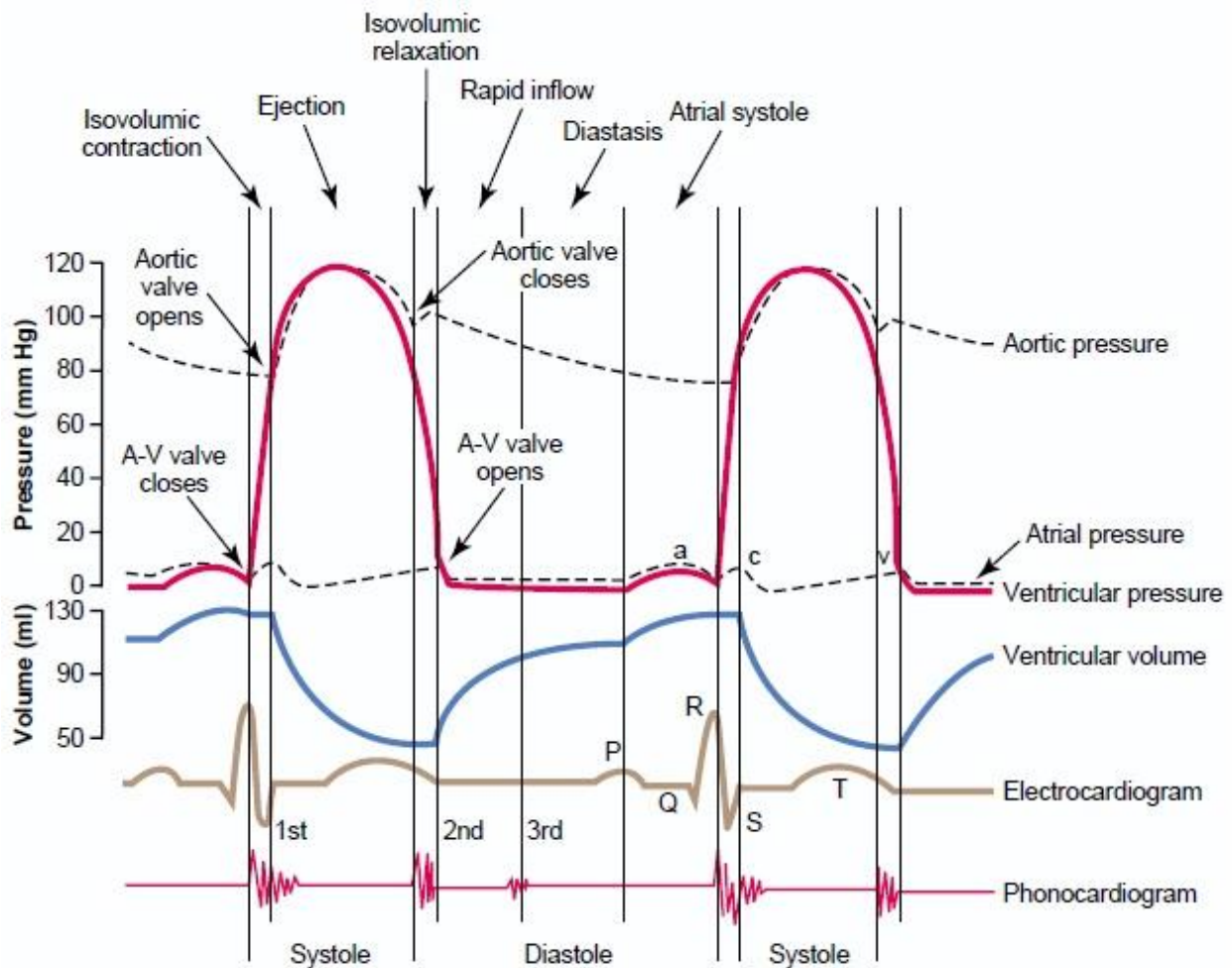


Figure 2.5 Events of the Cardiac Cycle for Left Ventricular Function [25]

Phase 1: isovolumic contraction. The left ventricle starts contracting when R wave of QRS complex that represents the potential and time changes in the ventricular depolarization and most primitive repolarization in the electrocardiogram (see Figure 2.5) reaches its peak value. LVP sharply increases due to the powerful contraction of the ventricular myocardium. When LVP overcomes LAP, blood in the left ventricle impels the corresponding mitral valve in the left atrio-ventricular orifice to make it closed. The mitral valve is tightened due to the papillary

muscle and chordae tendineae, and the contraction of the circular muscle decreases the caliber in the atrio-ventricular junction area, hence blood in the left ventricle is prevented from regurgitating into the left atrium. At this point, LVP increases fast but when it doesn't exceed AoP (around 80 mmHg in end-systole), the aortic valve in the aorta orifice is still closed. During this short period (around 0.05 s), both mitral and aortic valves are not open, the size between the apex and the base of the heart decreases, the left ventricle turns round, the tension of the ventricular myocardium enhances but LVP is not changed, this is called isovolumic contraction.

Phase 2: rapid ejection. The ventricular myocardium keeps contracting and its tension continues to rise, causing LVP to exceed AoP shortly then the aortic valve is blown out, blood is ejected into the aorta and reaches its maximum flow velocity fast. During end-rapid ejection LVP can reach its peak value (around 120 mmHg in the left ventricle). In this phase it takes only 0.09 s but the volume of ejected blood occupies 80%-85% of SV.

Phase 3: slow ejection. During this period, the contractility of the left ventricle is weak, LVP decreases, the ejection velocity becomes slow. Although LVP is slightly less than AoP (only several mmHg), the total energy in the left ventricle (pressure energy plus kinetic energy) is still higher than that in the aorta due to the ventricular contraction. Therefore, blood can still be ejected from the left ventricle. This phase uses 0.13 s on average then the cardiac cycle goes into the phase of diastole (relaxation).

Phase 4: pre-diastole. The left ventricle begins to relax and the ejection stops, LVP suddenly drops. LVP is less than AoP and the aortic valve is quickly shut down to stop blood regurgitating into the left ventricle, hence the period from the onset of the ventricular diastole to the closure of the aortic valve is called pre-diastole with the duration of 0.04 s.

Phase 5: isovolumic relaxation. When the aortic valve is closed, LVP still overcomes LAP, so the mitral valve remains closed, which will not be open until LVP keeps dropping to be less than LAP. During this short phase (0.08 s), LVP sharply decreases but LVV is basically constant, which is the phase of isovolumic relaxation.

Phase 6: rapid filling. With the mitral valve opening, LVV increases fast and LVP is lower than LAP, making blood in the left atrium and great cardiac veins rapidly flow into the left ventricle with a period of 0.11 s. During this period two-thirds of blood in the left ventricle is filling.

Phase 7: slow filling (end diastole). With blood in the left ventricle rapidly filling, the velocity of blood flow in veins entering back to the left ventricle via the left atrium gradually decreases, the pressure difference between the left atrium and the left ventricle decreases but LVV is still increasing. This phase is called slow filling that takes about 0.19 s then the left atrium starts contracting.

Phase 8: atrium contraction. The left atrium contracts by the end of the ventricle diastole; the remaining blood in the left atrium is ejected into the left ventricle due to the increasing LAP, improving the fullness degree of the left ventricle and increasing LVP. When the left atrium contracts, it makes LAP decrease and the mitral valve closed, hence, before the left ventricle contracts, the mitral valve has the trend of closure. Therefore, before next isovolumic contraction, the aforementioned eight phases form a complete cardiac cycle.

CHAPTER 3: THE COMBINED CARDIOVASCULAR-LVAD MODEL

The heart is known as a complex dynamic, time-varying, and nonlinear system that is difficult to model mathematically. In order to simulate the heart, numerous simplified and complex mathematical models of the cardiovascular system have been studied for several years. Wu et al. [26] modeled a complicated bi-ventricular human cardiovascular system. Chen [17] used a simplified uni-ventricular model of the cardiovascular system in state space form that was developed by using a minimal number of state variables to make the system identification as simple as possible; Simaan et al. [19] proposed a modified cardiovascular model, consisting of five state variables with the assumption that both pulmonary circulation and the right ventricle can work normally, hence their effect can be neglected.

In this research, Simaan's model [19] is adopted as the cardiovascular system. This chapter is organized as follows: In Section 3.1 the cardiovascular model is described. Section 3.2 presents the current-based cardiovascular-LVAD model and analyzes its open-loop response.

3.1 Cardiovascular Model

In this section, the cardiovascular equivalent circuit model and its state equations are introduced. Then the simulation results of corresponding hemodynamic variables for a normal heart are presented.

3.1.1 Cardiovascular Circuit Model

A cardiovascular equivalent circuit model is shown in Figure 3.1. In this model, preload and pulmonary circulations are represented by a single capacitor C_R , and afterload is described as a four-element windkessel model that consists of R_S , R_C , C_S , and L_S . Notice that in [17] there was no capacitor C_A , representing the aortic compliance used in this model. The mitral valve is described as a resistor R_M and an ideal diode D_M , and the aortic valve is represented by a resistor R_A and an ideal diode D_A . Table 3.1 lists the state variables and Table 3.2 lists all the system parameters in the cardiovascular model and their corresponding values [17]-[19].

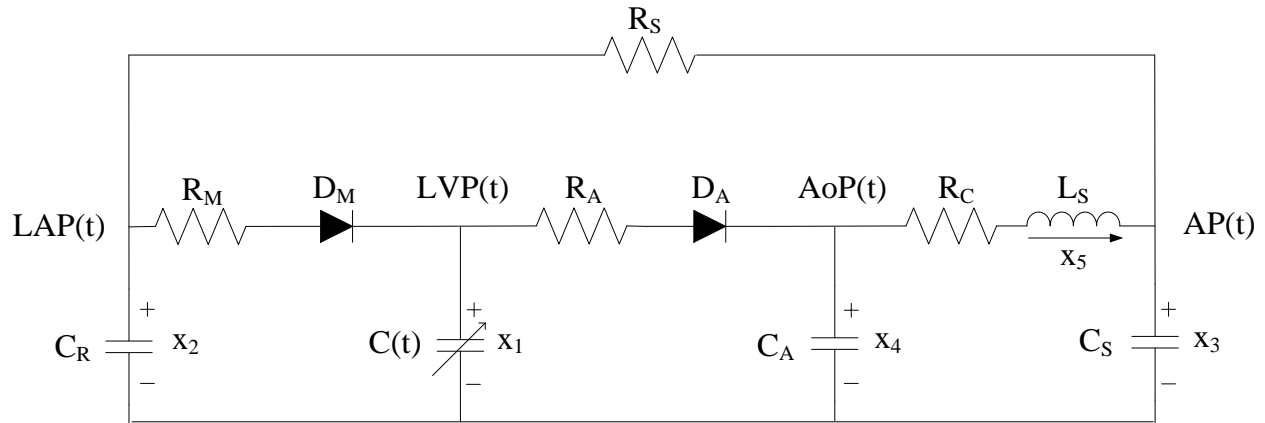


Figure 3.1 Cardiovascular Circuit Model

In this model, the left ventricle is represented by a time-varying compliance $C(t)$. In order to model its response, one way is to use the ventricle's elastance function $E(t)$, which is the reciprocal of $C(t)$ and associated with the contractility of the heart. The elastance theory was

presented by Suga and Sagawa [27]. It is defined as the ratio of LVP to LVV, which means to describe the relationship between pressure and volume of the left ventricle such that

$$E(t) = \frac{LVP(t)}{LVV(t)-V_0} = \frac{1}{c(t)} \quad (3.1)$$

where V_0 is a reference volume, the theoretical volume in the ventricle at zero pressure (10 ml for a normal heart).

Some mathematical derivations have been used to describe the elastance function $E(t)$. In this model, a so called “double hill” function [28] is used. The expression is as follows:

$$E_n(t_n) = 1.55 \cdot \left[\frac{\left(\frac{t_n}{0.7}\right)^{1.9}}{1 + \left(\frac{t_n}{0.7}\right)^{1.9}} \right] \cdot \left[\frac{1}{1 + \left(\frac{t_n}{1.17}\right)^{21.9}} \right] \quad (3.2)$$

Table 3.1 State Variables of the Cardiovascular Model

Variables	Name	Physiological Meaning (units)
$x_1(t)$	LVP(t)	Left Ventricular Pressure (mmHg)
$x_2(t)$	LAP(t)	Left Atrial Pressure (mmHg)
$x_3(t)$	AP(t)	Arterial Pressure (mmHg)
$x_4(t)$	AoP(t)	Aortic Pressure (mmHg)
$x_5(t)$	$Q_T(t)$	Total Flow (ml/s)

Table 3.2 Parameters of the Cardiovascular Model

Parameters	Value	Physiological Meaning
R_S (mmHg·s/ml)	1.0	Systemic Vascular Resistance (SVR)
R_M (mmHg·s/ml)	0.005	Mitral Value Resistance
R_A (mmHg·s/ml)	0.001	Aortic Value Resistance
R_C (mmHg·s/ml)	0.0398	Characteristic Resistance
$C(t)$ (ml/mmHg)	Time-varying	Left Ventricular Compliance
C_R (ml/mmHg)	4.4	Left Atrial Compliance
C_S (ml/mmHg)	1.33	Systemic Compliance
C_A (ml/mmHg)	0.08	Aortic Compliance
L_S (mmHg·s ² /ml)	0.0005	Inertance of Blood in Aorta
D_M		Mitral Value
D_A		Aortic Value

The scaled elastance function is defined as follows:

$$E(t) = (E_{max} - E_{min}) \cdot E_n(t_n) + E_{min} \quad (3.3)$$

where the constant E_{\max} and E_{\min} are related to the End-Systolic Pressure Volume Relationship (ESPVR) and the End-Diastolic Pressure Volume Relationship (EDPVR), respectively, $E(t)$ is a re-scaled version of $E_n(t_n)$, the normalized elastance. In addition, $t_n = t/T_{\max}$, $T_{\max} = 0.2 + 0.15 \cdot t_c$, and t_c is the cardiac cycle interval (i.e., $t_c = 60/\text{HR}$). Also, Figure 3.2 shows the elastance $E(t)$ with $E_{\max} = 2 \text{ mmHg/ml}$, $E_{\min} = 0.06 \text{ mmHg/ml}$, and $\text{HR} = 75 \text{ bpm}$ as a normal heart.

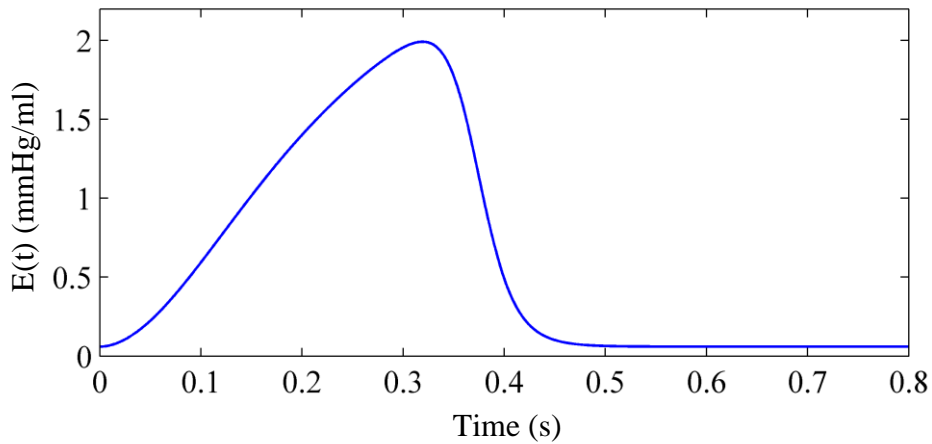


Figure 3.2 Elastance Function $E(t)$

According to the analysis of the cardiac cycle in Section 2.2.2, the mitral and aortic valves can determine the phases of the cardiac cycle. In view of this work, the phases can be divided into three different modes (isovolumic contraction and relaxation, ejection, and filling) with the open and closed states of the mitral and aortic valves. Notice that it is not feasible to open both mitral and aortic valves. Table 3.3 lists the phases of the cardiac cycle.

Table 3.3 Phases of the Cardiac Cycle

Modes	Valves		Phases
	D _M	D _A	
1	closed	closed	Isovolumic contraction
2	closed	open	Ejection
1	closed	closed	Isovolumic relaxation
3	open	closed	Filling
-	open	open	Not feasible

3.1.2 State Equations

According to Table 3.3, since there are three available modes, three sets of differential equations for describing the cardiovascular model for every mode can be derived. However, as the nonlinear elements of the two diodes, one feasible way to describe this model is to write only one set of state equations by using some basic circuit analysis methods such as KVL, KCL, etc., hence the state equations for this time-varying and nonlinear cardiovascular circuit model shown in Figure 3.1 can be derived as follows:

$$\dot{x} = f(x, t) = A_c(t)x + P_c(t)P(x) \quad (3.4)$$

where $A_c(t)$ and $P_c(t)$ are (5×5) and (5×2) time-varying matrices, respectively, and $P(x)$ is a (2×1) vector, used to model the nonlinear behavior of the two diodes previously mentioned. Note that the expression of $P_c(t)$ is not associated with the three modes such that

$$P_c(t) = \begin{bmatrix} \frac{1}{C(t)} & \frac{-1}{C(t)} \\ \frac{-1}{C_R} & 0 \\ 0 & 0 \\ 0 & \frac{1}{C_A} \\ 0 & 0 \end{bmatrix} \quad (3.5)$$

Both $A_c(t)$ and $P(x)$ are changed with respect to the three different modes of the cardiac cycle previously discussed.

Mode 1: Isovolumic phase. In this phase, both mitral and aortic valves are closed; therefore, the two corresponding diodes in Figure 3.1 are the open circuits as shown in Figure 3.3.

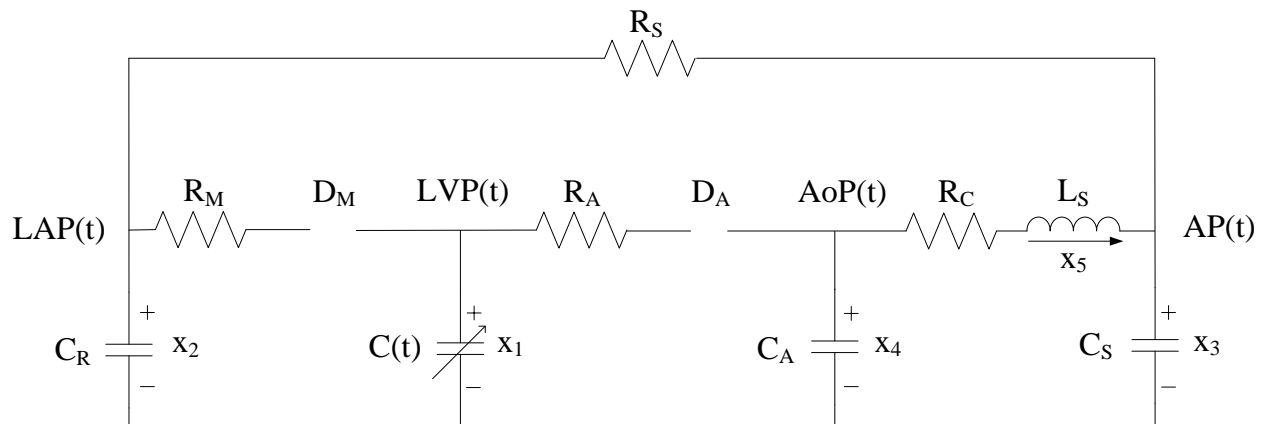


Figure 3.3 Isovolumic Phase for a Cardiovascular Circuit Model

$A_c(t)$ and $P(x)$ in this phase are as followed:

$$A_c(t) = \begin{bmatrix} \frac{-\dot{C}(t)}{C(t)} & 0 & 0 & 0 & 0 \\ 0 & \frac{-1}{R_S C_R} & \frac{1}{R_S C_R} & 0 & 0 \\ 0 & \frac{1}{R_S C_S} & \frac{-1}{R_S C_S} & \frac{1}{C_S} & 0 \\ 0 & 0 & 0 & 0 & \frac{-1}{C_A} \\ 0 & 0 & \frac{-1}{L_S} & \frac{1}{L_S} & \frac{-R_C}{L_S} \end{bmatrix} \quad (3.6)$$

$$P(x) = \begin{bmatrix} 0 \\ 0 \end{bmatrix} \quad (3.7)$$

Mode 2: Ejection phase. In this phase, since blood is ejected from the left ventricle to the aorta, as a result, the mitral valve is still closed but the aortic valve is open. In Figure 3.4, it is shown that at this time, D_M is still an open circuit but D_A is a short circuit.

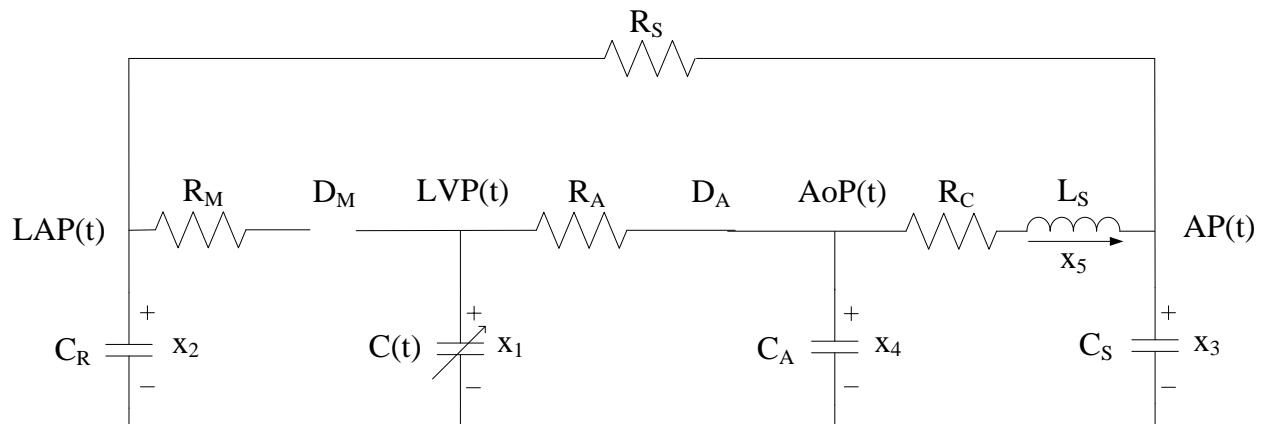


Figure 3.4 Ejection Phase for a Cardiovascular Circuit Model

$A_c(t)$ and $P(x)$ are rewritten as follows:

$$A_c(t) = \begin{bmatrix} \frac{-\dot{C}(t)}{C(t)} - \frac{1}{C(t)R_A} & 0 & 0 & \frac{1}{C(t)R_A} & 0 \\ 0 & \frac{-1}{R_S C_R} & \frac{1}{R_S C_R} & 0 & 0 \\ 0 & \frac{1}{R_S C_S} & \frac{-1}{R_S C_S} & 0 & \frac{1}{C_S} \\ \frac{1}{C_A R_A} & 0 & 0 & \frac{-1}{C_A R_A} & \frac{-1}{C_A} \\ 0 & 0 & \frac{-1}{L_S} & \frac{1}{L_S} & \frac{-R_C}{L_S} \end{bmatrix} \quad (3.8)$$

$$P(x) = \begin{bmatrix} 0 \\ r(x_1 - x_4) \\ R_A \end{bmatrix} \quad (3.9)$$

Mode 3: Filling phase. In this phase, blood is filled from the left atrium into the left ventricle, the mitral valves turns to be open and the aortic valve is closed. The corresponding Figure 3.5 shows that D_M is a short circuit and D_A is an open circuit.

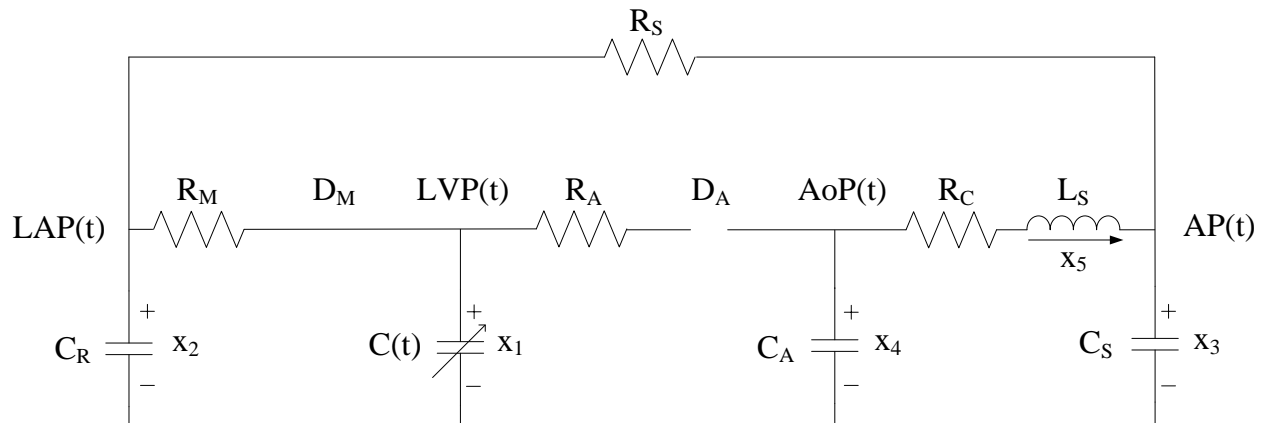


Figure 3.5 Ejection Phase for a Cardiovascular Circuit Model

$A_c(t)$ and $P(x)$ are rewritten as below:

$$A_c(t) = \begin{bmatrix} \frac{-\dot{C}(t)}{C(t)} - \frac{1}{C(t)R_M} & \frac{1}{C(t)R_M} & 0 & 0 & 0 \\ \frac{1}{R_M C_R} & \frac{-1}{C_R} \left(\frac{1}{R_M} + \frac{1}{R_S} \right) & \frac{1}{R_S C_R} & 0 & 0 \\ 0 & \frac{1}{R_S C_S} & \frac{-1}{R_S C_S} & 0 & \frac{1}{C_S} \\ 0 & 0 & 0 & 0 & \frac{-1}{C_A} \\ 0 & 0 & \frac{-1}{L_S} & \frac{1}{L_S} & \frac{-R_C}{L_S} \end{bmatrix} \quad (3.10)$$

$$P(x) = \begin{bmatrix} r(x_2 - x_1) \\ R_M \\ 0 \end{bmatrix} \quad (3.11)$$

where $r(x)$ is the ramp function:

$$r(x) = \begin{cases} x, & \text{if } x \geq 0 \\ 0, & \text{if } x < 0 \end{cases} \quad (3.12)$$

3.1.3 Simulation Results

In order to check the performance of the cardiovascular circuit model, simulation tests have been implemented by MATLAB¹. Figure 3.6 illustrates the simulation results of several hemodynamic variables in the model such as LVP, LAP, AoP, LVV, and Q_T (cardiac cycle is 0.8 s). The model validation can be found in [19].

¹ The MathWorks Inc., Natick, MA.

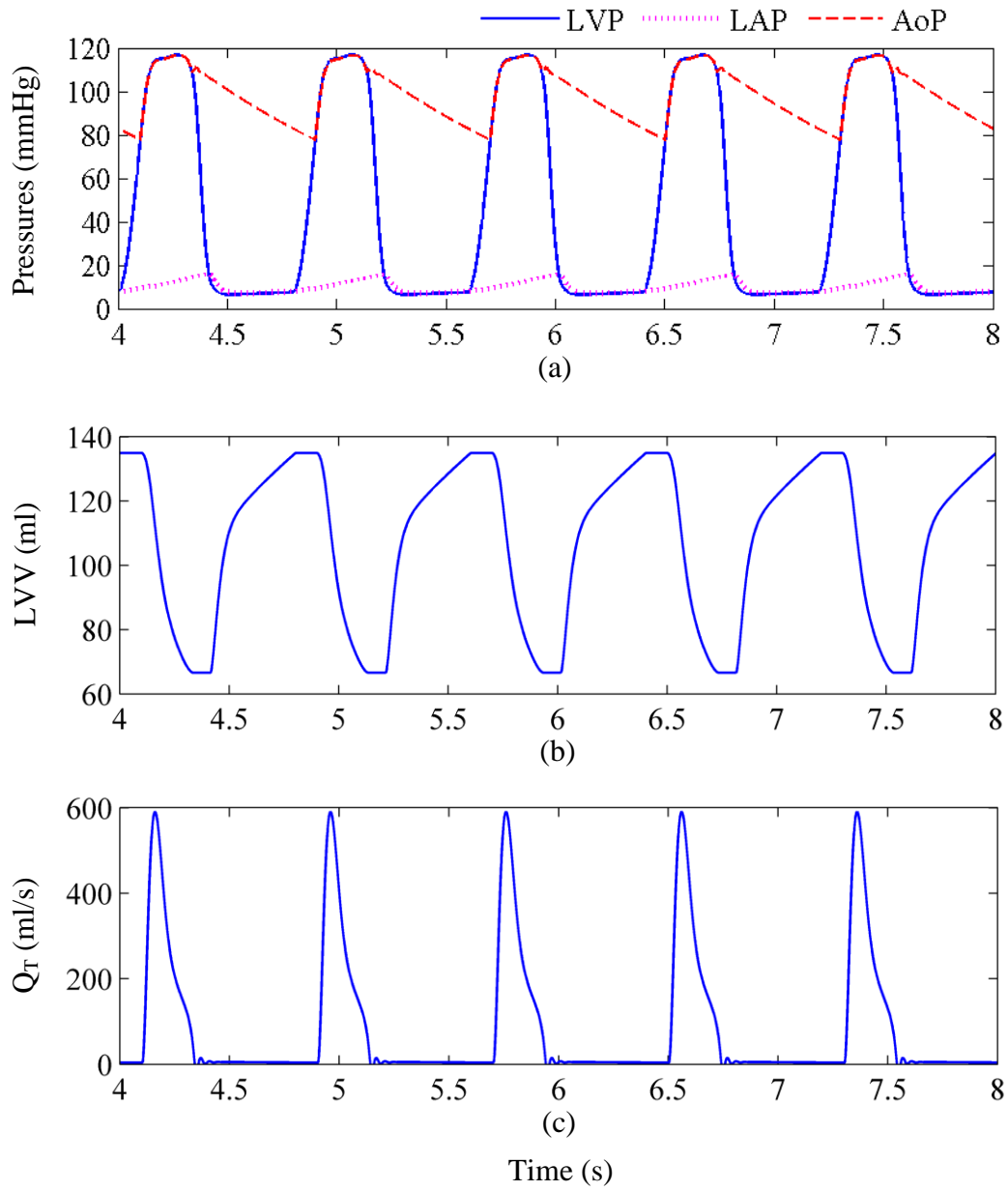


Figure 3.6 Simulation of Main Hemodynamic Parameters for a Normal Heart

3.2 The Combined Cardiovascular-Pump Model

In this section, the 1st LVAD model is described, and the current-based model of the combined cardiovascular and rotary LVAD system is presented with its state equations. Finally the simulation results of the open-loop response for a sick heart are discussed.

3.2.1 Cardiovascular-LVAD Model

The LVAD considered in this work is a rotary blood pump connected as a bridge between the left ventricle and the aorta as illustrated in the schematic in Figure 3.7. A combined cardiovascular-LVAD model is shown in Figure 3.8. Table 3.4 lists the state variables of this cardiovascular-LVAD model. Table 3.5 lists all parameters with their values for the LVAD.

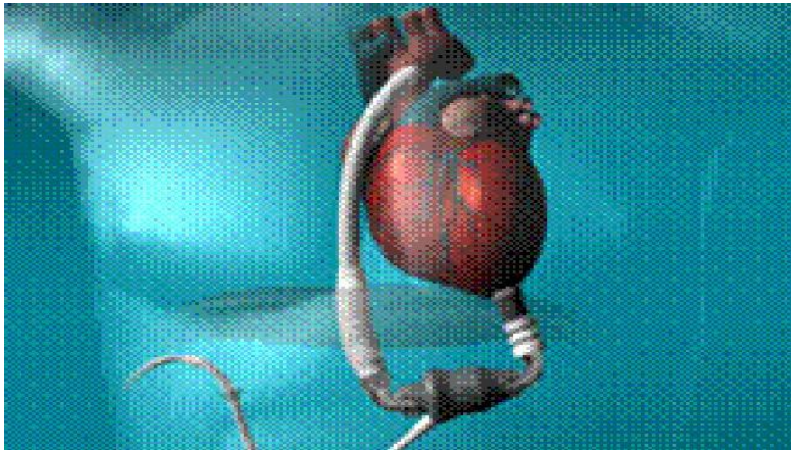


Figure 3.7 Schematic of a Rotary LVAD [19]

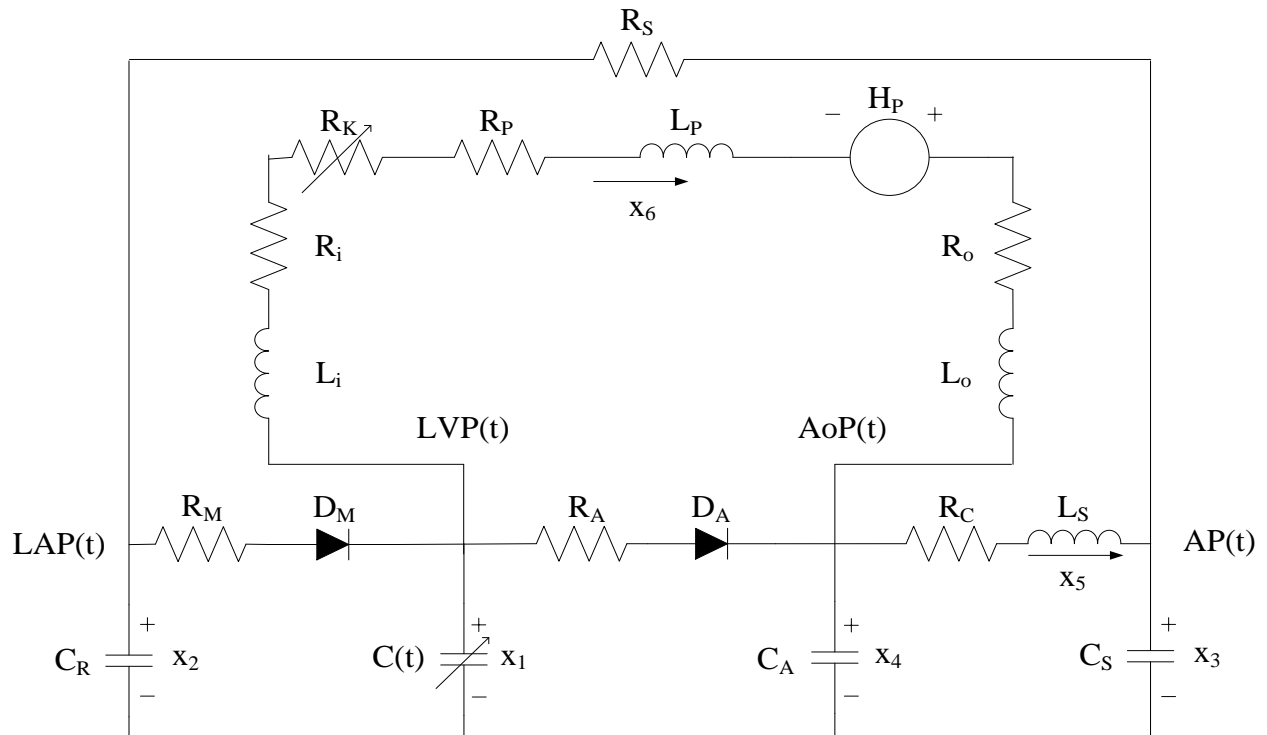


Figure 3.8 Combined Cardiovascular-LVAD Circuit Model

Table 3.4 State Variables of the Combined Model

Variables	Name	Physiological Meaning (units)
$x_1(t)$	LVP(t)	Left Ventricular Pressure (mmHg)
$x_2(t)$	LAP(t)	Left Atrial Pressure (mmHg)
$x_3(t)$	AP(t)	Arterial Pressure (mmHg)
$x_4(t)$	AoP(t)	Aortic Pressure (mmHg)
$x_5(t)$	$Q_T(t)$	Total Flow (ml/s)
$x_6(t)$	PF(t)	Pump Flow (ml/s)

Table 3.5 Parameters of the LVAD Model

Parameters	Value	Physiological Meaning
R_k (mmHg·s/ml)	See (3.14)	Suction Resistance with parameters
R_i (mmHg·s/ml)	0.0677	Inlet Resistance of Cannulae
R_o (mmHg·s/ml)	0.0677	Outlet Resistance of Cannulae
L_i (mmHg·s ² /ml)	0.0127	Inlet Inertance of Cannulae
L_o (mmHg·s ² /ml)	0.0127	Outlet Inertance of Cannulae
R_p	0.1707	Pressure Difference Parameter
L_p	0.02177	Pressure Difference Parameter

The LVAD pumps blood continuously from the left ventricle to the aorta. Therefore, the pressure difference between the left ventricle and the aorta is expressed by the following equation [20]:

$$LVP(t) - AoP(t) = R_i Q + L_i \frac{dQ}{dt} + R_o Q + L_o \frac{dQ}{dt} + R_p Q + L_p \frac{dQ}{dt} - H_p + R_k Q \quad (3.13)$$

where H_p is the pressure (head) gain across the pump and Q is the blood flow rate through the pump. The parameters R_i , R_o , and R_p represent the flow resistances and L_i , L_o , and L_p represent the flow inertances of the cannulae² and pump, respectively. The resistance R_k is a special

² The cannula is a plastic rigid tube that connects the rotary pump to the heart.

nonlinear time-varying element, called suction element model developed by Schima et al. [29]. It is an empirical model such that its resistance varies with the LVP, which is zero when LVP is larger than a given threshold \bar{x}_1 and linearly increases if LVP is below \bar{x}_1 at a given rate α . In another word, this suction model is a pressure-dependent resistance. The mathematical expression of R_k is given as

$$R_k = \begin{cases} 0, & \text{if } x_1(t) > \bar{x}_1 \\ \alpha(x_1(t) - \bar{x}_1), & \text{if } x_1(t) \leq \bar{x}_1 \end{cases} \quad (3.14)$$

where α is -3.5 s/ml and \bar{x}_1 is 1 mmHg.

The pressure gain across the pump H_p is modeled using the direct relation between the electric power supplied to the pump motor P_e and the hydrodynamic power generated by the pump P_p scaled by the pump efficiency η as:

$$P_p = \eta P_e \quad (3.15)$$

Additionally, the electric power may be written in terms of the supplied voltage V and the supplied current $i(t)$ to the pump motor while the hydrodynamic power may be written in terms of the pump head or pressure gain H_p and the Pump Flow (PF) Q as:

$$P_e = V \cdot i(t) \quad (3.16)$$

$$P_p = \rho g H_p Q \quad (3.17)$$

where ρ is the density of the reference fluid and g is the acceleration of gravity ($\rho_{\text{Hg}} = 13600 \text{ kg/m}^3$, $g = 9.8 \text{ m/s}^2$). Using Equation (3.16) and (3.17) and then substituting in Equation (3.15) yields:

$$\rho g H_p Q = \eta V i(t) \quad (3.18)$$

Solving for the pump pressure gain H_p , we obtain the following expressions:

$$H_p = \frac{\eta V}{\rho g} \cdot \frac{i(t)}{Q} \quad (3.19)$$

Or

$$H_p = \gamma \frac{i(t)}{Q} \quad (3.20)$$

where $\gamma = \eta V / \rho g$. After applying the appropriate conversion factors and assuming a pump motor supplied voltage $V = 12$ volts as well as a pump efficiency of 100% (assuming that most losses are accounted for by the pressure losses induced by R_p and L_p), the constant γ can be computed to be $\gamma = 89,944 \text{ mmHg}\cdot\text{ml/s}\cdot\text{amp}$. This relation leads to a non-linear state equation governing the behavior of the LVAD as:

$$LVP(t) - AoP(t) = R^*Q + L^* \frac{dQ}{dt} - \gamma \frac{i(t)}{Q} \quad (3.21)$$

Where $R^* = R_i + R_o + R_p + R_k$ and $L^* = L_i + L_o + L_p$. Notice that it is crucial to validate the numerical solution scheme of the state equations to guarantee that the system does not operate at zero (or negative) pump flow Q at any point during the cardiac cycle as the state equation in (3.21) exhibits its non-linearity with the pump flow Q in the denominator.

The rotary LVAD state equation in (3.21) allows forming a combined model where the primary control variable is the supplied current to the pump motor. Furthermore, the resulting time-varying Pump Speed (PS) – $\omega(t)$ may be estimated at a post-processing stage after solving for the state variables, using the relation between the pump pressure H_p and the pump speed $\omega(t)$ such that:

$$H_p = \beta \omega^2(t) \quad (3.22)$$

where $\beta = 9.9025 \cdot 10^{-7} \text{ mmHg}/(\text{rpm})^2$. Comparing with Equation (3.20), an expression for the pump speed in terms of the Pump Current (PC) can be derived as follows:

$$\omega(t) = \sqrt{\frac{\gamma i(t)}{\beta Q(t)}} \quad (3.23)$$

Note that now it is clear how the heart hemodynamics through $Q(t)$ influence directly, in a highly nonlinear manner, the pump speed $\omega(t)$.

3.2.2 State Equations

According to the state equations in Section 3.1.2, the state equations for the combined cardiovascular-LVAD model can be written as follows:

$$\dot{x} = f(x, t, i) = A_c(t)x + P_c(t)P(x) + bi(t) \quad (3.24)$$

where $A_c(t)$ and $P_c(t)$ are (6×6) and (6×2) time-varying matrices, respectively. $P(x)$ is the same as shown in Section 3.1.2 and $P_c(t)$ is expressed as follows:

$$P_c(t) = \begin{bmatrix} \frac{1}{C(t)} & \frac{-1}{C(t)} \\ \frac{-1}{C_R} & 0 \\ 0 & 0 \\ 0 & \frac{1}{C_A} \\ 0 & 0 \\ 0 & 0 \end{bmatrix} \quad (3.25)$$

In addition, note that in Equation (3.24) the pump motor current $i(t)$ is the control variable, and b is a (6×1) vector, given as

$$b = \begin{bmatrix} 0 \\ 0 \\ 0 \\ 0 \\ 0 \\ \frac{\gamma}{L^*x_6} \end{bmatrix} \quad (3.26)$$

$A_c(t)$ varies according to the three different modes previously mentioned. Figure 3.9, 3.10, and 3.11 show the combined cardiovascular-LVAD circuit model with three different phases, respectively.

Mode 1: Isovolumic phase.

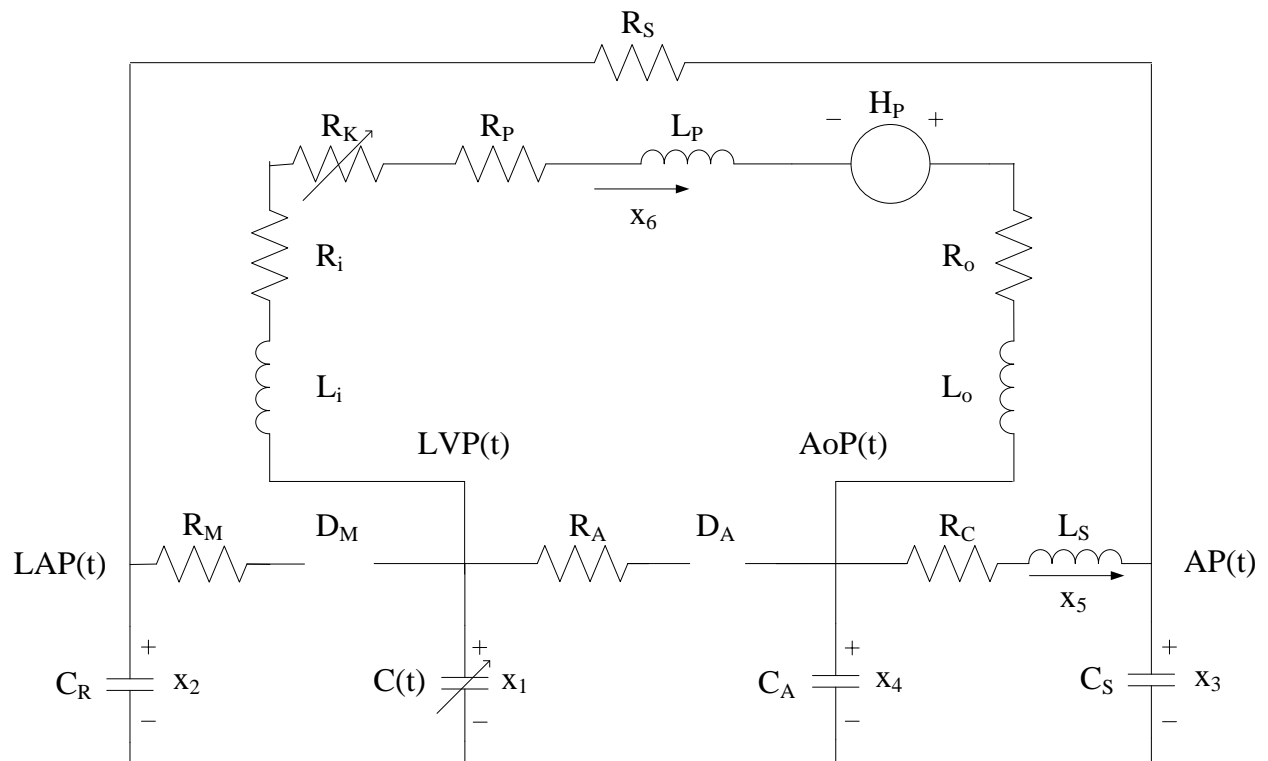


Figure 3.9 Isovolumic Phase for a Combined Cardiovascular-LVAD Circuit Model

$$A_c(t) = \begin{bmatrix} \frac{-\dot{C}(t)}{C(t)} & 0 & 0 & 0 & 0 & \frac{-1}{C(t)} \\ 0 & \frac{-1}{R_S C_R} & \frac{1}{R_S C_R} & 0 & 0 & 0 \\ 0 & \frac{1}{R_S C_S} & \frac{-1}{R_S C_S} & \frac{1}{C_S} & 0 & 0 \\ 0 & 0 & 0 & 0 & \frac{-1}{C_A} & \frac{1}{C_A} \\ 0 & 0 & \frac{-1}{L_S} & \frac{1}{L_S} & \frac{-R_C}{L_S} & 0 \\ \frac{1}{L^*} & 0 & 0 & \frac{-1}{L^*} & 0 & \frac{-R^*}{L^*} \end{bmatrix} \quad (3.27)$$

Mode 2: Ejection phase.

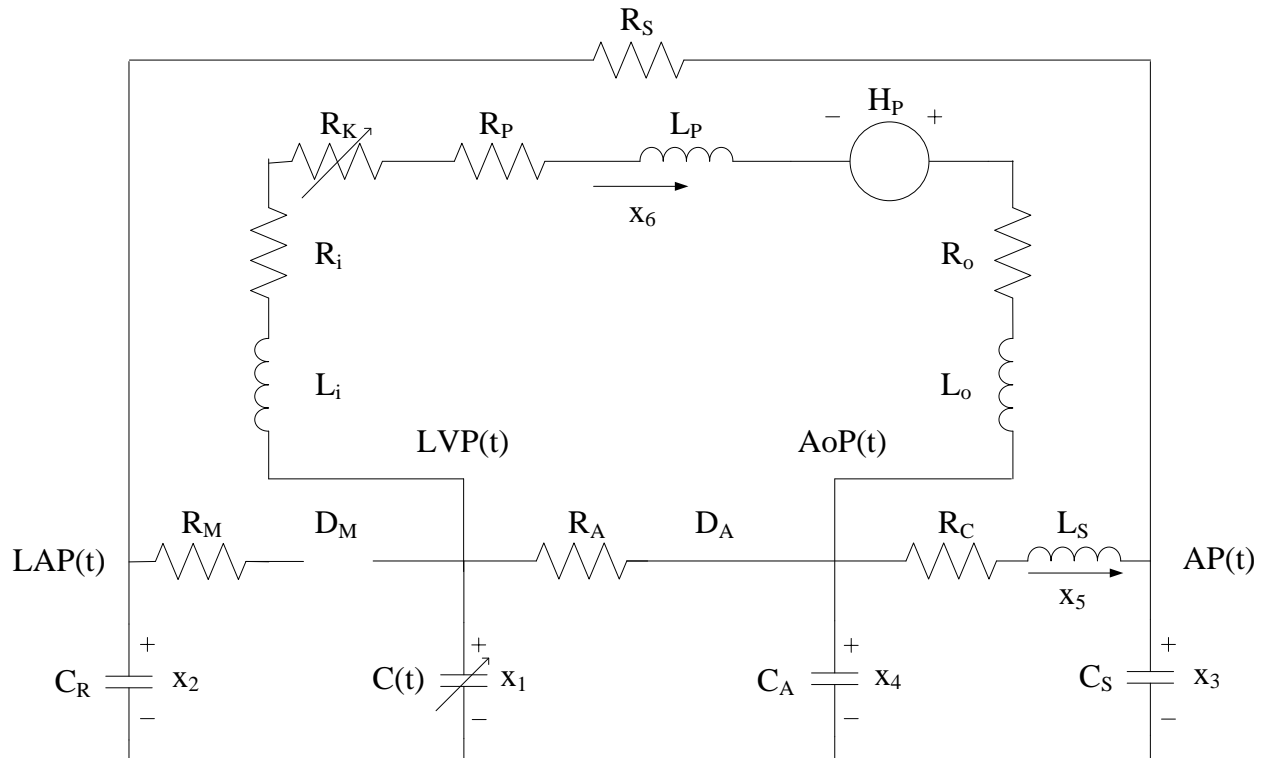


Figure 3.10 Ejection Phase for a Combined Cardiovascular-LVAD Circuit Model

$$A_c(t) = \begin{bmatrix} \frac{-\dot{C}(t)}{C(t)} - \frac{1}{C(t)R_A} & 0 & 0 & \frac{1}{C(t)R_A} & 0 & \frac{-1}{C(t)} \\ 0 & \frac{-1}{R_S C_R} & \frac{1}{R_S C_R} & 0 & 0 & 0 \\ 0 & \frac{1}{R_S C_S} & \frac{-1}{R_S C_S} & \frac{1}{C_S} & 0 & 0 \\ \frac{1}{C_A R_A} & 0 & 0 & \frac{-1}{C_A R_A} & \frac{-1}{C_A} & \frac{1}{C_A} \\ 0 & 0 & \frac{-1}{L_S} & \frac{1}{L_S} & \frac{-R_C}{L_S} & 0 \\ \frac{1}{L^*} & 0 & 0 & \frac{-1}{L^*} & 0 & \frac{-R^*}{L^*} \end{bmatrix} \quad (3.28)$$

Mode 3: Filling phase.

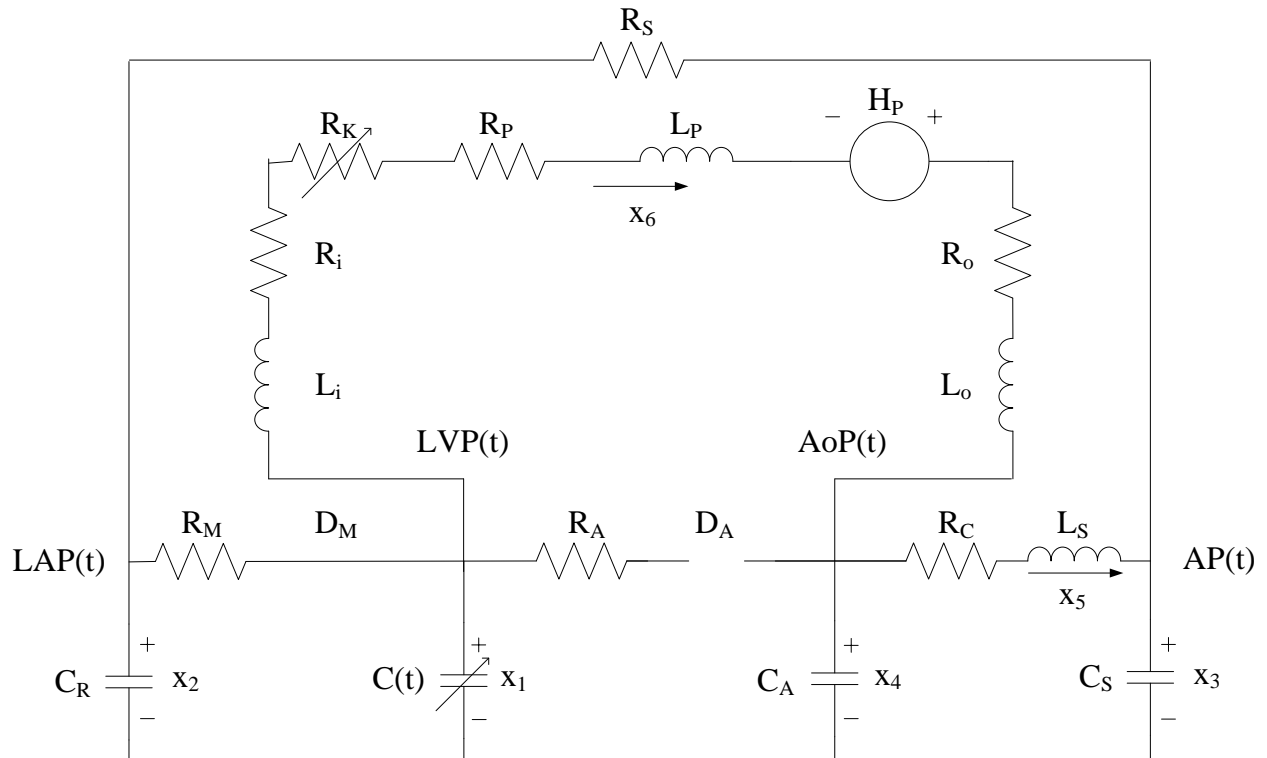


Figure 3.11 Filling Phase for a Combined Cardiovascular-LVAD Circuit Model

$$A_c(t) = \begin{bmatrix} \frac{-\dot{C}(t)}{C(t)} - \frac{1}{C(t)R_M} & \frac{1}{C(t)R_M} & 0 & 0 & 0 & \frac{-1}{C(t)} \\ \frac{-1}{R_M C_R} & \frac{-1}{C_R} \left(\frac{1}{R_M} + \frac{1}{R_S} \right) & \frac{1}{R_S C_R} & 0 & 0 & 0 \\ 0 & \frac{1}{R_S C_S} & \frac{-1}{R_S C_S} & \frac{1}{C_S} & 0 & 0 \\ 0 & 0 & 0 & 0 & \frac{-1}{C_A} & \frac{1}{C_A} \\ 0 & 0 & \frac{-1}{L_S} & \frac{1}{L_S} & \frac{-R_C}{L_S} & 0 \\ \frac{1}{L^*} & 0 & 0 & \frac{-1}{L^*} & 0 & \frac{-R^*}{L^*} \end{bmatrix} \quad (3.29)$$

3.2.3 Open Loop Simulations

In the open loop simulations for the LVAD, E_{\max} equals to 1.0 mmHg/ml for a sick heart since E_{\max} is considered to be 2.0 mmHg/ml for a healthy heart in the cardiovascular model. In addition, note that Equation (2.2) will not be available any more since the pump can replace the natural heart to provide continuous blood flow. The actual cardiac output will be the combination of the blood flow pumped by the heart and that through the LVAD.

Figure 3.12 shows the effect of the ramp PC on LVP, AoP, Q_T , and PF. The ramp pump current linearly increases, starting at 0.1 A with the slope of 0.01 over the period of 60 seconds shown in Figure 3.12(a). Note that in Figure 3.12(b), AoP is larger than LVP at all time since the aortic valve is not open during the ejection, and the phases of the aortic valve (i.e., open or closed) depend on the contractility strength of the heart and the values of the control input. In this case, since the weak left ventricle is not strong enough to open the aortic valve, the cardiac output

(total flow) is equal to the pump flow, meaning that the cardiac output is totally provided by the LVAD. This can also be proven in Figure 3.12(c).

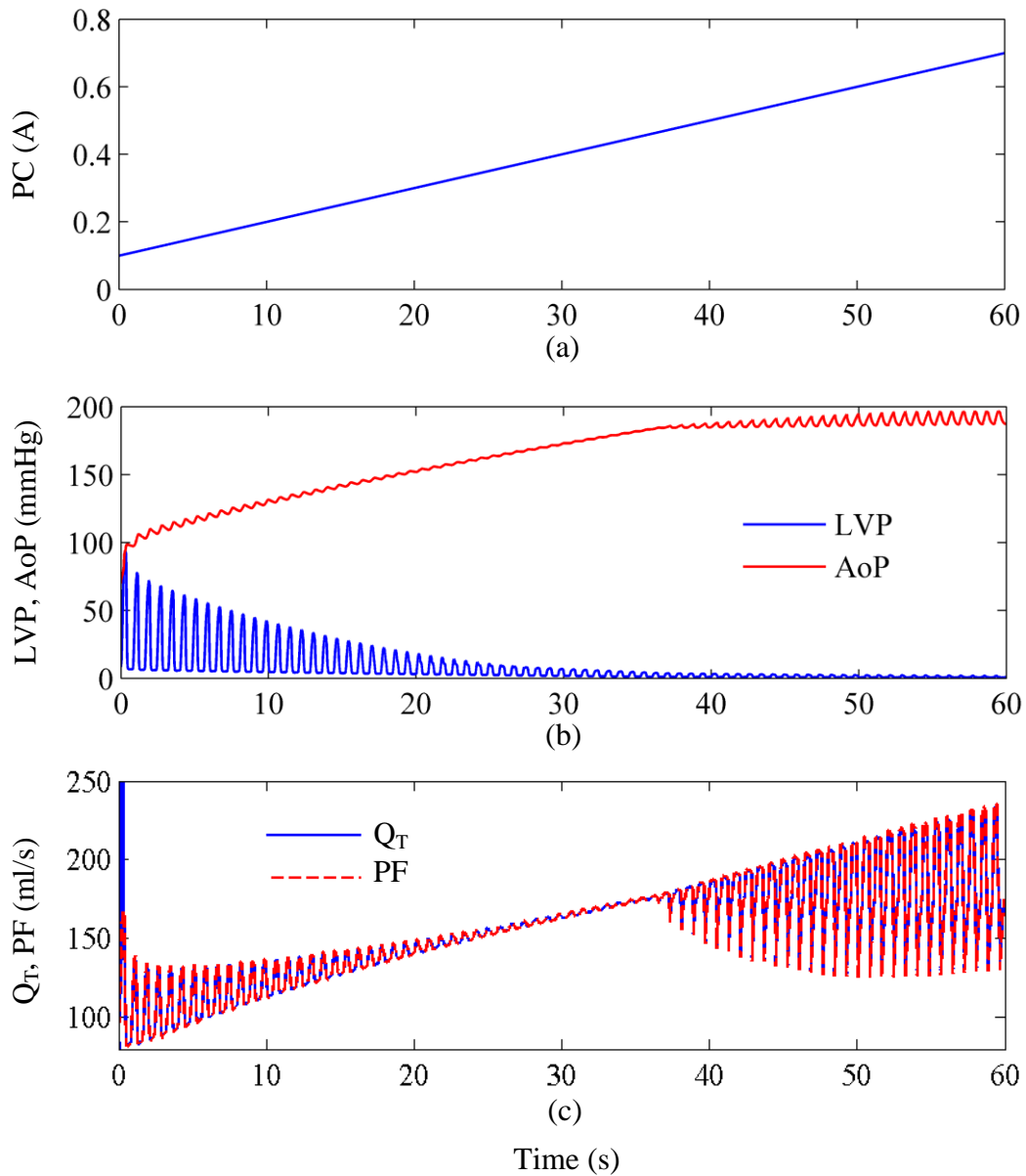


Figure 3.12 Simulations of Ramp PC, LVP, AoP, Q_r , and PF

In addition, according to Equation (3.23), it is also important to examine how the pump speed signal is affected by the supplied pump motor current. Figure 3.13 shows a plot of the pump speed when the model, with a heart rate of 75 bpm, is driven with a linearly increasing pump current shown in Figure 3.12(a). There are two important observations that can be made from Figure 3.13. First, note that the resulting pump speed $\omega(t)$ does not also increase linearly. Instead, it increases nonlinearly with a decreasing rate of increase. Second, the pump speed has a superposed oscillatory component that has the same pulsatility as the heart rate of 75 bpm. This is a very interesting and extremely important new phenomenon that has recently been observed in in-vivo data obtained through clinical studies of intensive care patients implanted with LVADs [30]. This is the first time that such a phenomenon has been reproduced from a combined cardiovascular and LVAD model and represents a breakthrough in accurately modeling this complex bio-mechanical system [20].

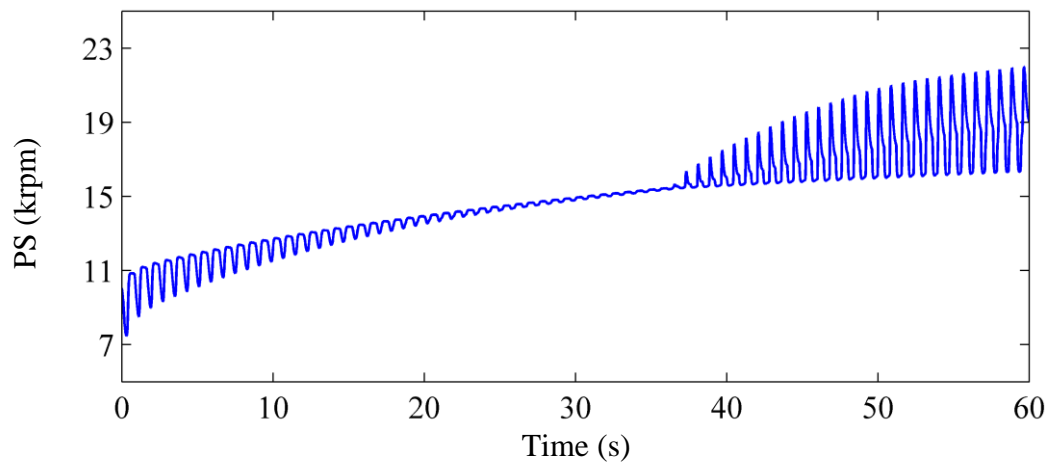


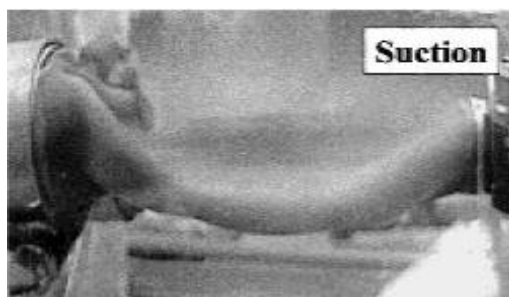
Figure 3.13 PS as a Function of Time When PC is Increased Linearly

CHAPTER 4: SUCTION PHENOMENON AND INDICES

The suction phenomenon is known as one of the major complications in the development of implantable rotary blood pumps. Suction can be defined as the collapse of the ventricle or tissues and cells damage. The reason is that the pumped blood outflow exceeds the blood flow to the heart, which means the heart is over-pumping more blood than normally needed. Figure 4.1 shows the normal and collapsed ventricle sacs in a mock loop experiment that simulates a healthy ventricle and an auxiliary pump with a pneumatically actuated artificial heart and an unsealed centrifugal pump, respectively [6].



(a)



(b)

Figure 4.1 The Mock Loop Experiment of Normal and Suction Cases [6]

In this dissertation, we present a new suction detection and classification method based on the Lagrangian Support Vector Machine (LSVM) approach in pattern recognition. The LSVM is a modified original Support Vector Machine (SVM) and has high accuracy, stable performance, and fast learning speed (i.e., training time). In addition, LSVM is the most widely used algorithm, for its well-known mathematical foundation, robustness, and relatively simple implementation.

Figure 4.2 shows a flowchart of the proposed LSVM algorithm for the LVAD. The algorithm is composed of four modules [14], [15]: (1) a *pre-processing module* whose purpose is to filter the pump flow signal, eliminating high frequency noise components using a low pass filter. (2) a *feature extraction module* which calculates six suction indices from the filtered pump signal. Three of the six indices are based on time domain, two on frequency domain, and one on time-frequency domain. Both of the two modules mentioned above are implemented during both the training as well as during the test phases. (3) a *classifier training module* whose purpose is to perform the training phase and (4) a *classification module* whose purpose is to perform the final classification. Note that the classifier training module and the classification module must operate on two distinct and different sets of data.

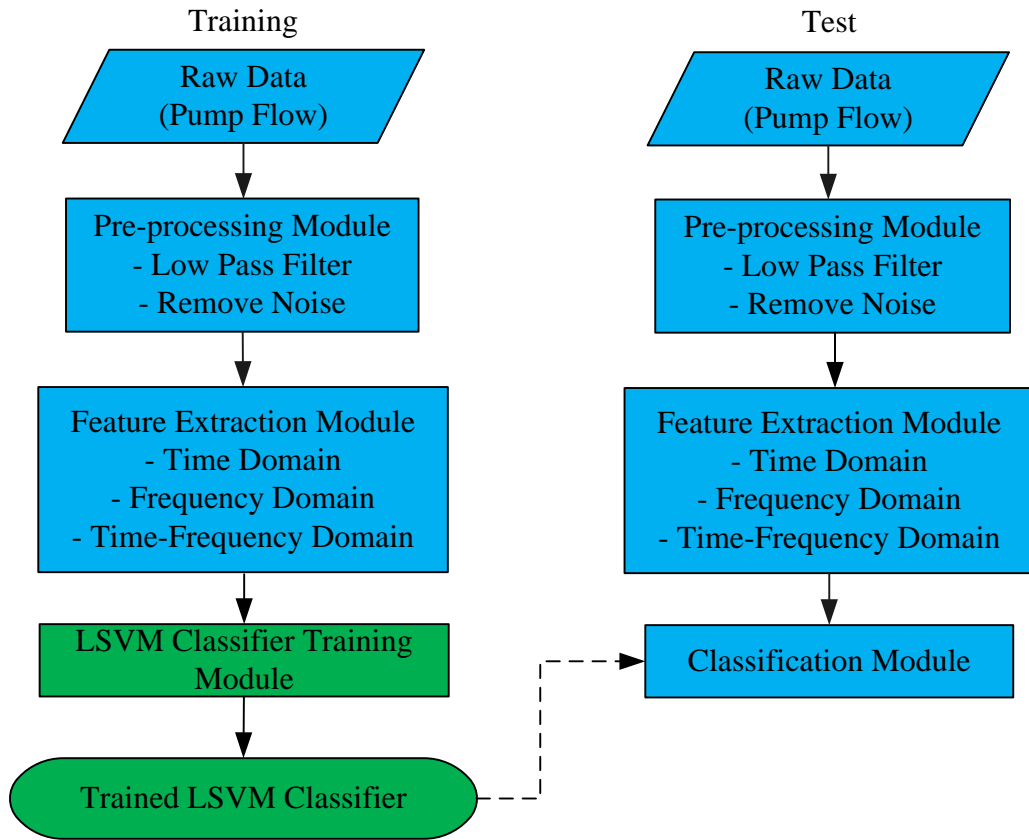


Figure 4.2 Flow Chart of the Proposed Suction Detection Algorithm

This chapter is organized as follows. Section 4.1 introduces the data acquisition. Section 4.2 describes the feature extraction of pump flow in details, including definition of pump states, window length issue, and suction indices extracted based on time, frequency, and time-frequency domains, respectively.

4.1 Data Acquisition

The in vivo data used in this study were obtained from experiments, as described in Table 4.1, performed at the University of Pittsburgh in 1998 and 2005 [31]. One calf of average weight (~250Kg) was implanted with a centrifugal MedQuest pump and four calves, also of average weight, were implanted with axial Nimbus pumps. The inflow cannulation was achieved via the left ventricle and the blood flow was measured using two transonic flow probes; the first placed either in the aorta and pulmonary artery to measure cardiac output and the second in the pump outflow cannula to measure pump flow. The pump inlet pressure was measured by a pressure sensor placed at the inlet of the pump. Suction was induced either by overpumping (most of the times) or by clamping the vena cava. Overpumping was achieved by increasing the pump speed from 1,000 rpm to 3,100 rpm for the MedQuest pump and from 7,000 rpm to 15,000 rpm for the Nimbus pump, respectively. Once suction was encountered the pump speed was decreased to avoid any injury to the myocardium. Clamping the vena cava caused less blood to return to the calves' hearts and as a result, the pump drew less blood, causing suction. Note that at the end of the experiment, Esmolol (a cardioselective drug that decreases heart rate and contractility) was used for the animals to validate how changes in the heart contractility affect the pump flow and the occurrence of suction. Additional details on the experiment and data acquisition procedure can be found in [31].

Table 4.1 Description of the Study on In-vivo Data for Two Pumps

Pump name	MedQuest ³	Nimbus ⁴
Pump Type	Centrifugal	Axial
Subject used	One calf	Four calves
Study type	Acute	Chronic
Sampling rate (Hz)	500	135/150

4.2 Feature Extraction of Pump Flow

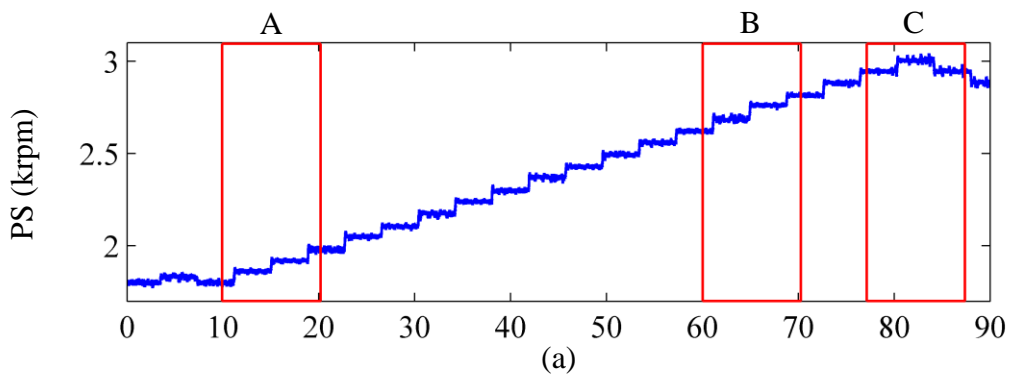
Suction could be easily identified if reliable pressure sensors are implanted at some locations in the left ventricle to continuously measure hemodynamic variables such as x_1 through x_5 (presented in the cardiovascular model in Section 3.1.1), or at the inlet of the pump to evaluate the pump inlet pressure. However, currently such implantable sensor technology is not available for real-time monitoring. Hence, due to the lack of available information, most suction detection methods are tentative and depend on the extraction of features from other available signals, which can be continuously measured for a long time. Due to these constraints, most researchers use pump flow, pump speed, or pump current to extract features for suction detection. In this work, the pump flow signal is adopted to extract features.

³ LaunchPoint, LLC (Goleta, CA) and WorldHeart, Inc.

⁴ Nimbus, Inc., Rancho Cordova, CA.

4.3 Definition of Pump States

Pump states are usually defined by clinical experts. However, the definition of such states is generally not consistent due to the subjectivity of the experts and the complexity of different types of pump signals available in real time. In this paper, we will develop the LSVM algorithm with two possible classes of pump states. The first is a 3-state classification which admits three states of suction patterns: No Suction (NS), Approaching Suction (AS), and Suction (S), and the second is a 2-state classification which admits two states of suction patterns: No Suction (NS) and Suction (S). Clearly in the 2-state case NS and AS are merged together as NS, and consequently this case is simpler to analyze but does not provide a warning that suction is approaching. Figure 4.3 and 4.4 show several plots of the in vivo data for MedQuest and Nimbus pumps, respectively. These plots include Pump Speed (PS), Left Ventricular Pressure (LVP), Pump Inlet Pressure (PIP), and Pump Flow (PF). On these plots three pump states are identified and indicated by the three time windows labeled A, B, and C, respectively.



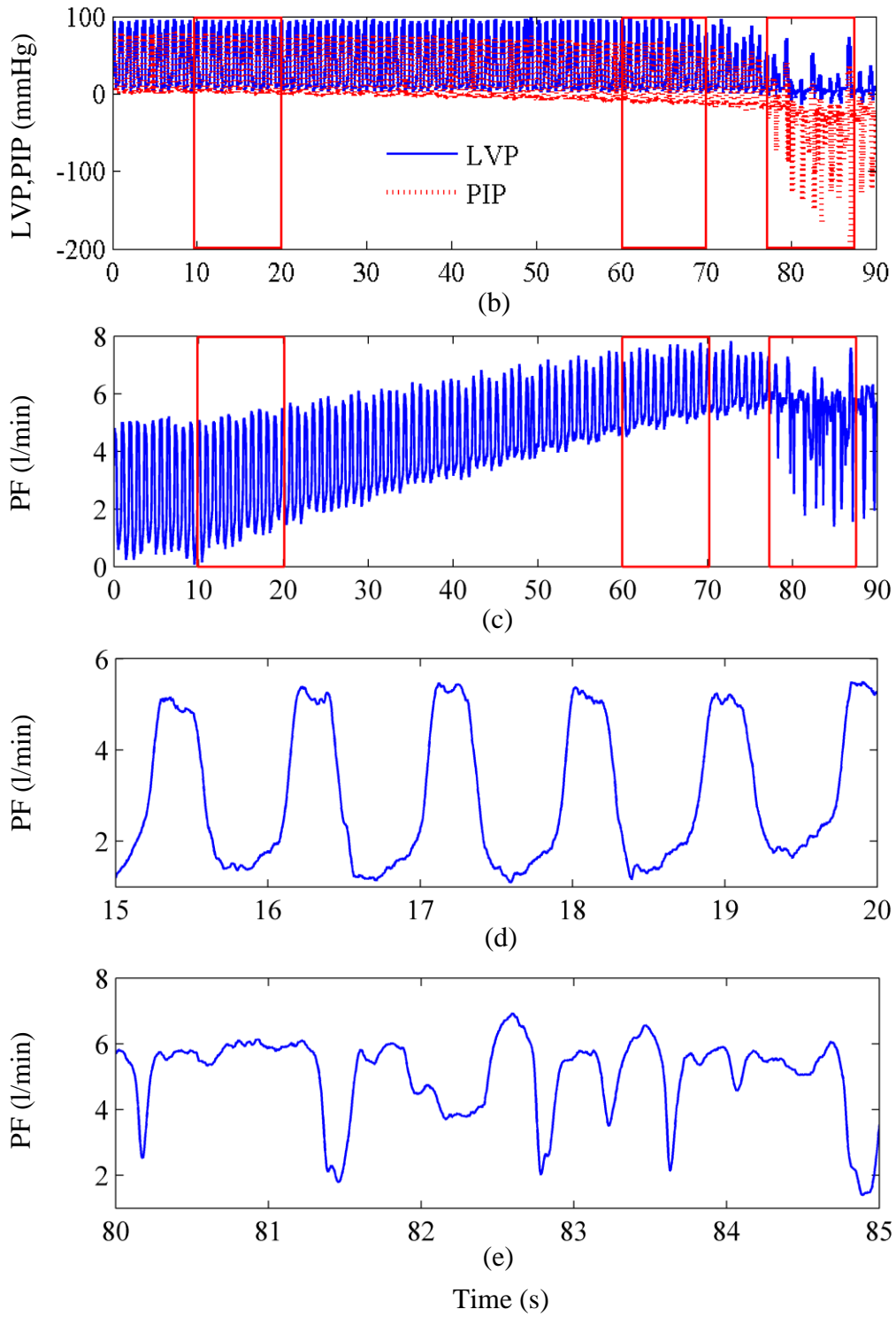
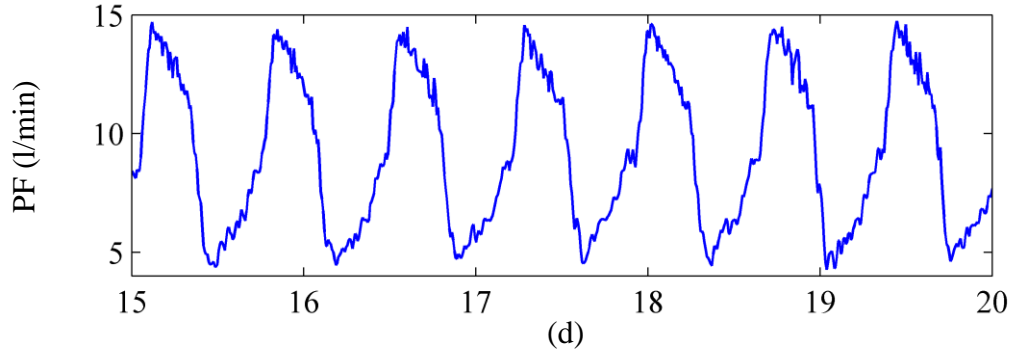
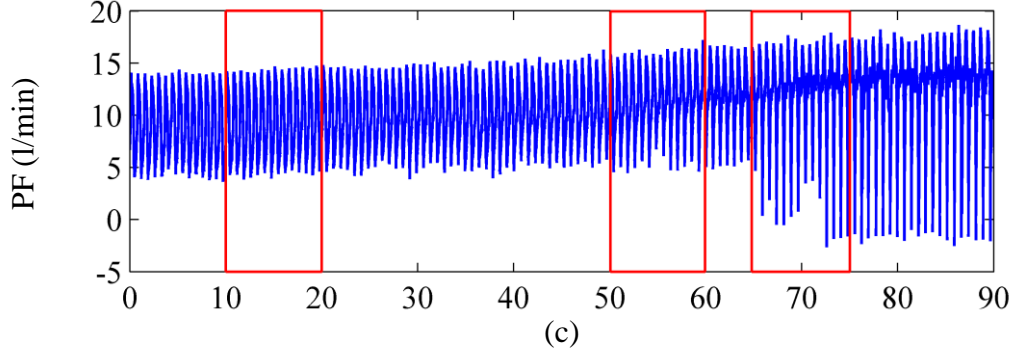
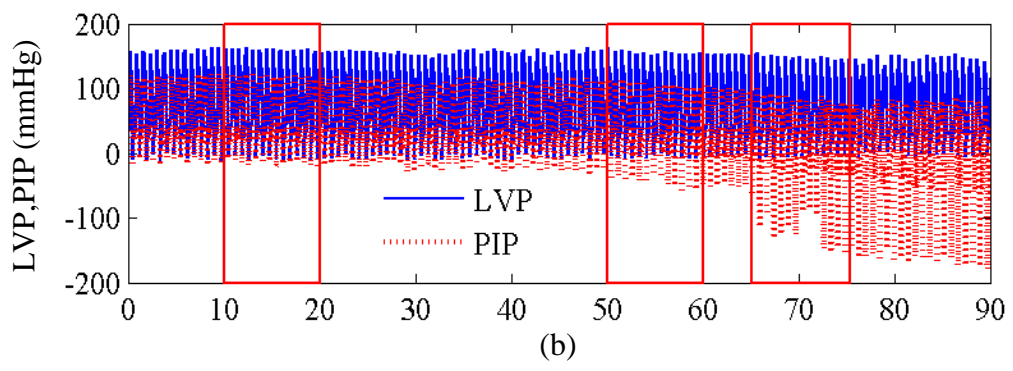
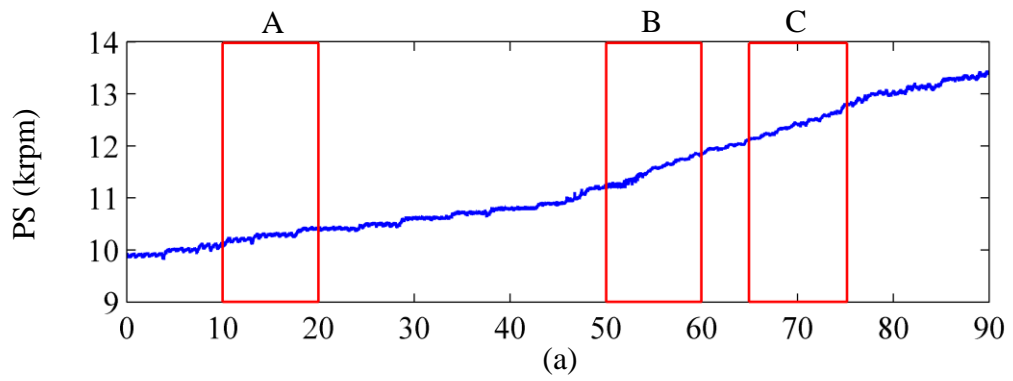


Figure 4.3 Example of In Vivo Data Based on MedQuest Pump. (a) PS. (b) LVP, PIP. (c) PF. (d) Zoomed PF for NS Case. (e) Zoomed PF for S Case



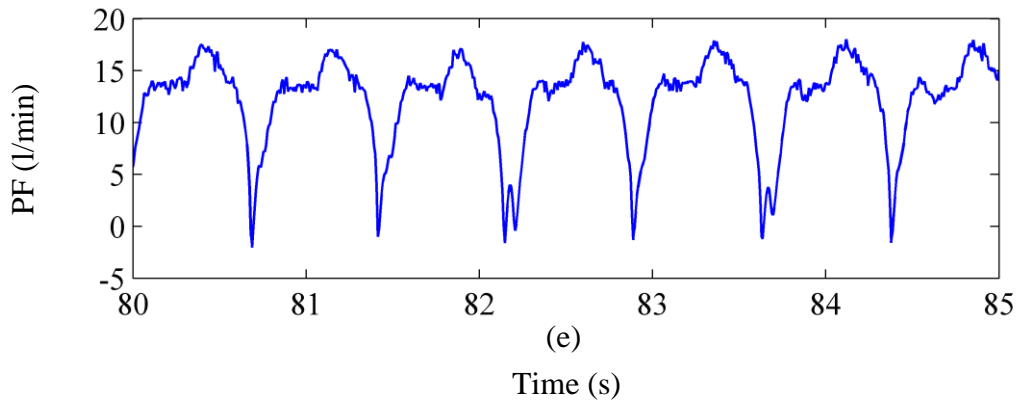


Figure 4.4 Example of In Vivo Data Based on Nimbus Pump. (a) PS. (b) LVP, PIP. (c) PF. (d) Zoomed PF for NS Case. (e) Zoomed PF for S Case

In time window A, No Suction (NS) corresponds to the normal operating condition of the pump. Within each cardiac cycle, the Minimum Pump Inlet Pressure (MPIP) is generally close to zero and its difference from the Minimum Left Ventricular Pressure (MLVP) is small, (i.e., $\Delta P = MLVP - MPIP \leq \Delta P_{NS}$, where ΔP_{NS} is the low No Suction threshold on ΔP). In addition, during NS the pump flow signal has a periodic characteristic with a large sinusoidal component [19] shown in Figure 4.3(d) and Figure 4.4(d).

The Approaching Suction (AS) state is shown in time window B. As the pump speed increases, MPIP decreases much faster than MLVP causing ΔP to increase (i.e., $\Delta P_{NS} < \Delta P \leq \Delta P_S$, where ΔP_S the high Suction threshold on ΔP). In this state, the pump flow signal becomes less pulsatile than in the NS state. Furthermore, an optimal PS could be found during AS case since the flow drawn by the pump tends to match the flow coming back to the heart (venous return).

The third state shown in time window C is the Suction (S) state. In this state, the inlet cannula is evidently obstructed, MPIP exhibits very large negative spikes and MLVP is slightly less than zero (i.e., $\Delta P > \Delta P_S$). Furthermore, the pump flow signal loses the periodic with a large sinusoidal component characteristic that it had during NS and instead, exhibits a sudden large drop in the slope of the envelope of the minimum pump flow signal [19] shown in Figure 4.3(e) and Figure 4.4(e). The suction state is quite dangerous in that if it continues for some time, the patient may experience extreme discomfort and in some cases may die due to damage in the cardiac tissue, ventricular collapse, or ventricular arrhythmia.

4.4 The Window Length Issue

In order to effectively extract suction indices, the window length (i.e., the time period over which the indices are calculated) should be considered. Most existing suction detection approaches reported in the literature extract features using different-size windows that vary from 2 to 6 seconds [10]-[12], [32], and [33]. Currently, there does not exist a “perfect” method or technology for choosing the length of this window. In general, a shorter window length allows for faster data processing but the resulting features may not be accurate. On the other hand, a longer window will provide more accurate features but may not be appropriate for real-time processing. Therefore a tradeoff must be considered among several options that include a requirement for the classifier to be both highly accurate and responsive and to have sufficient

samples available to estimate the indices and minimize the delay that is inherent in such systems since it is necessary to buffer the pump flow before extracting the features. In the final analysis, we used a 5-second window as a compromise which is determined to be the most appropriate time window for our study.

In the following three subsections, the time, frequency, and time-frequency indices derived from the pump flow signal are described. SI_1 , SI_2 , and SI_3 are based on time domain, SI_4 and SI_5 are based on frequency domain, and SI_6 is based on time-frequency domain, respectively.

4.5 Time Domain Based Suction Indices

Our LSVM was designed to work with six Suction Indices, SI_i , $i=1, 2, \dots, 6$ covering the characteristics of the pump flow signal in three different domains: time, frequency, and time-frequency. While in general it is not known a priori which of these domains will provide the most discriminating power among the three states of NS, AS and S, the LSVM classifier will have the advantage of relying on all three domains simultaneously by using these six indices.

The time index SI_1 is defined based on the mean, minimum, and maximum values of the pump flow [32] according to the expression:

$$SI_1 = \frac{2mean(PF) - (\max(PF) + \min(PF))}{\max(PF) - \min(PF)} \quad (4.1)$$

When suction is absent, the mean pump flow value is approximately half of the sum of the maximum and minimum values of PF, which shifts slightly towards minimum PF while approaching suction. When suction occurs, the mean pump flow value is close to the maximum pump flow value. Hence, SI_1 increases dramatically.

Time indices SI_2 and SI_3 are calculated with respect to the derivative of the pump flow signal as follows:

$$SI_2 = \frac{\max\left[\frac{d(PF)}{dt}\right]}{\max(PF) - \min(PF)} \quad (4.2)$$

$$SI_3 = \frac{\min\left[\frac{d(PF)}{dt}\right]}{\max(PF) - \min(PF)} \quad (4.3)$$

where $\max\left[\frac{d(PF)}{dt}\right]$ is the maximum derivative of PF and $\min\left[\frac{d(PF)}{dt}\right]$ is the minimum derivative of PF, respectively. SI_2 increases obviously during suction, whereas SI_3 decreases at the beginning of suction.

4.6 Frequency Domain Based Suction Indices

The frequency domain indices can detect the changes in the harmonic and subharmonic energy content of the pump flow. Let $Q_p(\omega)$ as the Fourier transform of the pump flow signal and ω_0 as the fundamental frequency. Also, let $\omega_1 = \omega_0 - \omega_c$ and $\omega_2 = \omega_0 + \omega_c$, where $2\omega_c$ is a threshold (in radians/sec) that defines an interval centered at ω_0 . In this study, $\omega_0 = 1.0$ Hz and $\omega_c = 0.5$ Hz.

The harmonic index SI_4 is defined as the ratio of the signal's total energy in the fundamental component frequency band to the total energy in the harmonic component frequency band [33], given by the following expression

$$SI_4 = \frac{\int_{\omega_1}^{\omega_2} |Q_P(\omega)| d\omega}{\int_{\omega_2}^{\infty} |Q_P(\omega)| d\omega} \quad (4.4)$$

Another frequency index SI_5 is defined [33] as the ratio of the subharmonic energy to the fundamental energy as follows:

$$SI_5 = \frac{\int_0^{\omega_1} |Q_P(\omega)| d\omega}{\int_{\omega_1}^{\omega_2} |Q_P(\omega)| d\omega} \quad (4.5)$$

When approaching suction, SI_4 starts to decrease and SI_5 starts to increase. In the case of suction event, SI_4 decreases and SI_5 increases abruptly due to the shift of energy from the fundamental band to both harmonic and subharmonic bands, indicating the occurrence of suction.

4.7 Time-Frequency Domain Based Suction Index

This method is used to supplement the frequency-domain approach. The index SI_6 is defined [33] as the standard deviation of instantaneous mean frequency of PF, expressed as

$$SI_6 = \sqrt{\text{var}(\langle \omega \rangle_t^{SP})} \quad (4.6)$$

In Equation (4.6), the instantaneous frequency is defined as the average frequency at a given

time [34] such that

$$\langle \omega \rangle_t^{SP} = \frac{\int \omega P_{SP}(\omega, t) d\omega}{\int P_{SP}(\omega, t) d\omega} \quad (4.7)$$

where $P_{SP}(\omega, t)$ is the squared magnitude of the Short-Time Fourier Transform (STFT) defined as follows:

$$P_{sp}(\omega, t) = \left| \int q_p(\tau) f^*(\tau - t) e^{-j\omega\tau} d\tau \right|^2 \quad (4.8)$$

In Equation (4.8), $f(t)$ can be considered as a window that chooses a local section of the signal $q_p(t)$ for Fourier analysis. Two extreme cases can occur, depending on the selection of the window. If $f(t)$ is a very long window, a high resolution spectrogram can be obtained, but time resolution is reduced. On the contrary, if $f(t)$ is a very short window, Equation (4.8) gives a low resolution spectrogram [31].

As previously discussed, we assume that under desired circumstances PF is approximately periodic and its fundamental frequency ω_0 is the patient's cardiac frequency. If the window $f(t)$ is selected such that the spectrogram of pump flow presents "good" resolution in frequency, we expect to see a line parallel to the time axis in the "time \times frequency" plane [31]. In other words, the spectrogram of the pump flow is similar to that of a pure tone signal. This implies that the average frequency at a given time $\langle \omega \rangle_t^{SP} \approx \omega_0$ [31].

The value of SI_6 is small without suction and increases slightly when suction is approaching, and it increases abruptly during a suction event.

The six indices described above are the final inputs to the LSVM classifier, which will be discussed in the next chapter.

CHAPTER 5: SUCTION DETECTION FOR THE ROTARY LVADS

The purpose of the decision system (i.e., consists of classifier training and classification modules in Figure 4.2) is to combine the six features described in the previous section in order to classify the pump states. Therefore, a learning system required. Several methods in statistical pattern recognition have been proposed to design learning systems, such as Discriminant Analysis, Neural Networks and, more recently, Support Vector Machines (SVM). Among these, Support Vector Machines are the most widely used algorithms for the advantages of its classification performance over other pattern recognition algorithms. Furthermore, there is a modified SVM, called LSVM, whose performances are better than the standard SVM. These reasons motivated us to use LSVM to design a classifier for the suction detection.

5.1 Support Vector Machine

The Support Vector Machine algorithm was first proposed by Vapnik [35] in 1998, as a reliable and powerful classification technology that has been successfully applied to various pattern recognition problems [36]-[39]. Figure 5.1 shows the main idea of the standard SVM for a two-dimension, two-class linearly separable pattern. The squares and circles represent two different classes. H is the classification line that correctly classifies the two-class samples. H_1 and H_2 are two lines, which pass the samples of every class that are closest to H . Furthermore, both H_1 and H_2 are parallel to H . Therefore, the distance between H_1 and H_2 is the classification

margin. The optimal classification line is required such that it cannot only correctly classify the samples, but maximize the margin. Extending to the high dimension space, the optimal classification line becomes the optimal hyperplane.

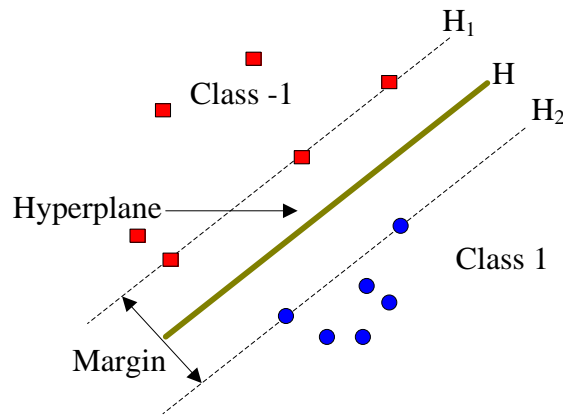


Figure 5.1 The Structure of a Simple SVM

Consider a training set (x_i, y_i) , $i = 1, \dots, n$, where $x_i \in \mathbb{R}^n$ and $y_i \in \{+1, -1\}$, where +1 and -1 represent the classification identification of the two classes. Assume that the equation of classification face is as follows:

$$\omega \cdot x + b = 0 \quad (5.1)$$

where ω and b are the weight vector and constant bias, respectively. To correctly classify all the samples, there exists the following expression such that:

$$y_i(x_i \cdot \omega + b) - 1 \geq 0 \Leftrightarrow \begin{cases} x_i \cdot \omega + b \geq +1 & \text{for } y_i = +1 \\ x_i \cdot \omega + b \leq -1 & \text{for } y_i = -1 \end{cases} \quad (5.2)$$

Thus, the classification margin can be calculated as follows:

$$\min_{(x_i|y_i=1)} \frac{\omega \cdot x_i + b}{\|\omega\|} - \max_{(x_i|y_i=-1)} \frac{\omega \cdot x_i + b}{\|\omega\|} = \frac{2}{\|\omega\|} \quad (5.3)$$

Now the question is to maximize the margin, which means to minimize its reciprocal, hence Equation (5.3) can be considered as a quadratic programming problem such that:

$$\Phi(\omega) = \frac{1}{2} \|\omega\|^2$$

Subject to
$$y_i(x_i \cdot \omega + b) \geq 1, \quad i = 1, 2, \dots, n \quad (5.4)$$

In order to solve the above quadratic programming problem, we can use Lagrange multiplier method as follows:

$$L = \frac{1}{2} \|\omega\|^2 - \sum_{i=1}^n \alpha_i y_i (x_i \cdot \omega + b) + \sum_{i=1}^n \alpha_i \quad (5.5)$$

where $\alpha_i > 0$ the Lagrange parameter. Now the question is to minimize L with respect to ω and b. By calculating partial differential with respect to ω and b and let the results be 0, the problem in Equation (5.4) is transformed to a simple dual problem: maximize L with the constraints such that the gradients of L with respect to both ω and b would be 0, and the Lagrange parameter α_i is non-negative, which means under the following constraints:

$$\sum_{i=1}^n y_i \alpha_i = 0 \quad (5.6)$$

$$\alpha_i \geq 0, \quad i = 1, 2, \dots, n \quad (5.7)$$

Maximize the following function with respect to α such that

$$J(\alpha) = \sum_{i=1}^n \alpha_i - \frac{1}{2} \sum_{i,j=1}^n \alpha_i \alpha_j y_i y_j (x_i \cdot x_j) \quad (5.8)$$

If α_i^* is the optimal solution then

$$\omega^* = \sum_{i=1}^n \alpha_i^* y_i x_i \quad (5.9)$$

That means the weight vector ω of the optimal hyperplane is a linear combination of the sample vector.

The problem above is the quadratic programming with inequality constraints. According to the optimality condition—Karush-Kuhn-Tucher (KKT) condition, the solution of the quadratic programming problem can satisfy the following condition:

$$\alpha_i \{[(x_i \cdot \omega) + b]y_i - 1\} = 0, \quad i = 1, 2, \dots, n \quad (5.10)$$

Therefore, for many samples, α_i is 0, and the non-zero α_i corresponds to the special samples that make the equality hold in Equation (5.2). They are called support vectors. In addition, b^* can be calculated from any support vector using Equation (5.2) such that:

$$b^* = \frac{1}{y_s} - \omega^* \cdot x_s \quad (5.11)$$

where x_s is a support vector.

Finally the optimal classification decision function is as follows:

$$f(x) = \text{sgn}\{\sum_{i=1}^n y_i \alpha_i^* (x_i \cdot x) + b^*\} \quad (5.12)$$

When the samples are linearly separable, the decision function can be obtained using Equation (5.12). However, if the data are linearly inseparable, the constraint in Equation (5.2) cannot be satisfied. Thus, a non-negative slack variable will be added in Equation (5.2) in order to widen the constraint condition such that:

$$y_i[(\omega \cdot x_i) + b] \geq 1 - \varepsilon_i, \quad i = 1, 2, \dots, n \quad (5.13)$$

When the classification error occurs, $\varepsilon_i > 0$, therefore, $\sum_i \varepsilon_i$ is the upper bound of the number of incorrectly classified samples in the dataset. Then it is necessary to add an extra cost term in the objective function (5.4) such that:

$$\Phi(\omega, \varepsilon) = \frac{1}{2}(\omega \cdot \omega) + C(\sum_{i=1}^n \varepsilon_i) \quad (5.14)$$

where the positive C is a constant cost parameter that controls the tradeoffs between the margin and error penalty. Now, the problem is to find the minimum in Equation (5.14) with the constraint in Equation (5.13). By balancing the maximum margin and the least number of the incorrectly classified samples, the optimal hyperplane with linearly inseparable samples can be

obtained. Note that the difference between linear separable and linear inseparable cases is that Equation (5.7) is the constraint for the linear separable case, which is considered as $0 \leq \alpha_i \leq C$ for the linear inseparable case.

The previous discussions are under the assumption that the data samples are linear. However, in real time, in most cases the data samples are nonlinear. To correctly identify the nonlinear samples, the input vectors can be mapped into a high-dimension eigenvector space, where the optimal hyperplane can be made. That is the SVM-based algorithm for the nonlinear data. Furthermore, with the appropriate mapping function, most linear inseparable samples in the input space can be solved by transforming them to linear separable samples.

However, while mapping data from the low-dimension input space to the high-dimension feature space, in most cases it is impossible to obtain the optimal hyperplane in the high-dimension feature space due to the rapid increase of the space dimension. SVM can solve this problem in the input space by defining Kernel Function [40], the theory is as follows:

Since the previous discussions in this section only involve inner product, therefore, assume that there exists a nonlinear mapping $\Psi: R^n \rightarrow H$ that maps samples from the input space to high dimension feature space H , the optimal hyperplane can be established in the feature space by only using dot product (i.e., $\Psi(x_i) \cdot \Psi(x_j)$). Therefore, if there exists a function K to satisfy the

condition such that $K(x_i, x_j) = \Psi(x_i) \cdot \Psi(x_j)$, then in the high dimension space only dot-product operation is required.

According to functional theory, if a certain function K satisfies Mercer condition [41], it can correspond to dot-product in a certain transformed space; hence the linear classification after a certain nonlinear transform can be implemented using the dot-product function $K(x_i, x_j)$ that satisfies Mercer condition in the optimal hyperplane, and the computational complexity is not increased. Therefore, the final decision function is summarized as follows:

$$f(x) = \text{sgn}(\sum_{i=1}^n y_i \alpha_i^* K(x_i, x) + b^*) \quad (5.15)$$

where $K(x_i, x_j)$ is the kernel function [40]. Several popular models of kernel include linear, polynomial, and radial basis function, etc. In this study, a linear kernel is selected since using other kernels didn't result in any improvement in performance of the suction detection issue for our study.

Figure 5.2 shows a schematic diagram of SVM. The decision function of SVM is formally similar to a Neural Networks. The output is the linear combination of several interlayer nodes, and every interlayer node corresponds to an inner product of an input sample and a support vector. Therefore, SVM is also called support vector network.

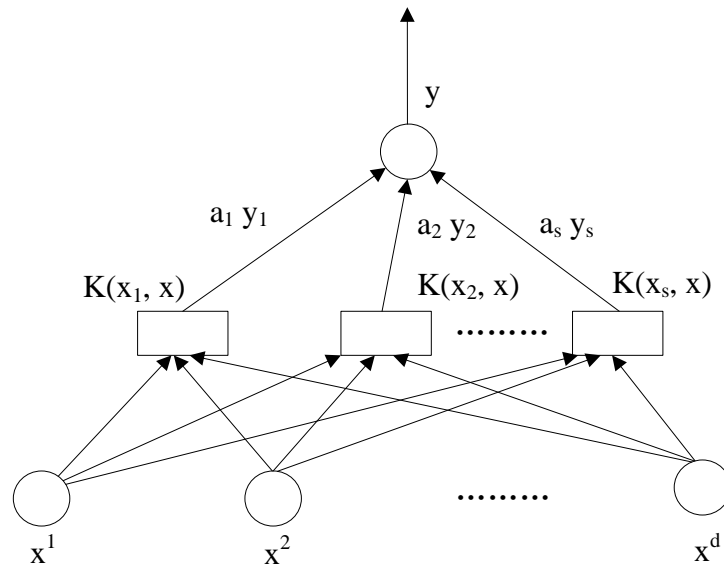


Figure 5.2 The Schematic Diagram of SVM

Although SVM-based algorithm has been proven to be effective in many practical applications, it still has some disadvantages in computation such as slow learning speed (training time), complex computation, and great arithmetic demand, etc. To solve these limitations, a Lagrangian Support Vector Machine could be adopted.

5.2 Lagrangian Support Vector Machine

The Lagrangian Support Vector Machine (LSVM) was first proposed by Mangasarian et al. [42] in 2001, as a modified SVM. Compared to the standard SVM and many of other existing pattern recognition approaches, the LSVM is a very fast and simple algorithm, based on an implicit Lagrangian formulation of the dual of a simple reformulation of the standard quadratic problem

of SVM [43]. In general, the LSVM requires inversion of a single matrix whose much smaller dimensions are of the order of the original input space plus only one.

Consider an $m \times n$ matrix A representing m data points in the n -dimensional real space and an $m \times m$ diagonal matrix D with plus ones or minus ones along its diagonal, also assume that e is an $m \times 1$ vector of ones and I is an $m \times m$ identity matrix, and then two matrices are defined as follows:

$$H = D[A \quad -e], \quad Q = \frac{I}{\gamma} + HH' \quad (5.16)$$

where Q is a symmetric positive definite matrix and γ equals to C in Equation (5.14). With these definitions in Equation (5.16), the corresponding dual problem becomes

$$\min_{0 \leq u \in R^m} f(u) = \frac{1}{2} u' Q u - e' u \quad (5.17)$$

where u equals to α in the equations in Section 5.1. Same as SVM, the LSVM algorithm is also based on KKT necessary and sufficient optimality conditions for the dual problem such that:

$$0 \leq u \perp (Qu - e) \geq 0 \quad (5.18)$$

With the simply established identity between any two real numbers (or vectors) p and q , we can obtain the following expression:

$$0 \leq p \perp q \geq 0 \Leftrightarrow p = (p - \tau q)_+, \tau > 0 \quad (5.19)$$

Hence Equation (5.18) can be rewritten as followed with any positive τ

$$Qu - e = ((Qu - e) - \tau u)_+ \quad (5.20)$$

The iterative scheme that forms the LSVM algorithm is as follows:

$$u^{i+1} = Q^{-1} \left\{ e + [(Qu^i - e) - \tau u^i]_+ \right\}, \quad i = 0, 1, \dots, \quad (5.21)$$

The global linear convergence from any starting point could be established under the following condition such that

$$0 < \tau < \frac{2}{\gamma} \quad (5.22)$$

where τ is set as $1.9/\gamma$ in all the experiments. In addition, the optimality condition (5.20) is also the necessary and sufficient condition for the unconstrained minimum of the implicit Lagrangian associated with the dual problem (5.17) such that:

$$\min_{u \in R^m} L(u, \tau) = \min_{u \in R^m} f(u) + \frac{1}{2\tau} (\|(-\tau u + Qu - e)_+\|^2 - \|Qu - e\|^2) \quad (5.23)$$

Setting the gradient with respect to u of Equation (5.23) to zero gives

$$(\tau I - Q) \left[(Qu - e) - ((Q - \tau I)u - e)_+ \right] = 0 \quad (5.24)$$

where Equation (5.24) is equivalent to the Equation (5.20) under the assumption that τ is positive and not an eigenvalue of Q . Mangasarian et al. established the LSVM algorithm and its global linear convergence of the iteration (5.21) under condition (5.22) such that starting with an arbitrary $u^0 \in \mathbb{R}^m$, the optimal solution \bar{u} will converge at the following linear rate [42]

$$\|Qu^{i+1} - Q\bar{u}\| \leq \|I - \tau Q^{-1}\| \cdot \|Qu^i - Q\bar{u}\| \quad (5.25)$$

Details on the LSVM algorithm and the proof of Equation (5.25) can be found in [42].

Similar to the original SVM algorithm, although both the SVM and LSVM algorithms are originally designed as binary classifiers, classification into additional classes is possible. In this work, a decision tree method is adopted for the multiclass problem. In general, at the top of the decision tree, the hyperplane is made to separate one or some classes from the remaining classes in the feature space. If plural classes are in the separated subspace, at the node connected to the top node, we determine the hyperplane that separates the classes. This procedure is repeated until there is only one-class data in the separated regions. This method only needs to construct $k-1$ (k is the total number of classes) classifiers. Therefore, in this work, a 2-step LSVM decision tree method is adopted for the 3-state case. First, we separate the S state from the NS and AS states and then the NS and AS states are classified by another LSVM.

5.3 Classification Performance Evaluation Criteria

In order to evaluate the performance of our suction detection algorithm, we will use seven criteria. Three of these criteria relate to the sensitivity, specificity, and accuracy of the algorithm [44]. The expressions for these criteria are given as follows:

$$\text{sensitivity}(ST) = \frac{TP}{TP+FN} \times 100\% \quad (5.26)$$

$$\text{specificity}(SF) = \frac{TN}{TN+FP} \times 100\% \quad (5.27)$$

$$\text{accuracy}(AC) = \frac{TP+TN}{TP+TN+FP+FN} \times 100\% \quad (5.28)$$

where the definitions of TP, TN, FP, FN, and AC are as follows:

True Positive rate (TP): the proportion of positive cases that were correctly classified.

True Negative rate (TN): the proportion of correctly identified negative cases.

False Positive rate (FP): the proportion of negative cases that were incorrectly identified as positive.

False Negative rate (FN): the proportion of positive cases that were incorrectly classified as negative.

Accuracy (AC): the proportion of the total number of predictions that were correctly identified.

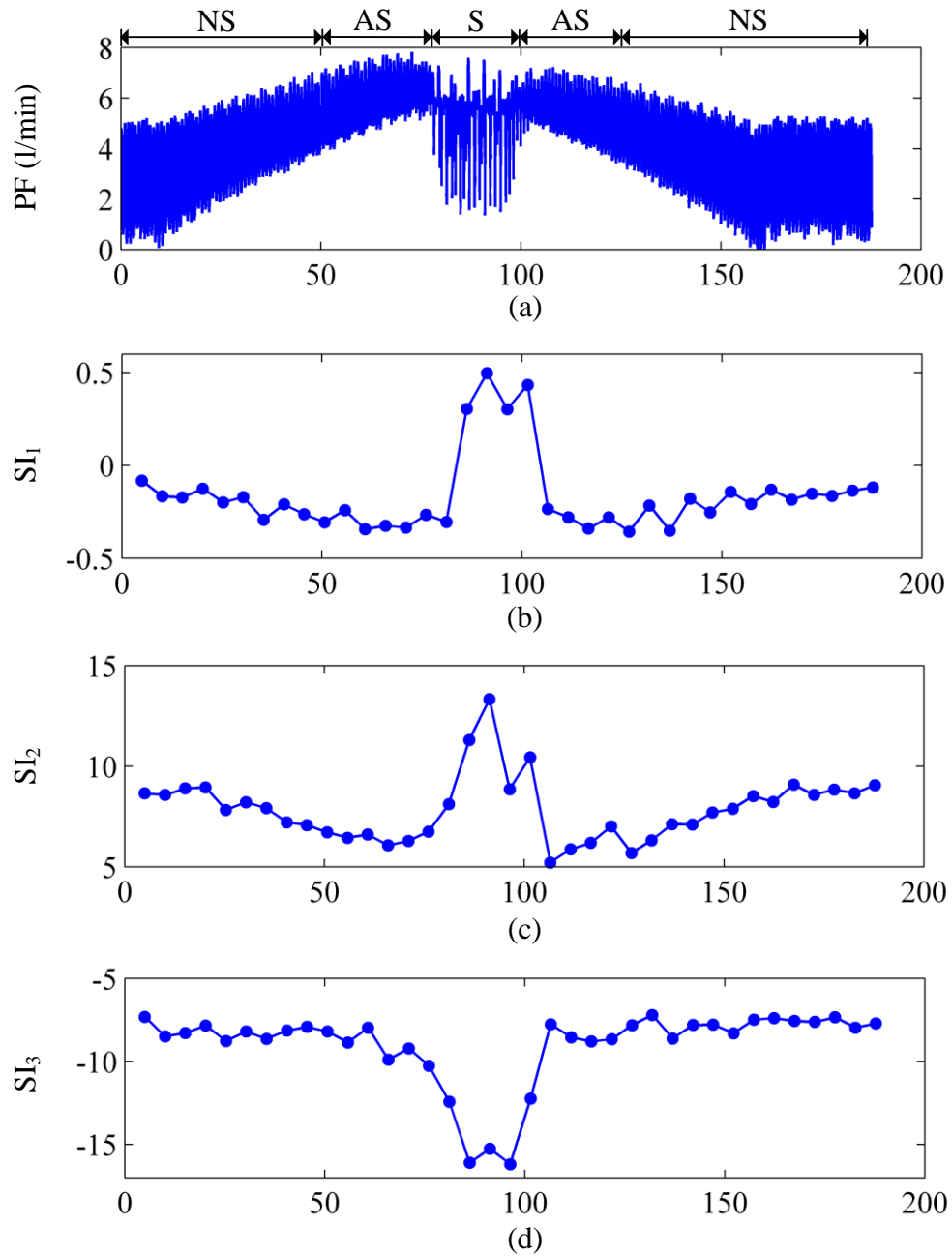
The fourth and fifth criteria relate to the training and test times of the algorithm. The last two criteria are the Receiver Operating Characteristic (ROC) curve and the Area under ROC Curve (AUC). The ROC curve is a technique for visualizing, analyzing, and choosing classifiers based on their performance. ROC curves have been extensively applied in medical decision making, radiology, and other areas for several decades, and more recently they have been used in machine learning and data mining. The ROC curve is a two-dimensional graphical plot of a binary classifier system in which sensitivity is plotted on the y-axis and 1-specificity is plotted on the x-axis. The ROC describes the relative tradeoffs between benefits (sensitivity) and costs (1-specificity) [45]. Once ROC is determined, the AUC, which is an index of the quantitative measure of the overall performance of the classifiers, can be easily calculated [45].

5.4 In Vivo Data Analysis

This section describes how experimental data were used for the proposed suction detection system. These data were analyzed off-line.

Figure 5.3(a) shows an example of the pump flow signal from the MedQuest pump experiment. The six suction indices derived from this signal are calculated and plotted on the same figure.

The changes in these indices as the pump flow signal transitions from NS to AS and from AS to S are clearly evident in Figure 5.3(b)-(g).



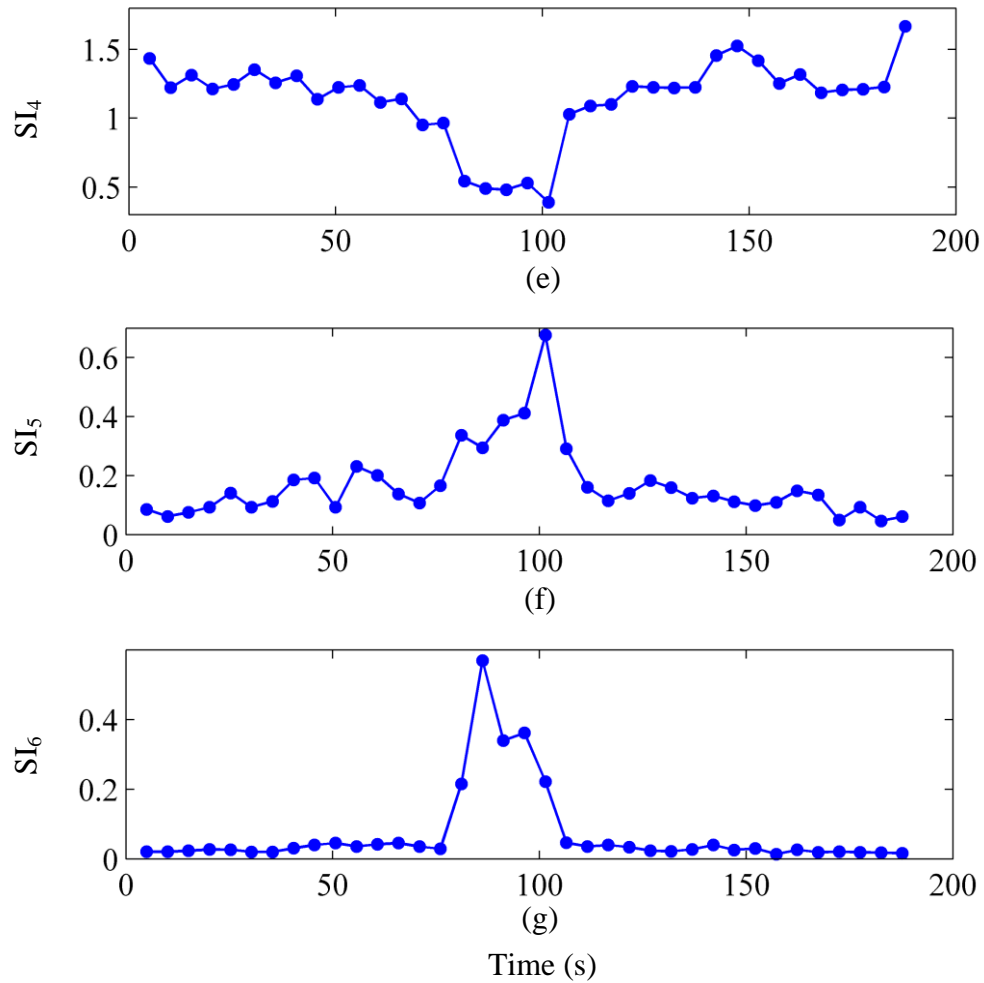


Figure 5.3 Suction Indices Extracted from PF Based on MedQuest pump. (a) PF. (b) SI_1 . (c) SI_2 . (d) SI_3 . (e) SI_4 . (f) SI_5 . (g) SI_6

A total of 11 in-vivo data files were recorded for the MedQuest pump, and a total of 23 in vivo data files were adopted for the Nimbus pump, respectively. The data were previously classified by three human experts into three states, (i.e., NS, AS, and S) according to the three pump states previously defined. This classification procedure was based on the analysis of PF, PS, LVP, and

PIP, resulting in a total number of 1527 samples of the pump flow signal for the MedQuest pump and a total number of 1432 samples for the Nimbus pump in a data base. Table 5.1 and Table 5.2 show the data statistics, including Mean Values (Mean) and Standard Deviations (SD) of each feature variable for each type of indices for the two pumps. For the MedQuest pump, nearly half of the samples, 759 (49.7%), belongs to NS, whereas AS and S present 646 (42.3%) and 122 (8.0%), respectively, of the data. For the Nimbus pump, the number of the samples for NS, AS, and S is 784 (54.75%), 310 (21.65%), and 338 (23.6%), respectively.

Table 5.1 In-Vivo Data Statistics for the MedQuest Pump

Samples	NS		AS		S	
	759 (49.7%)		646 (42.3%)		122 (8.0%)	
Feature	Mean	SD	Mean	SD	Mean	SD
SI ₁	-0.16	0.07	-0.26	0.13	0.46	0.17
SI ₂	7.95	1.05	6.25	1.31	10.40	2.11
SI ₃	-7.76	0.52	-9.03	3.37	-14.44	3.83
SI ₄	1.47	0.25	1.01	0.23	0.42	0.14
SI ₅	0.09	0.05	0.22	0.24	0.77	0.56
SI ₆	0.03	0.03	0.08	0.08	0.36	0.14

Table 5.2 In-Vivo Data Statistics for the Nimbus Pump

Samples	NS		AS		S	
	784 (54.75%)		310 (21.65%)		338 (23.6%)	
Feature	Mean	SD	Mean	SD	Mean	SD
SI ₁	-0.03	0.08	-0.08	0.12	0.25	0.10
SI ₂	9.73	1.48	8.55	1.33	9.46	1.58
SI ₃	-7.97	0.81	-8.40	0.98	-11.37	2.04
SI ₄	2.12	0.44	1.44	0.52	0.56	0.27
SI ₅	0.08	0.05	0.19	0.25	1.77	1.94
SI ₆	0.02	0.02	0.05	0.05	0.17	0.11

Table 5.1 and Table 5.2 also show that the difference among the three pump states is numerically significant, except for SI₂ of the Nimbus pump. Also note that, due to the similarities from a physiologic stand point between NS and AS, the mean values of all six indices between NS and AS for both pumps are reasonably close (as expected) and are closest in the cases of SI₅ and SI₆, which also can be illustrated by using box-plots in Figure 5.4.

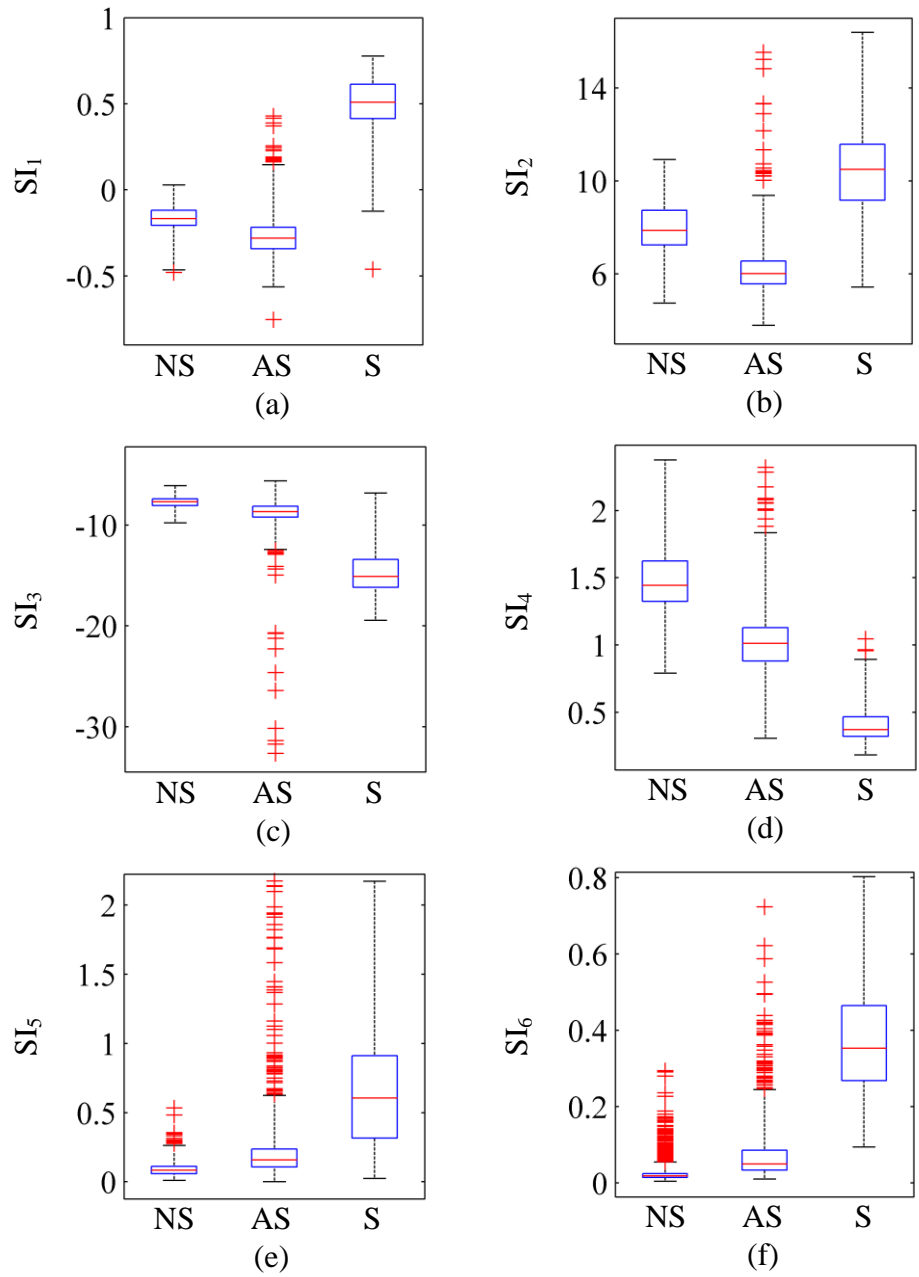


Figure 5.4 Box Plots of the Features per Pump State for MedQuest Pump. (a) SI_1 . (b) SI_2 . (c) SI_3 . (d) SI_4 . (e) SI_5 . (f) SI_6

The box-plots shown in Figure 5.4 illustrate the distribution of the six indices for the three pump

states, for the MedQuest pump data (similar plots can also be obtained for the Nimbus pump data). Note that the median values (the red lines in each box) are different across the three states (meaning that each state has distinct distributions compared to the other states) and are almost identical to the mean values in Table 5.1, for each feature. Also note that the separation between NS and AS is slightly difficult to distinguish for indices SI_5 and SI_6 as observed earlier.

Table 5.3 and Table 5.4 show the correlation among the six derived indices for both pumps. In our data base, none of the indices are very strongly correlated; the strongest correlation (0.69) is between SI_3 and SI_4 for the MedQuest pump and the strongest correlation (-0.71) is also between SI_3 and SI_4 for the Nimbus pump, respectively.

Table 5.3 Correlation Coefficients from Six Indices for MedQuest Pump

	SI_1	SI_2	SI_3	SI_4	SI_5	SI_6
SI_1	1					
SI_2	-0.54	1				
SI_3	-0.34	0.51	1			
SI_4	0.03	0.29	0.69	1		
SI_5	0.51	-0.36	-0.48	-0.28	1	
SI_6	-0.66	0.63	0.66	0.39	-0.66	1

Table 5.4 Correlation Coefficients from Six Indices for Nimbus Pump

	SI ₁	SI ₂	SI ₃	SI ₄	SI ₅	SI ₆
SI ₁	1					
SI ₂	-0.56	1				
SI ₃	-0.38	0.42	1			
SI ₄	0.53	-0.40	-0.71	1		
SI ₅	-0.63	0.40	0.47	-0.62	1	
SI ₆	0.26	0.03	0.21	-0.34	0.05	1

In this work, the LSVM classifier is trained on a randomly selected set of 50% of the in vivo data samples and then tested on the remaining 50% of the samples in the same data set for both the 2-state and 3-state classifications. Due to the random selection of samples, the classification is repeated 500 times. The two thresholds on ΔP used in the classifier, as mentioned in Section 4.3, are chosen as $\Delta P_{NS} = 10$ mmHg and $\Delta P_S = 35$ mmHg for the MedQuest pump and $\Delta P_{NS} = 25$ mmHg and $\Delta P_S = 50$ mmHg for the Nimbus pump, respectively due to the different nature of the two pumps. The mean values and standard deviations of all the results reported in this study (i.e., performance criteria ST, SF, AC, training and test times, ROC and AUC) are averaged over 500

runs. All experimental procedures are implemented using MATLAB implemented on a 2-GHz Intel Pentium Dual CPU desktop computer with 3 gigabytes of memory.

5.5 Two-State Classification Task for the MedQuest Pump

For the MedQuest pump 763 total samples (379 NS, 323 AS and 61 S) were available for classification. The 2-state (the AS samples are considered as NS) classification results of the LSVM algorithm over 500 runs on the test set are shown in Table 5.5. On average, only 6.35 of the 702 NS samples (i.e., 0.90%) are incorrectly classified as S and 3.02 of the 61 S samples (i.e., 4.95%) are incorrectly classified as NS.

Table 5.5 Classification Results of the LSVM Classifier on the Test Set for 2-State Problem Based on MedQuest Pump ^a

	NS	S	Total
NS	695.65	6.35	702
S	3.02	57.98	61

^a Actual classes are in rows, predicted in columns.

Table 5.6 shows the performance analysis of the LSVM classifier on the test set for the 2-state case. It indicates that a sensitivity of 99.10% is achieved with the related standard deviation of 0.35% in classifying NS cases, while for suction state the sensitivity and standard deviation are

95.05% and 2.71%, respectively. Therefore, the overall accuracy is 98.77% with the standard deviation of 0.29%. The training and test times are 0.008 s and 0.009 s, respectively.

Table 5.6 Performance Analysis of the LSVM Classifier on the Test Set for 2-State Problem Based on MedQuest Pump (Numbers Inside the Parenthesis is SD in %)

	NS	S
Sensitivity (%)	99.10 (0.35)	95.05 (2.71)
Specificity (%)	95.05 (2.71)	99.10 (0.35)
Accuracy (%)	98.77 (0.29)	98.77 (0.29)

5.6 Three-State Classification Task for the MedQuest Pump

For the 3-state case, the average correct classification results for each pump state together with the spread of the erroneous classifications into the other states are shown in Table 5.7. For NS, on average, there are 27.85 NS samples misclassified as AS (7.35%) and only 0.24 samples are wrongly classified as S (0.06%). For AS, 18.72 samples are misclassified as NS (5.79%) and only 6.16 samples are incorrectly classified as S (1.91%). Finally for S, the mean erroneous number of samples misclassified as NS and AS are as low as 0 (0%) and 3.05 (5%), respectively.

Furthermore, the detailed performance analysis of the LSVM algorithm over 500 runs on the test set is shown in Table 5.8. The proposed method can discriminate NS with sensitivity, specificity, accuracy of 92.59%, 95.13%, 93.87%, AS with 92.30%, 92.98%, 92.69%, and S with 95.00%, 99.09%, 98.76%, respectively. The training and test times are 0.031 s and 0.016 s, respectively.

Table 5.7 Classification Results of the LSVM Classifier on the Test Set for 3-State Problem Based on MedQuest Pump ^a

	NS	AS	S	Total
NS	350.91	27.85	0.24	379
AS	18.72	298.12	6.16	323
S	0	3.05	57.95	61

^a Actual classes are in rows, predicted in columns.

Table 5.8 Performance Analysis of the LSVM Classifier on the Test Set for 3-State Problem Based on MedQuest Pump (Numbers Inside the Parenthesis is SD in %)

	NS	AS	S
Sensitivity (%)	92.59 (1.13)	92.30 (1.45)	95.00 (2.76)
Specificity (%)	95.13 (1.12)	92.98 (1.04)	99.09 (0.34)
Accuracy (%)	93.87 (0.55)	92.69 (0.59)	98.76 (0.30)

5.7 Two-State Classification Task for the Nimbus Pump

For the Nimbus pump 716 total samples (392 NS, 155 AS and 169 S) were available for classification. Table 5.9 shows the 2-state (the AS samples are considered as NS) classification results of the proposed algorithm over 500 runs on the test set. On average, only 2.25 of the 547 NS samples are misclassified as S (0.41%) and 2.25 of 169 suction samples are incorrectly classified as NS (1.33%). In addition, Table 5.10 shows that for the NS case the sensitivity and the related SD is 99.59% and 0.29%, respectively. For the S case, a sensitivity of 98.67% is obtained and the corresponding standard deviation is 0.84%, giving an overall hit-rate of 99.37% with the standard deviation of 0.20%. Moreover, the training and test times are 0.007 s and 0.009 s, respectively.

Table 5.9 Classification Results of the LSVM Classifier on the Test Set for 2-State Problem Based on Nimbus Pump ^a

	NS	S	Total
NS	544.75	2.25	547
S	2.25	166.75	169

^a Actual classes are in rows, predicted in columns.

Table 5.10 Performance Analysis of the LSVM Classifier on the Test Set for 2-State Problem Based on Nimbus Pump (Numbers Inside the Parenthesis is SD in %)

	NS	S
Sensitivity (%)	99.59 (0.29)	98.67 (0.84)
Specificity (%)	98.67 (0.84)	99.59 (0.29)
Accuracy (%)	99.37 (0.20)	99.37 (0.20)

5.8 Three-State Classification Task for the Nimbus Pump

Correspondingly, for the 3-state classification, Table 5.11 shows the detailed classification results over 500 runs on the test set. For NS, on average, there are 19.78 NS samples incorrectly classified as AS (5.05%) and only 0.17 samples wrongly classified as S (0.04%). For AS 32.64 samples are incorrectly identified as NS (21.06%) and only 2.01 samples are misclassified as S (1.29%). For S, the mean erroneous number of samples incorrectly classified as NS and AS are as low as 0.31 (0.18%) and 2.04 (1.21%), respectively.

In addition, the performance analysis of the LSVM algorithm over 500 runs on the test set is shown in Table 5.12. From Table 5.12, we can conclude that NS has the sensitivity, specificity, accuracy of 94.91%, 89.83%, 92.61%. The related ST, SF, and AC are 77.65%, 96.11%, 92.11% for AS and 98.61%, 99.60%, 99.37% for S, respectively. The training and test times are 0.031 s

and 0.013 s, respectively. These results based on two different pumps demonstrate the effectiveness of the proposed pump status classification algorithm in discriminating three different pump states.

Table 5.11 Classification Results of the LSVM Classifier on the Test Set for 3-State Problem Based on Nimbus Pump ^a

	NS	AS	S	Total
NS	372.05	19.78	0.17	392
AS	32.64	120.35	2.01	155
S	0.31	2.04	166.65	169

^a Actual classes are in rows, predicted in columns.

Table 5.12 Performance Analysis of the LSVM Classifier on the Test Set for 3-State Problem Based on Nimbus Pump (Numbers Inside the Parenthesis is SD in %)

	NS	AS	S
Sensitivity (%)	94.91 (1.26)	77.65 (3.38)	98.61 (0.77)
Specificity (%)	89.83 (1.75)	96.11 (0.91)	99.60 (0.27)
Accuracy (%)	92.61 (0.75)	92.11 (0.76)	99.37 (0.20)

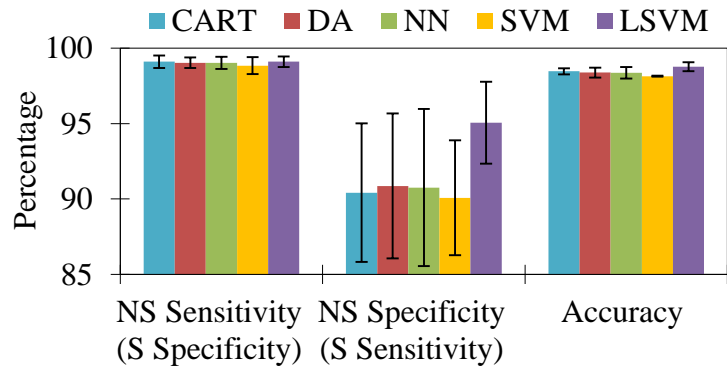
5.9 Comparison with Other Classifiers

As mentioned earlier, extensive studies for suction detection have been conducted by a number of research groups using different classification methods. Most efforts concentrate on signal processing and feature extraction of available pump signals such as PC, PS, or PF waveform. Therefore, considering most of earlier studies, the spread of classification accuracies obtained appears to be large. This is attributed to either the information content of the extracted features from the pump signals or the increasing complexity and effectiveness of computational technologies applied. However, it should be noticed that no quantitative, qualitative, or statistical comparisons among these suction detection methods have been made.

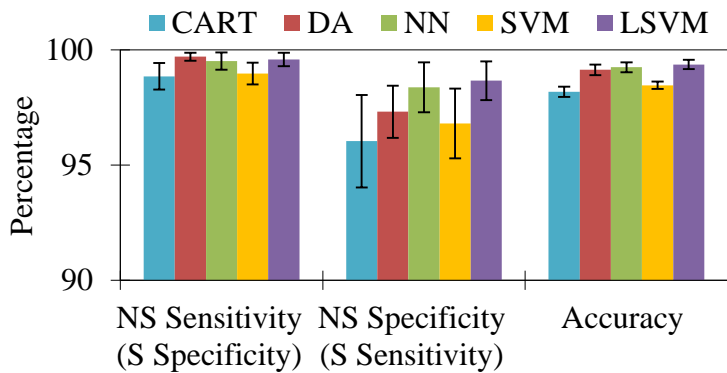
In this section, we will compare the performance of the LSVM classification algorithm with some recently existing suction detection algorithms: CART [10], DA [11], NN [12], and the original SVM-based algorithm for both 2-state and 3-state classification tasks based on the same two pumps. The classification procedures for CART, DA, NN, and SVM are also repeated 500 times with the same dataset and suction indices as used in the LSVM algorithm. The results of the comparison for both pumps are summarized in Figures 5.5 and 5.6, and Table 5.13 for the 2-state classification and in Figures 5.7, 5.8, 5.9, and Table 5.14 for the 3-state classification.

Figure 5.5 shows the means and standard deviations of the sensitivity, specificity and accuracy for all five classification methods for the 2-state classification. Generally, the LSVM algorithm

appears to outperform the other four approaches in terms of sensitivity, specificity and accuracy. Note also that because the standard deviations of these criteria are smallest in the LSVM algorithm, this may be interpreted that the LSVM algorithm is more stable than the other four. The only three exceptions are in the original SVM algorithm having the smallest standard deviation for accuracy for the MedQuest pump and the DA method having the highest NS sensitivity and the smallest standard deviation for NS sensitivity for the Nimbus pump.



(a) MedQuest pump



(b) Nimbus pump

Figure 5.5 Comparison of Classification Accuracy for 2-State Task (The Brackets Indicate the Standard Deviations)

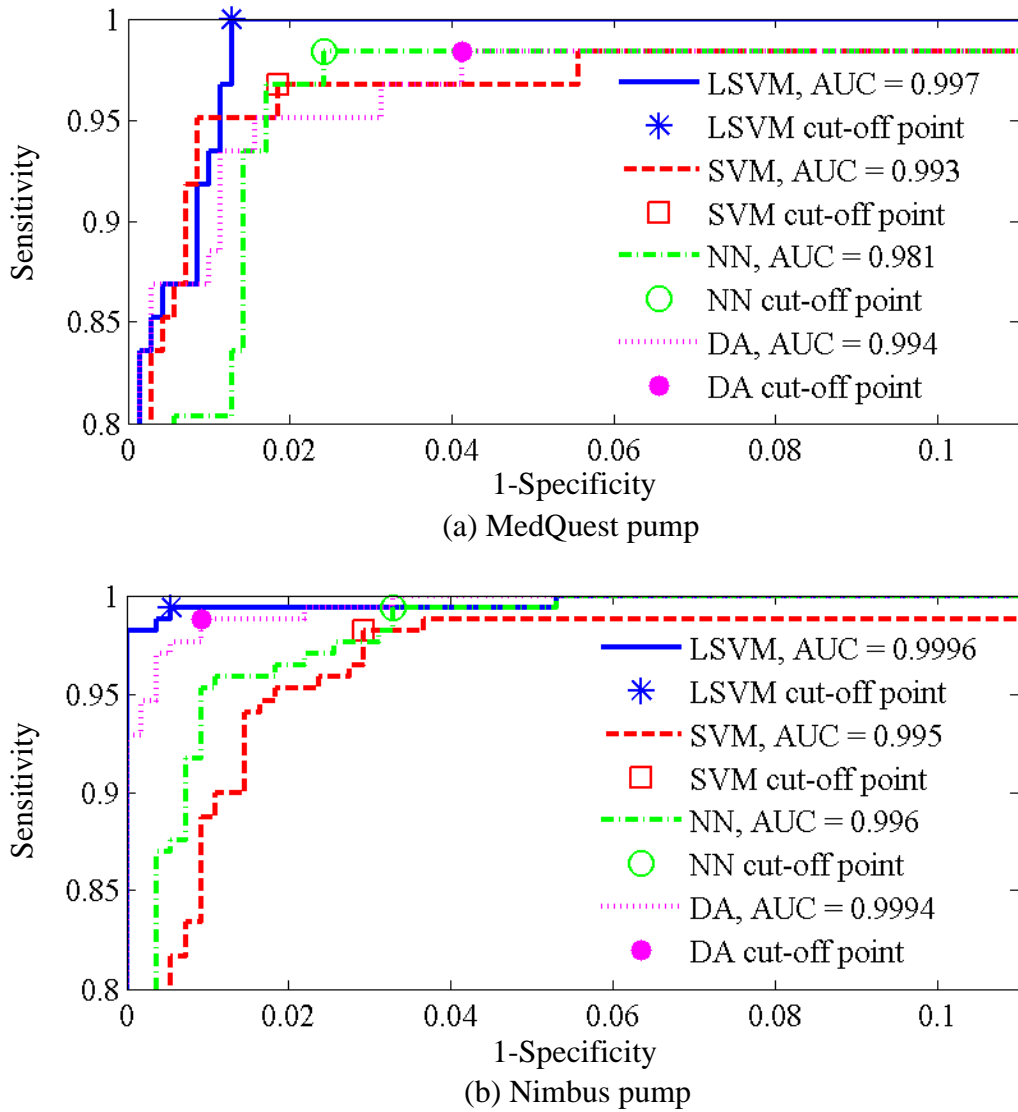


Figure 5.6 Comparison of ROC Curves for 2-State Problem

The related ROC curves and AUC values of the DA, NN, SVM, and LSVM algorithms for the two pumps for 2-state problem are shown in Figure 5.6 (the plots are zoomed to show only the regions of interest). Note that ROC curve is not made for the CART algorithm due to the discrete nature of this classifier. Based on these plots it is clear that the overall performance of the LSVM

algorithm is better than DA, NN, and SVM algorithms since the closer the ROC curve is to the upper left corner in the plot (i.e., the larger AUC) the higher the overall accuracy of the classifier. Comparisons of the training and test times for the five methods are shown in Table 5.13. The DA and LSVM algorithms appear to require the least training time compared to the remaining three.

Table 5.13 Comparison of Training/Test Time for 2-State Problem

	CART	DA	NN	SVM	LSVM
Training Time (s) ^a	0.016	0.009	1.413	4.080	0.008
Test Time (s) ^a	0.002	0.004	0.020	0.019	0.009
Training Time (s) ^b	0.019	0.008	1.419	5.913	0.007
Test Time (s) ^b	0.002	0.004	0.021	0.024	0.009

^aMedQuest Pump, ^bNimbus Pump.

Figure 5.7 and Figure 5.8 illustrate the means and standard deviations of the sensitivity, specificity and accuracy for all five classifiers for the 3-state classification. As can be seen, for both two pumps, the LSVM-based algorithm outperforms the other four classifiers in 5 out of 9 performance indices (sensitivity, specificity, and accuracy of three states, respectively). It also outperforms the other four classifiers in 4 out of 9 when it comes to stability of performance (i.e., smallest standard deviations). Note that for the Nimbus pump, the sensitivity of AS for all five

classifiers is lower than that of the other two states (NS and S). This may be due to the nature of the Nimbus pump design and the pump signal condition.

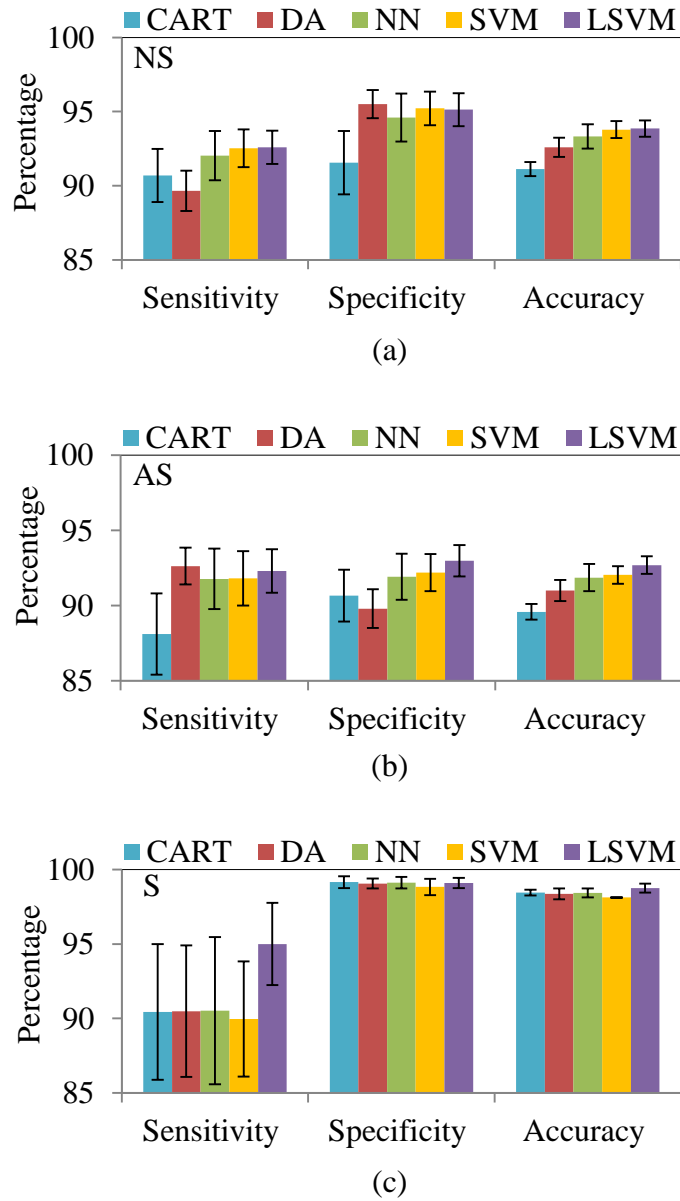
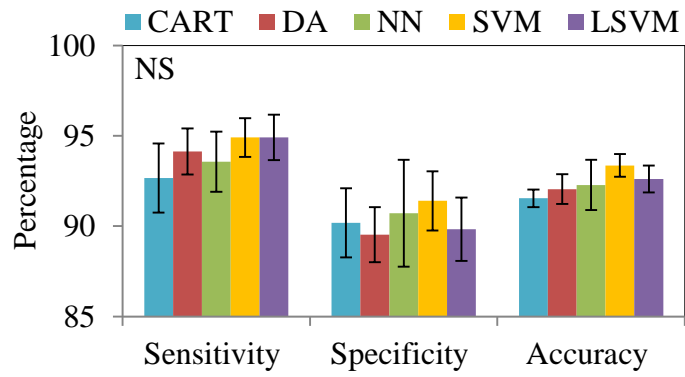
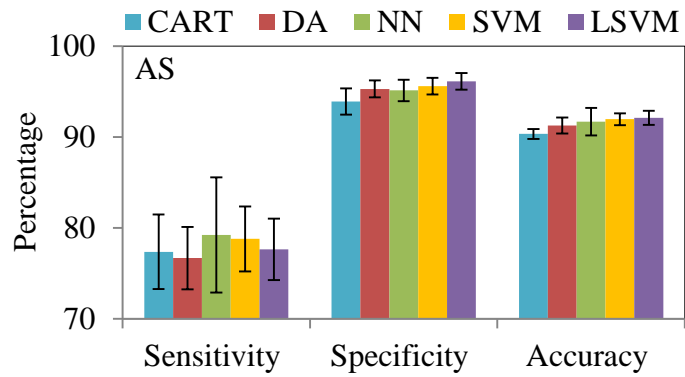


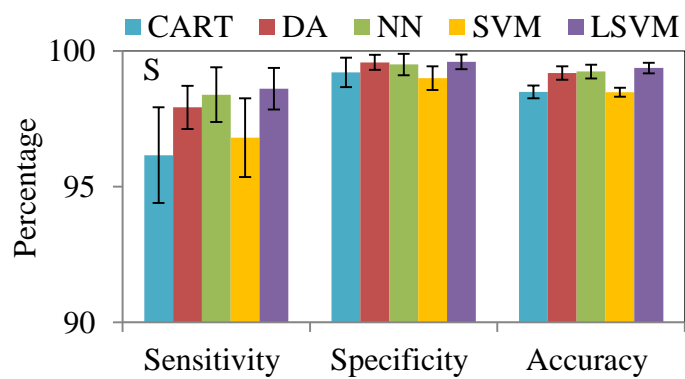
Figure 5.7 Comparison of Classification Accuracy for 3-State Problem for MedQuest Pump. (a) NS. (b) AS. (c) S. (The Brackets Indicate the Standard Deviations)



(a)

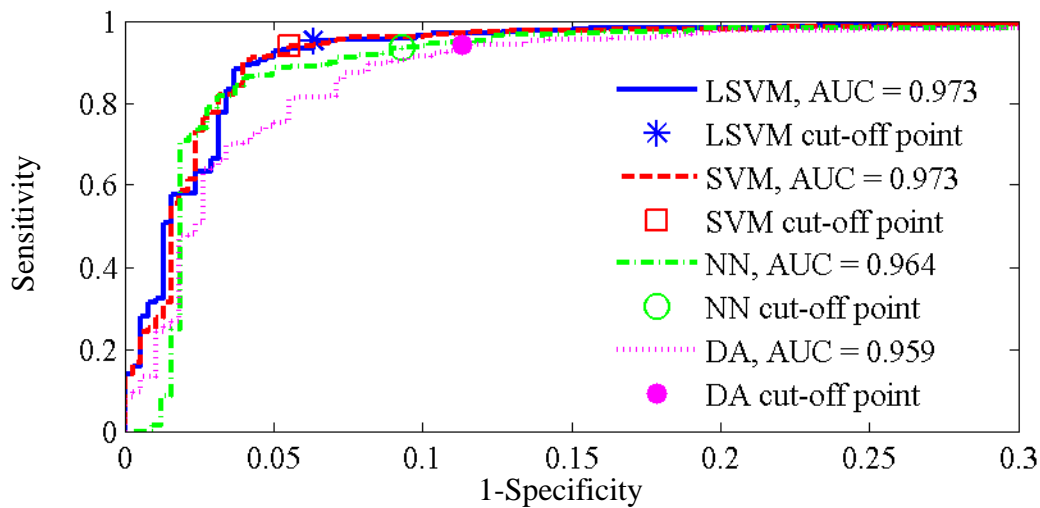


(b)

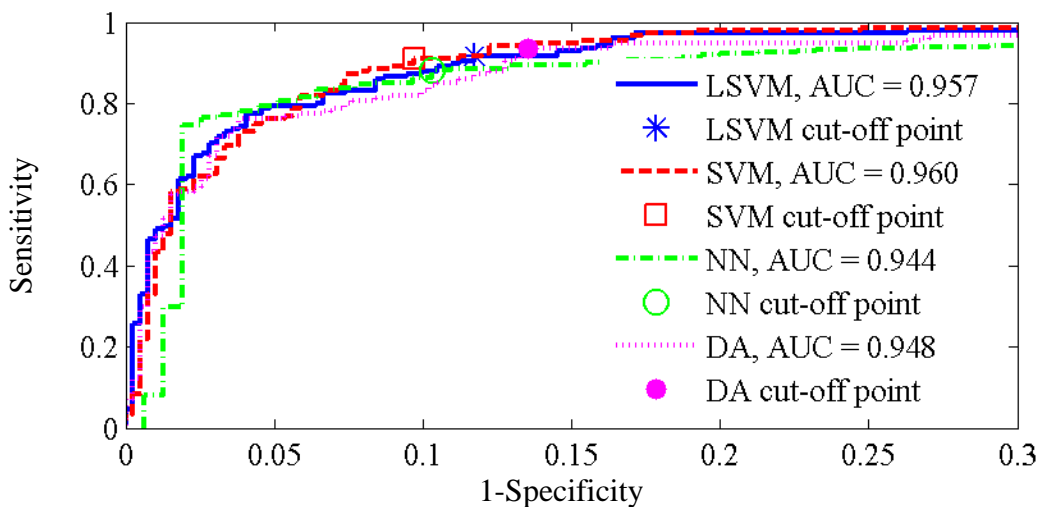


(c)

Figure 5.8 Comparison of Classification Accuracy for 3-State Problem for Nimbus Pump. (a) NS (b) AS (c) S (The Brackets Indicate the Standard Deviations)



(a) MedQuest pump



(b) Nimbus pump

Figure 5.9 Comparison of ROC Curves for 3-State Problem

The related ROC curves and AUC values of the DA, NN, SVM, and LSVM algorithms for the two pumps for 3-state problem are shown in Figure 5.9 (the plots are zoomed to show only the regions of interest). Note that since the ROC curve is a graphical plot for a binary classifier, it is implemented only for the NS and AS cases (the suction case has already been implemented in

Figure 5.6). As can be seen from Figure 5.9, for both pumps, the overall performance of NN and DA algorithms is obviously lower than that of SVM and LSVM algorithms, and the SVM algorithm performs slightly better than the LSVM algorithm. Furthermore, as can be seen in Table 5.14, the training time of the LSVM algorithm is longer than that of the DA algorithm but shorter than any other remaining algorithm for the two pumps.

Finally, we should note at this stage that the LSVM classifier appears to perform far better than the original SVM classifier for the 2-state classification and slightly better than SVM for the 3-state classification. From a clinical perspective, the more accurate the classification results are for suction detection, the more beneficial the method will be for the patients.

Table 5.14 Comparison of Training/Test Time for 3-State Problem

	CART	DA	NN	SVM	LSVM
Training Time (s) ^a	0.052	0.010	2.531	6.679	0.031
Test Time (s) ^a	0.002	0.004	0.027	0.047	0.016
Training Time (s) ^b	0.043	0.009	2.830	9.079	0.031
Test Time (s) ^b	0.002	0.004	0.023	0.047	0.013

^aMedQuest Pump, ^bNimbus Pump.

5.10 Robustness Analysis

Experimental validation on different pumps is the ultimate test for the robustness of such a detection system. In this research, the proposed method has been tested on two different pumps where in vivo data was available in an attempt to test its robustness. Figure 5.5, Figure 5.7, and Figure 5.8 show several performance indices for both 2-state and 3-state classifications for both pumps. Clearly despite differences between the two pumps, the LSVM-based algorithm demonstrates superior performance over all other algorithms. For the performance of all other algorithms, however, no significant conclusion can be drawn, which means generally the other four algorithms perform better for one pump but worse for the other, and generally all other four algorithms perform worse than the LSVM-based algorithm. Therefore, based on the above analysis, it is possible to conclude that the LSVM-based method shows not only best classification performance, but also best robustness for different blood pumps. This suggests that our suction detection method may be used in a clinical environment independent of the type or manufacturer of the rotary pump.

5.11 Statistical Significance Test

A statistical significance test regarding the significance of the classification results between the LSVM algorithm and the other four algorithms has been implemented based on the significance level of p-value [46]. According to Figure 5.5, Figure 5.7, and Figure 5.8 there are 24 correct classification performances yielding 96 paired significance tests for the LSVM algorithm against each of the remaining four. The p-values based on t-tests [46] for 2-state and 3-state

classification for both pumps are shown in Table 5.15-5.18. As can be seen, 80 out of the 96 tests are highly statistically significant (i.e., $p < 0.001$), 6 are very statistically significant (i.e., $0.001 \leq p < 0.01$), 3 are statistically significant (i.e., $0.01 \leq p < 0.05$), and only 7 are not statistically significant (i.e., $p \geq 0.05$).

Furthermore, as shown in Figure 5.5, Figure 5.7, and Figure 5.8, the LSVM algorithm occupied 14 out of 24 classifications as best correct classifications. Thus, the corresponding number of paired significance t-tests would be 56. The results of these tests also show that 53 out of 56 are highly statistically significant, 2 tests are statistically significant, and only 1 test is not statistically significant. These tests demonstrate the statistical significance of the superior performance of the LSVM classification algorithm as compared to the other four.

Table 5.15 P-Value of T-Test for 2-State Problem for the MedQuest Pump

LSVM Versus	CART	DA	NN	SVM
NS Sensitivity	0.0072	0.0017	0.0016	0
NS Sensitivity	0	0	0	0
Accuracy	0	0	0	0

Table 5.16 P-Value of T-Test for 2-State Problem for the Nimbus Pump

LSVM Versus	CART	DA	NN	SVM
NS Sensitivity	0	0	0.0017	0
NS Specificity	0	0	0	0
Accuracy	0	0	0	0

Table 5.17 P-Value of T-Test for 3-State Problem for the MedQuest Pump

LSVM Versus	CART	DA	NN	SVM
NS Sensitivity	0	0	0	0.4633
NS Specificity	0	0	0	0.169
NS Accuracy	0	0	0	0.615
AS Sensitivity	0	0	0	0
AS Specificity	0	0	0	0
AS Accuracy	0	0	0	0
S Sensitivity	0	0	0	0
S Specificity	0.0108	0.1519	0.2207	0
S Accuracy	0	0	0	0

Table 5.18 P-Value of T-Test for 3-State Problem for the Nimbus Pump

LSVM Versus	CART	DA	NN	SVM
NS Sensitivity	0	0	0	0.025
NS Specificity	0.0025	0.0036	0	0
NS Accuracy	0	0	0	0
AS Sensitivity	0.2568	0	0	0
AS Specificity	0	0	0	0
AS Accuracy	0	0	0	0.0446
S Sensitivity	0	0	0	0
S Specificity	0	0.2944	0	0
S Accuracy	0	0	0	0

CHAPTER 6: FEEDBACK CONTROL SYSTEM OF A ROTARY LVAD

Employing the proposed LSVM algorithm for suction detection has been shown to be effective. A very important use for such a suction detector is to be a part of a pump control strategy. The long-term need for a pump controller that automatically responds to the patient's physiological requirements would require a mechanism to detect the occurrence of suction, and hence establish the appropriate pump flow setting that allows for safe device operation. Practical considerations in developing such an intelligent controller are the hardware and computational requirements in real time. For a patient implanted with the LVAD, suction must be identified in the order of seconds, and the six suction indices examined in this paper can be computed at a high rate of 40 Hz and 50 Hz for the MedQuest and Nimbus pumps, respectively, which means that it can meet the LVAD requirements. Furthermore, with the current technology in batch processors, most conceivable features should be easy enough to extract in real time as some SVM-based real-time applications in different fields have already demonstrated [47]-[49]. In general, the proposed method is a valuable tool for suction detection.

In this chapter, we will discuss the control strategy for the rotary LVAD based on suction detection. This is a new patient-adaptive feedback controller for the rotary LVAD developed to automatically regulate the pump current of the device without introducing suction. This chapter

is organized as follows. Section 6.1 describes the development details of the feedback controller. Section 6.2 shows the simulation results. Discussion is presented in Section 6.3.

6.1 Feedback Control Design

The available mechanism to control a rotary LVAD is to adjust the pump motor current (control input) in order to meet certain goals typically related to the patient implanted with the LVAD. The objective of the feedback controller for the LVAD is to ensure that suction does not occur by unnecessary, excessive pumping, while at the same time to provide the patient with the amount of blood flow within acceptable range depending on the different levels of the patient's activity. This achievement has been a major challenge for the LVAD researchers for around 20 years and is considered as one of the most serious limitations of this technology at this time [19]. As previously discussed, a manual open-loop controller maybe a feasible way to achieve the above objectives; however, this method will not be able to achieve the above goals without the clinician or physician's ability to observe the pump flow and accordingly adjust the pump current. A full state feedback controller, on the other hand, may be available if the hemodynamic variables (x_1 through x_5 in Chapter 3) can be measurable continuously in real time; however, because of difficulties in measuring hemodynamic variables with current implantable sensors technology, this goal cannot be implemented. The pump flow (x_6), on the other hand, is the available state variable that can be measured in real time. This can be done, for example, by using the transonic

flow probes in the aorta and pulmonary artery or in the outflow cannula of the pump as mentioned previously. Therefore, the proposed control system will use the pump flow of the combined cardiovascular-LVAD model as the feedback variable. A general block diagram of the feedback controller is illustrated in Figure 6.1.

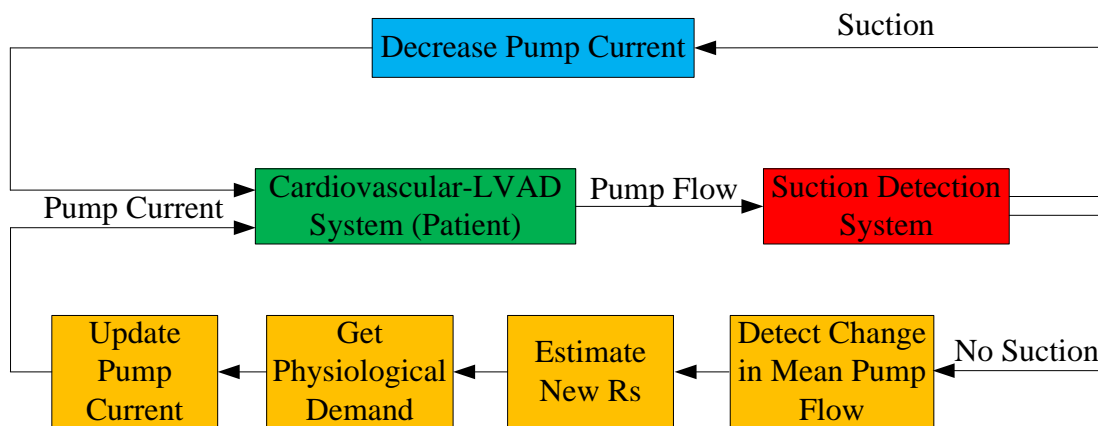


Figure 6.1 Block Diagram of the Proposed Control System

The controller mainly consists of two parts. The suction detection subsystem can determine which part is taking action, meaning that the suction detector could determine the pump status as NS or S. The first part, including four stages, will take action when the pump is operating normally (i.e., in NS case) ensured by the suction detector. During the first stage, labeled “Detect Change in Mean Pump Flow”, the mean pump flow signal is continuously read until a change is detected. This change means that the patient’s activity level is varying. Therefore, regulating the pump current is required to respond to the new physiological demand.

As mentioned above, the change in the mean pump flow is an indication of a change in the level of activity of the patient, which is modeled in terms of Systemic Vascular Resistance (SVR) denoted by R_S . If other conditions are not changed, as labeled “Estimate New R_S ” in the second stage, before calculating needed mean pump flow, the new R_S needs to be estimated using the approach proposed in [50]. Since changing R_S could cause obvious change in the mean pump flow if the values of other parameters in the cardiovascular-LVAD model are unchanged, therefore, the system will receive a signal as a response to change in the mean pump flow. As a result, the new R_S will be estimated by running the 6th order model under the same conditions as the Cardiovascular-LVAD system of the patient (i.e., using the same contractility of the left ventricle, HR, and PC). Initially the R_S will be determined based on the following non-linear equation:

$$R_{Snew} = \begin{cases} R_{Sold} + \Delta R_S & \text{if } Q_{old} > Q_{new} \\ R_{Sold} & \text{if } Q_{old} = Q_{new} \\ R_{Sold} - \Delta R_S & \text{if } Q_{old} < Q_{new} \end{cases} \quad (6.1)$$

where ΔR_S a preselected small positive constant. And afterwards a similar criterion will be used to determine the R_S at stage $k+1$ from the values at stage k :

$$R_S(k + 1) = \begin{cases} R_S(k) + \Delta R_S & \text{if } Q_k > Q_{k+1} \\ R_S(k) & \text{if } Q_k = Q_{k+1} \\ R_S(k) - \Delta R_S & \text{if } Q_k < Q_{k+1} \end{cases} \quad (6.2)$$

According to the rule above, the feedback controller will keep trying different values for R_S until

the mean pump flow generated by the 6th order model is equal to the new measurement of the actual mean pump flow of the patient. At this point the feedback controller determines that the final R_S is the same R_S for the patient.

Once R_S is determined, in the third stage labeled “Get Physiological Demand”, the required mean pump flow (physiological demand) under the current R_S could be easily calculated by using this R_S . In this dissertation, we assume that the physiological demand is a linear function of R_S , such that when R_S decreases (i.e., the patient’s activity level rises); the related mean pump flow is linearly increased.

Finally, in the fourth stage labeled as “Update Pump Current”, the pump motor current $i(t)$ will be adjusted until the mean pump flow reaches the physiological demand obtained in the third stage.

However, when the suction detector identified that suction occurs, the controller will lower the pump motor current immediately as follows:

$$i_{k+1} = i_k - K \cdot \text{mean}(PF) \quad (6.3)$$

where K represents the adjustment step size for adjusting the control variable. This procedure is labeled as “Decrease Pump Current” in Figure 6.1.

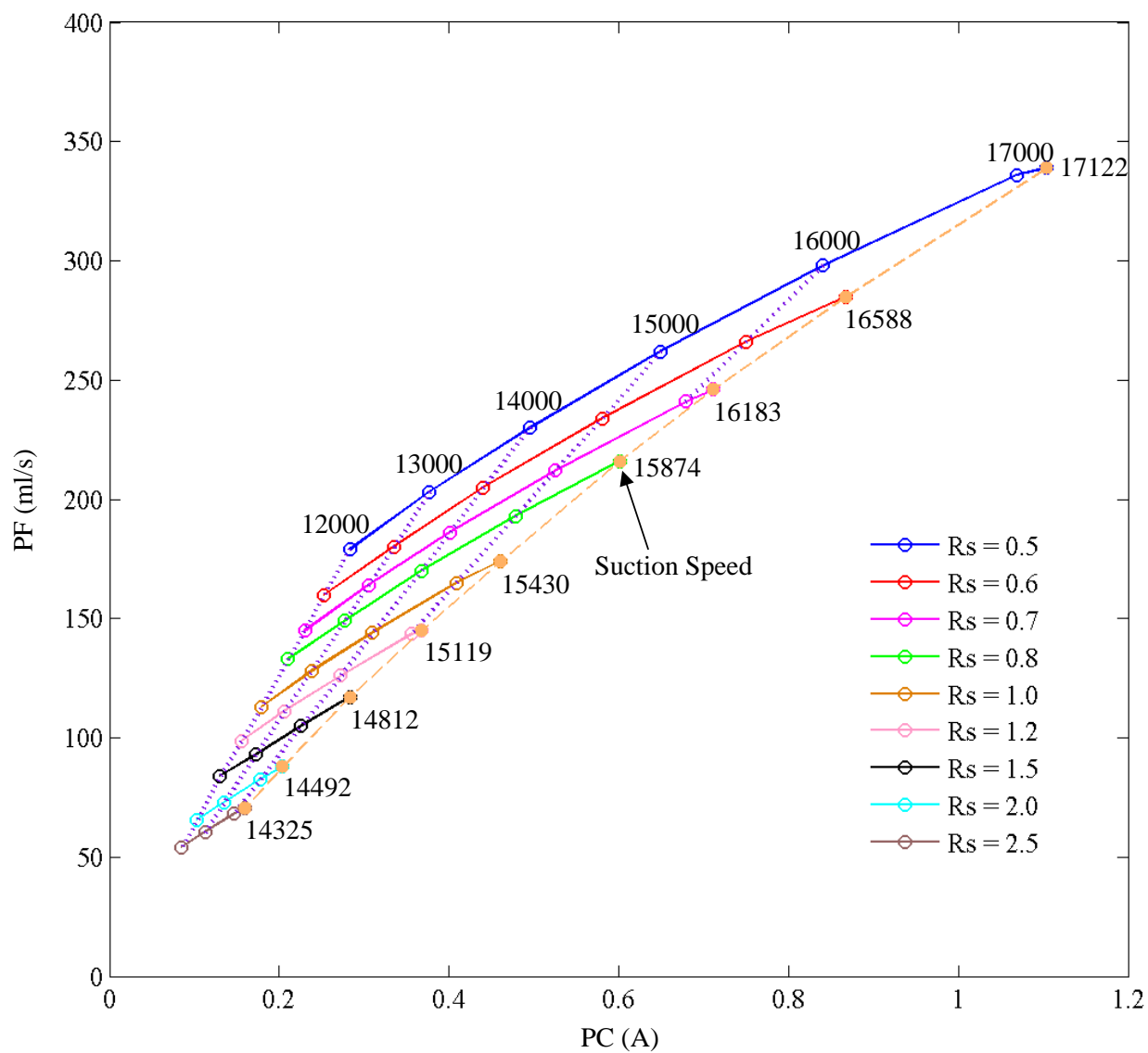


Figure 6.2 Relationships among PC, PF, and PS Described by Circle Symbols. Solid Circle Symbols Indicate PS When Suction Occurred

6.2 Simulation Studies

As mentioned earlier, one of the main aims of the controller is to regulate the pump current so that it remains below the level at which suction occurs. The suction current, however, varies depending on the level of activity of the patient. Thus, in order to assess the performance of the proposed controller, we need to determine the suction current as a function of R_S . This has been done by exciting the cardiovascular-LVAD model with an open-loop ramp current control and shown in Figure 6.2 (as the solid circle symbols). Figure 6.2 also shows the relationship among pump current, pump flow, and pump speed with different levels of activity of the patient. With each specific value of the pump current, when the level of the patient's activity increases, the corresponding values of both pump flow and pump speed increases. And clearly, the pump current should be controlled in the safe region (out of suction, on the left of the related solid symbols line in Figure 6.2) under each level of activity of the patient in order to ensure that the patient is not exposed to the suction event.

In addition, to assess the performance of the controller, we performed the following simulations. In all the simulations, the contractility of the left ventricle (E_{max}) is set at 1.0 mmHg/ml. In the first 25 s of the simulation period, the initial pump current is set at 0.146 amps to provide the required physiological demand. The corresponding initial R_S is set at 1.0 mmHg·s/ml representing a normal level of activity [3]-[5], [17]-[19]. After 25 s, the patient's activity level is

changed and the controller will take action. The simulations contain two different parts. In the first part we deactivate the suction detection subsystem. In the second part, we keep it active in the control system. This is done in order to assess the performance and the importance of the feedback controller without and with the embedded suction detector.

The simulations are to mimic a condition representing a patient with a changing level of activity. To accomplish this, we set $R_S = 1.0$ mmHg·s/ml for the first 25 s (i.e., the patient's level of activity is normal). Then we decreased R_S gradually in the next 10 s to $R_S = 0.5$ mmHg·s/ml so as to represent a changing level of activity from normal to active. For the remainder of the time interval R_S was kept at 0.5 mmHg·s/ml (i.e., the patient was very active). A plot of R_S as it was changed versus time is shown in Figure 6.3.

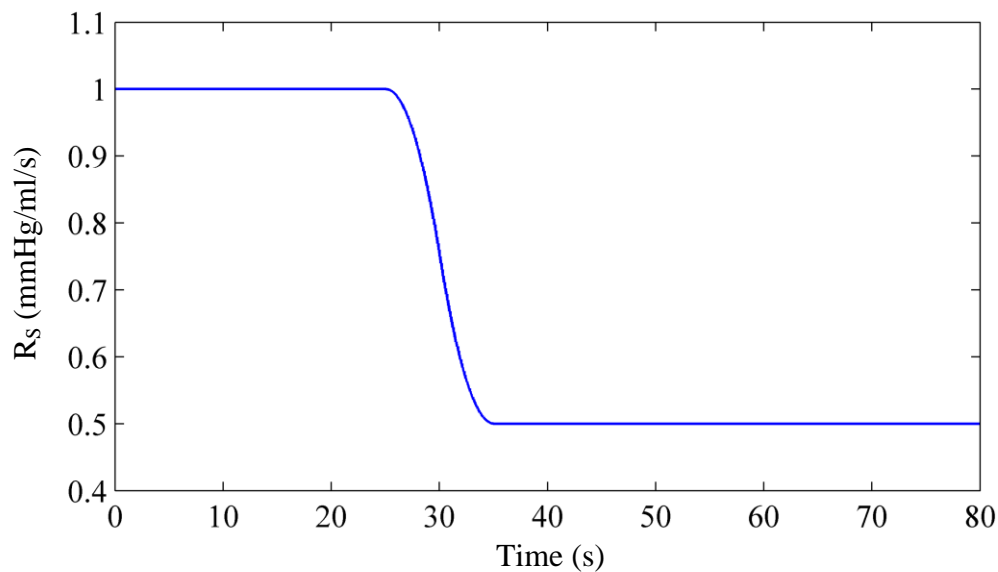


Figure 6.3 Changing R_S from 1.0 to 0.5 mmHg·s/ml

Figure 6.4 shows the simulation results of the feedback controller without the suction detector for the patient whose level of activity is represented by Figure 6.3. At first, the pump current is constant since all the conditions are not changed. After 25 s, due to the change in the patient's activity level, the pump current, pump flow, and pump speed have been increased by the controller in order to meet the physiological demand. Then at a certain point (around 60 s), ventricular suction occurred at the high values of the pump signals. Since there is no suction detector, the pump current will keep increasing until the physiological demand is met. However, once suction occurs, matching physiological demand will no longer be meaningful because at this point, the patient is in danger due to suction. Furthermore, if this phenomenon lasts for some time, it will cause permanent damage to the cells and tissues of the heart and may result in death of the patient. Therefore, ventricular suction must be prevented from occurring by the suction detection subsystem by reducing the pump current.

Figure 6.5 shows the simulation results of the feedback controller with the suction detector. As can be seen in Figure 6.5, at around 60 s, ventricular suction occurred briefly at the high values of the pump signals; however, since the suction detector was active, the controller lowered the pump current immediately, meaning that ventricular suction at the high pump speed was prevented from occurring. After that, the pump current was kept at a constant level meeting as much of the patient's cardiac demand while at the same time preventing suction.

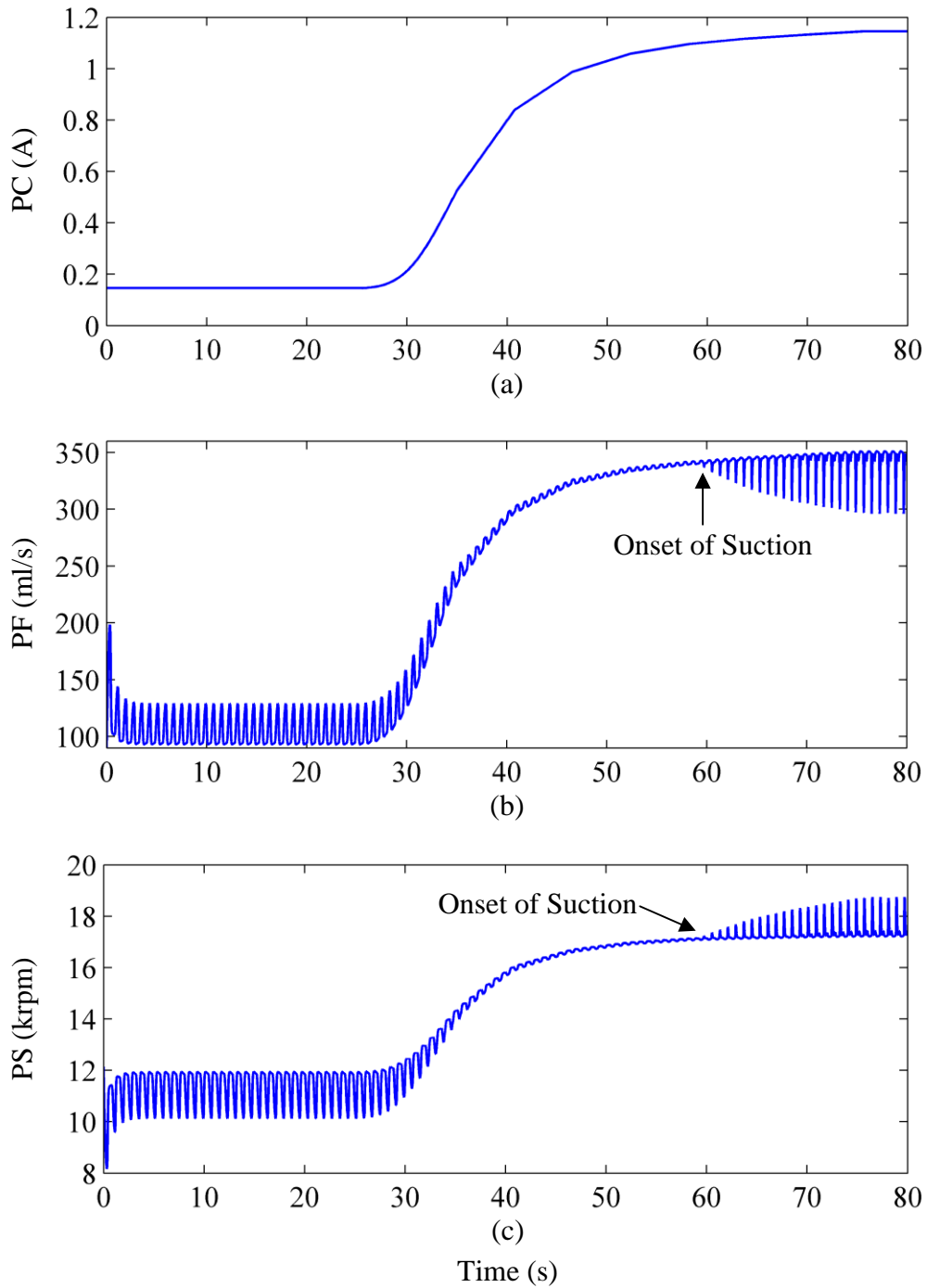


Figure 6.4 Simulation Results Generated by the Feedback Controller with Varying R_S from 1.0 to 0.5 without Suction Detector

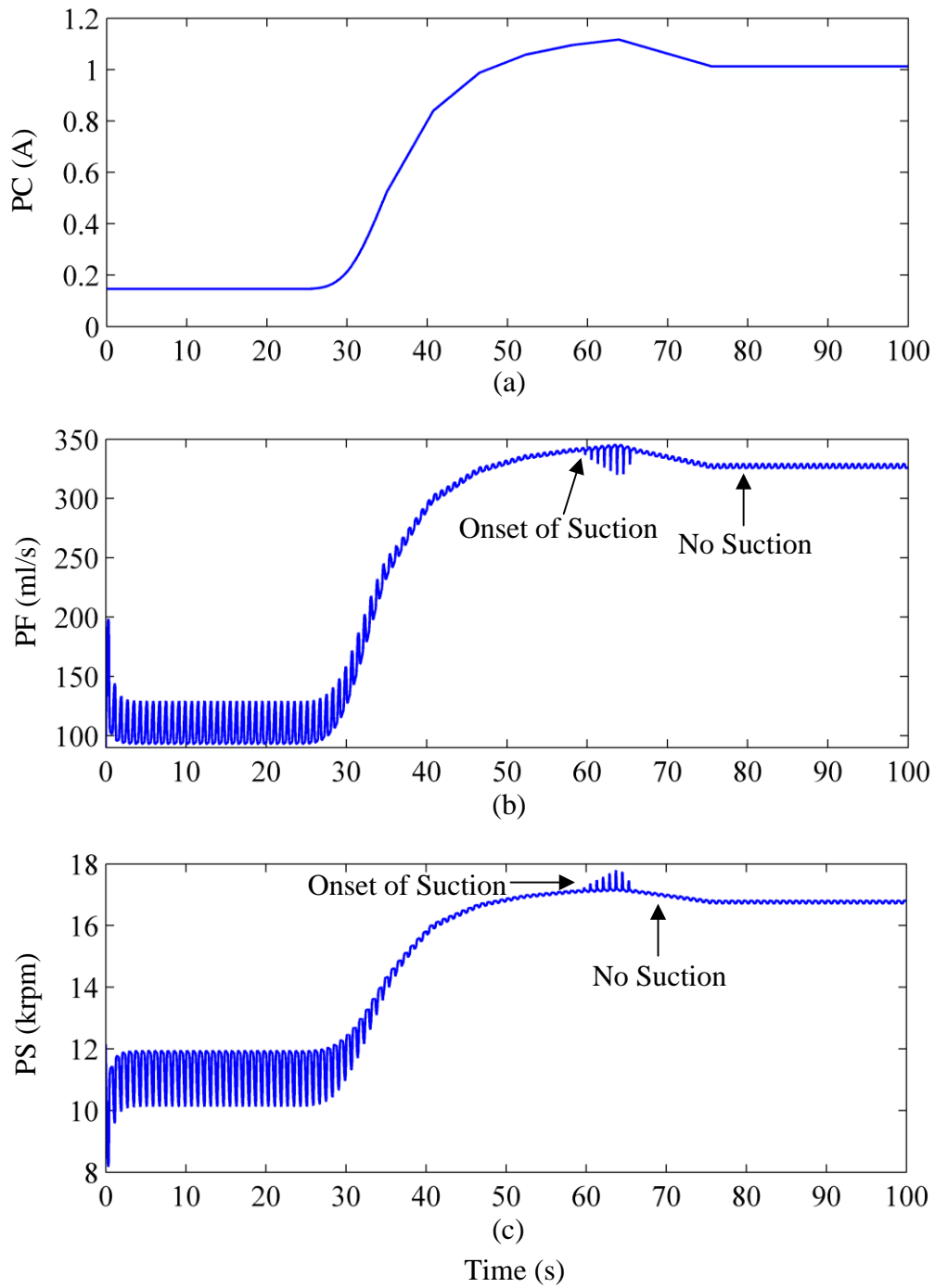


Figure 6.5 Simulation Results Generated by the Feedback Controller with Varying R_s from 1.0 to 0.5 with Suction Detector

By comparison, Figure 6.6, 6.7, and 6.8 show the varying patient's activity level from 1.0 to 0.6 mmHg·s/ml and the corresponding simulation results generated by the feedback controller without and with the suction detector. The simulation results also demonstrate that without suction detection subsystem, ventricular suction occurred and cannot be avoided. However, when the suction detector is incorporated, suction can be prevented from occurring effectively.

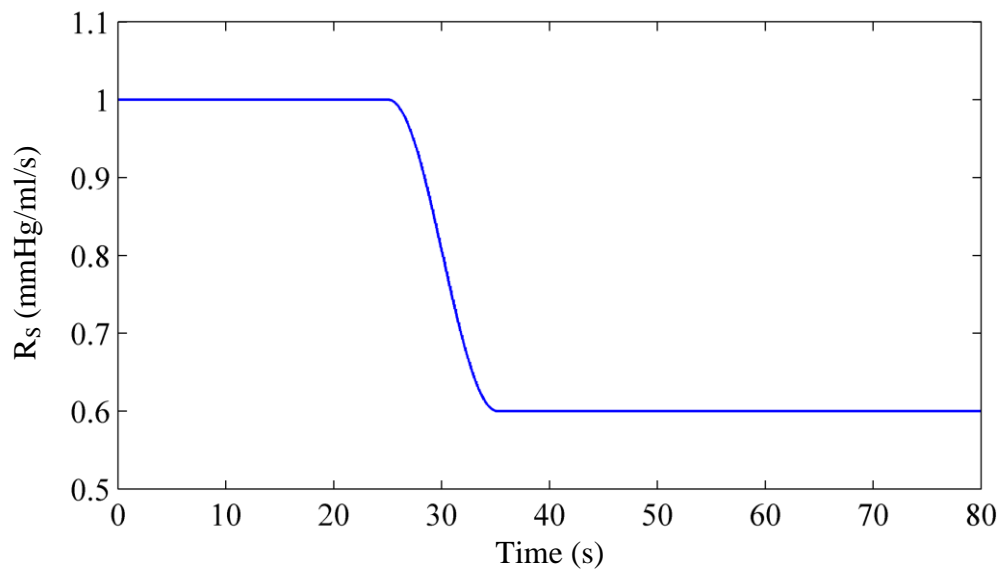


Figure 6.6 Changing R_s from 1.0 to 0.6 mmHg·s/ml

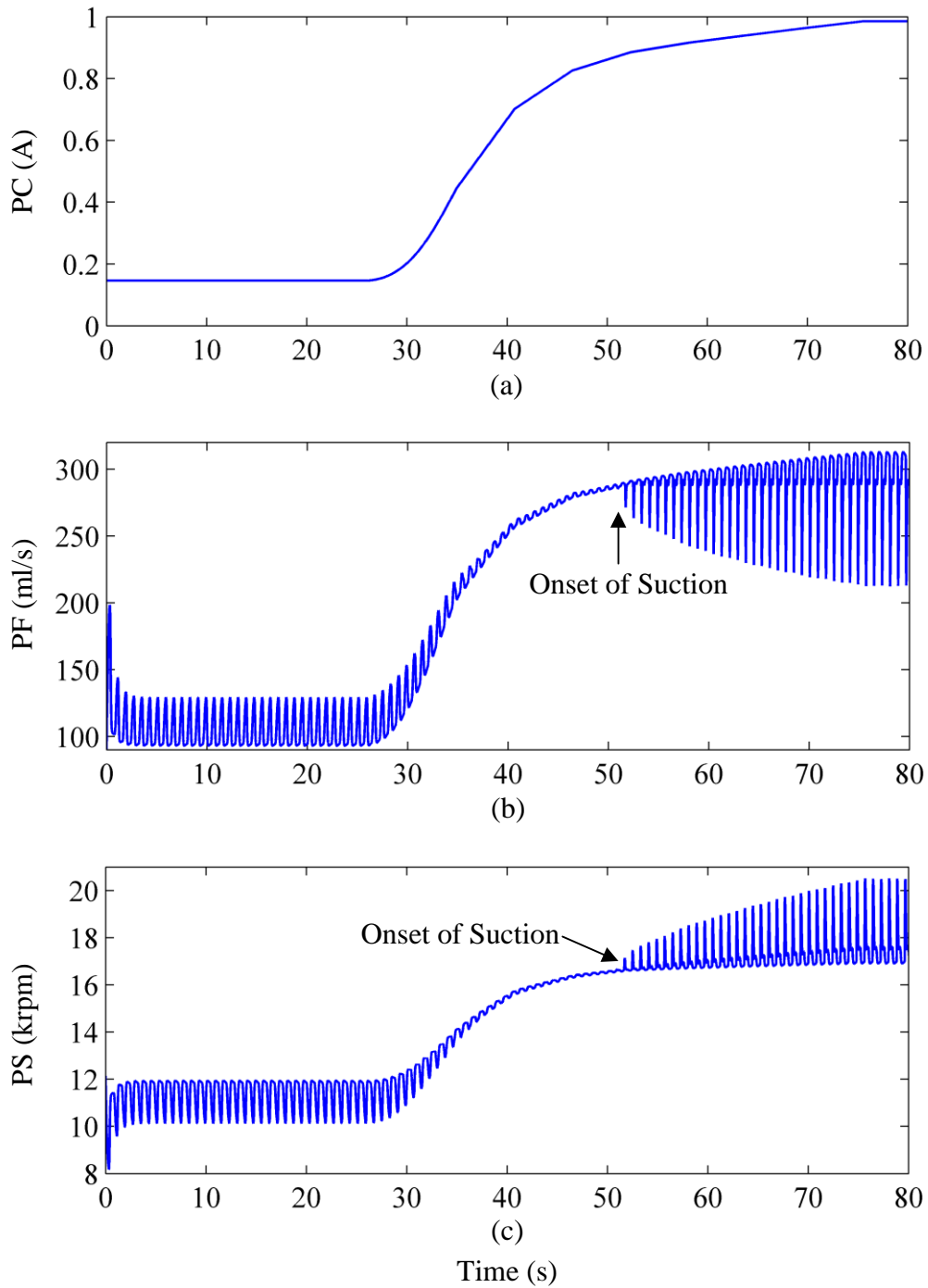


Figure 6.7 Simulation Results Generated by the Feedback Controller with Varying R_S from 1.0 to 0.6 without Suction Detector

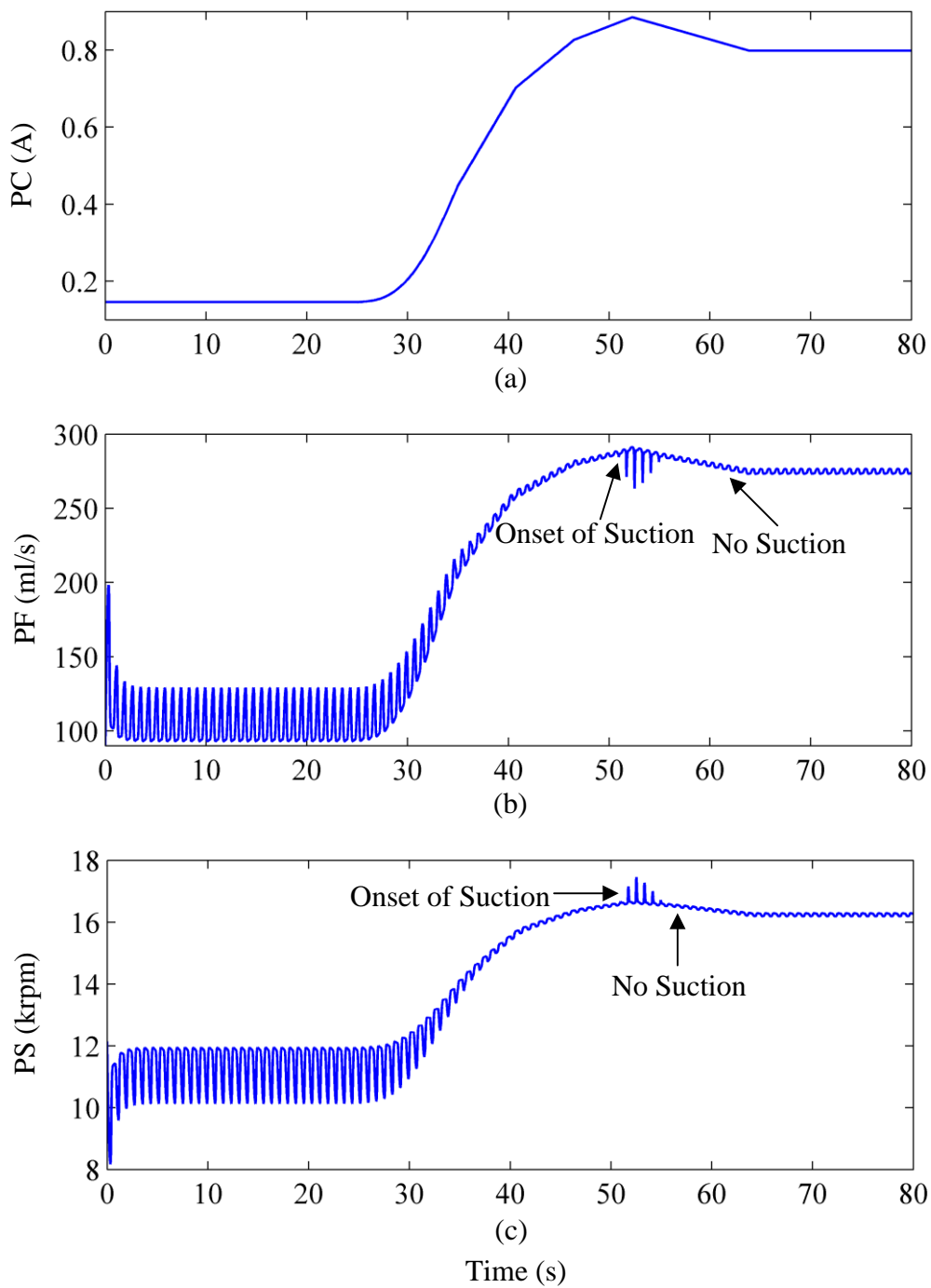


Figure 6.8 Simulation Results Generated by the Feedback Controller with Varying R_s from 1.0 to 0.6 with Suction Detector

Furthermore, Figure 6.9, 6.10, and 6.11 show the varying patient's activity level from 1.0 to 0.7 mmHg·s/ml and the related simulation results generated by the feedback controller without and with the suction detector, respectively. The results also show that when suction occurred, without suction detector embedded, ventricular suction kept lasting and cannot be avoided. Comparatively, when the suction detector is embedded, suction can be prevented by lowering the pump motor current quickly.

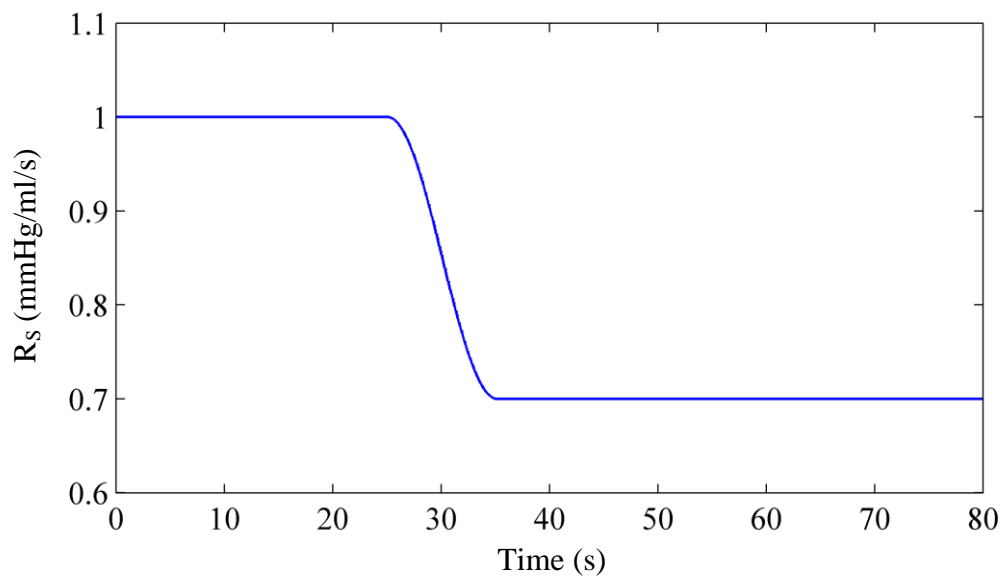


Figure 6.9 Changing R_S from 1.0 to 0.7 mmHg·s/ml

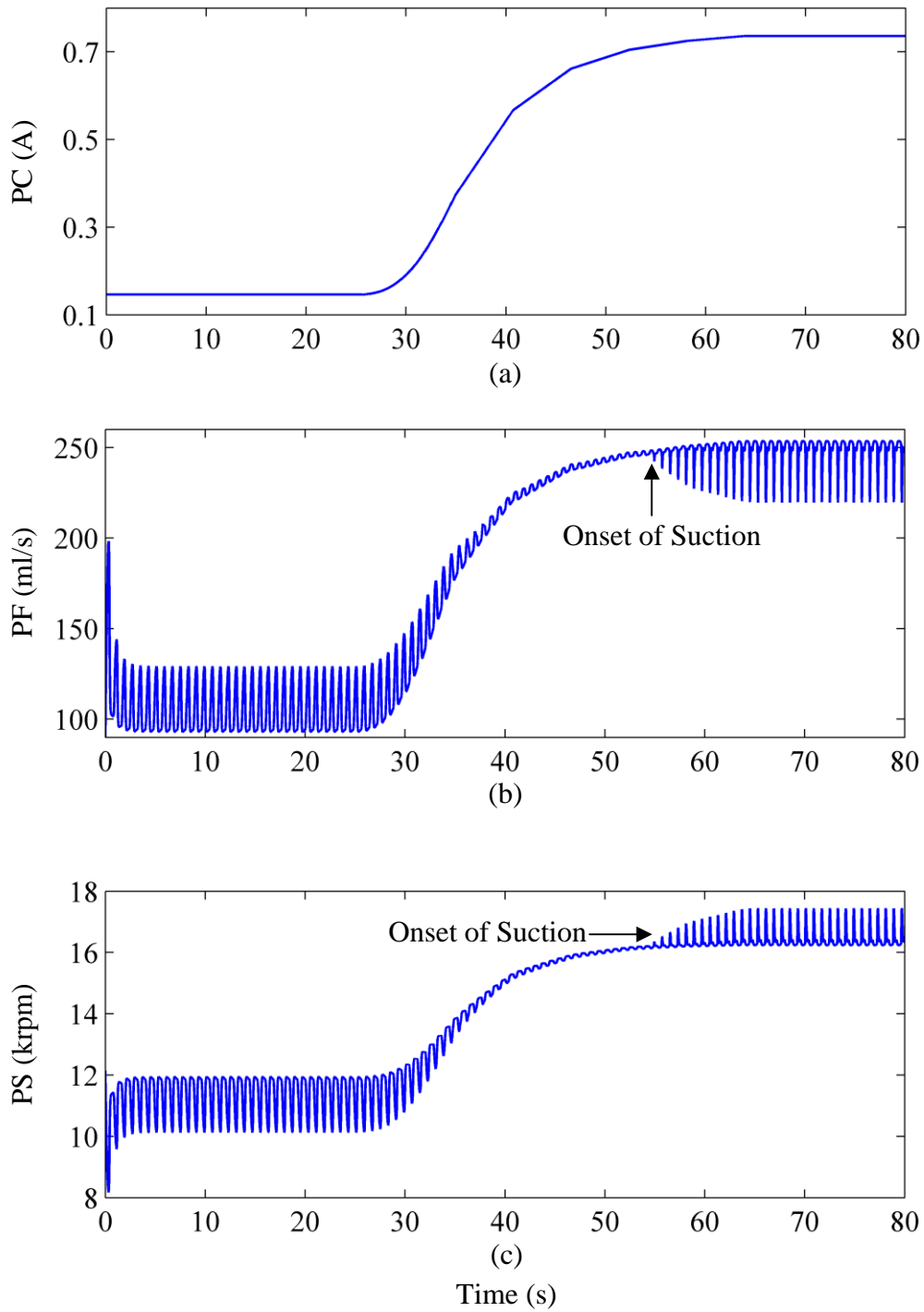


Figure 6.10 Simulation Results Generated by the Feedback Controller with Varying R_S from 1.0 to 0.7 without Suction Detector

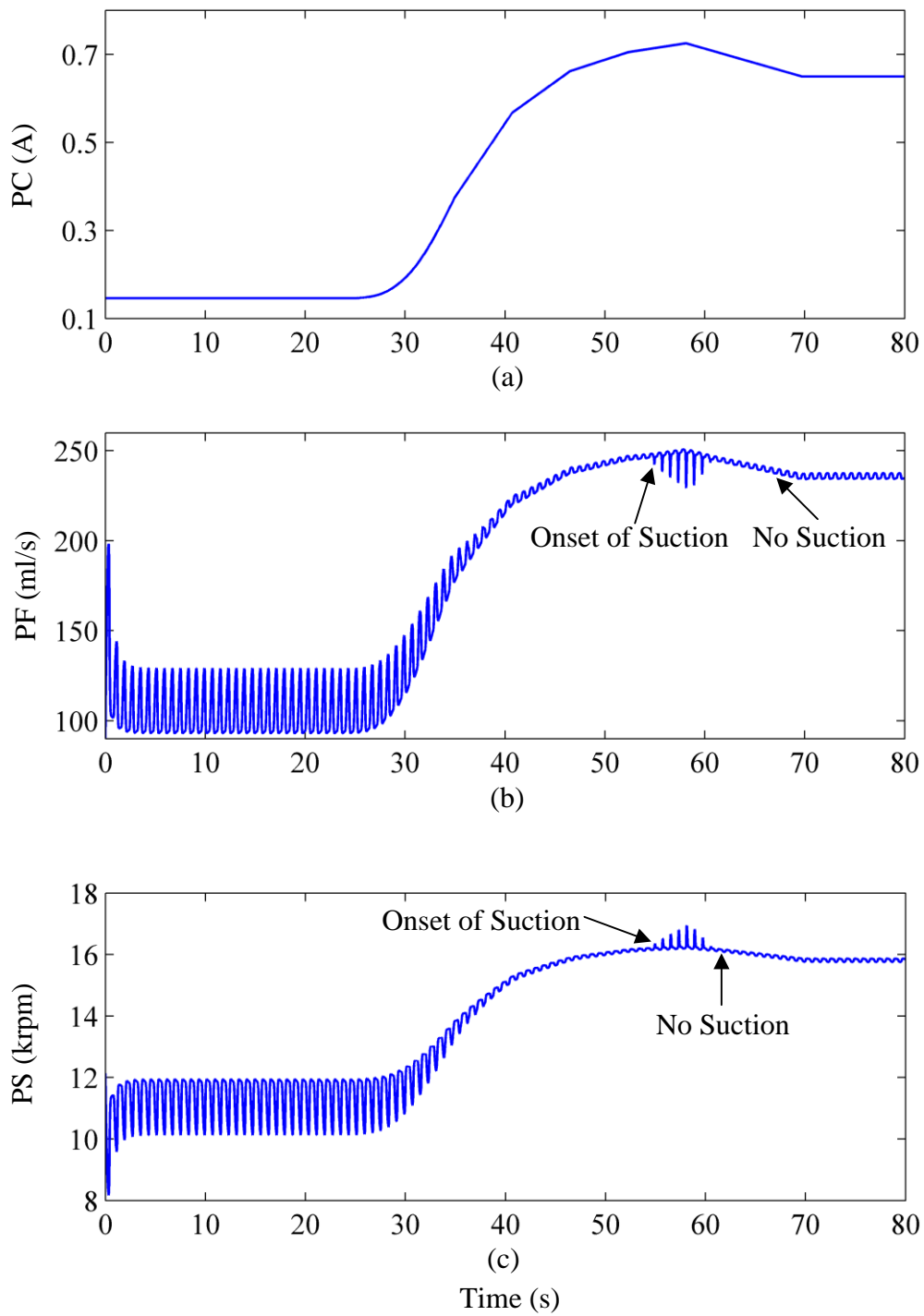


Figure 6.11 Simulation Results Generated by the Feedback Controller with Varying R_S from 1.0 to 0.7 with Suction Detector

6.3 Discussion

In this study, the proposed system is a combination of two main subsystems: a suction detector and a feedback controller. The control system for the rotary LVAD must be adaptable and safe. Adaptability means that the control system could automatically adjust the control variable (pump current) according to the level of activity of the patient. Safety means that suction must be avoided to protect the muscle, tissues and cells of the heart. With increasing adaptability and safety in continuously working LVADs, the demand for the automatic pump motor current regulation increases. Therefore, the key requirements of our proposed system are the adaptation of LVAD-generated signals to the changing physiological requirements of the patient by automatically adjusting the pump current, and avoidance of overpumping of the left ventricle – ventricular suction.

The developed controller provides one answer for the problem of updating PC in a rotary LVAD, but it may not be the definitive answer. There may be other developments that can generate similar or even better results. For instance, a multi-objective optimization approach could take into account all the criteria of interest to clinicians [51], however, more information about the patient's status would be considered to implement such a strategy.

The suction detection is an important step during the development of a feedback control strategy for LVADs. A number of control strategies have been proposed by research groups in the LVAD

field. Particular control factors were based on the pulsatility. However, as pointed out in [52], it is necessary to embed a suction detection mechanism in the pulsatility-based control system to classify between pulsatility in the normal pump status from that identified during the suction case. Furthermore, according to [53], only controlling an estimate of the certain pump variables without other constraints may lead to ventricular suction or an undesirable CO value under certain situations. Comparatively, our proposed suction detection system can classify the pumping states with a high degree of accuracy.

In general, the proposed system accomplished the objective of adapting the controller to variations in the physiologic state of the patient, while driving the pump out of the current range that would cause suction to the patient. Its main contribution to the LVAD field is to show the feasibility and reliability of this method in simulations. One limitation of our proposed controller is that the parameter K is an experimentally chosen value. A methodology for an intelligent estimation of adaptive values of K is currently under investigation. The other future step is to apply this proposed strategy to the in vivo animal experiments before it can be used as an alternative for human patients in the clinical study, which remains a significant challenge in real time.

CHAPTER 7: CONCLUSION

In this dissertation, a control system based on suction detection for rotary blood pumps was presented. The whole system is a combination of three subsystems: a combined cardiovascular-LVAD model, a suction detector, and a feedback controller.

The cardiovascular system model is a circuit analog model by using resistances, inductors, capacitors and diodes, respectively. A cardiovascular system model as a healthy heart has been introduced by using the data in the literatures as references. An empirical rotary Left Ventricular Assist Device model is coupled to the failing cardiovascular system model as a combined new sixth order state-space model. These models are capable of reproducing the real data in the literatures, such as the experimental data for the healthy people and patients with heart failure. The combined model provides a realistic simulation of the interaction between the pump and the native cardiovascular system. More useful changes in hemodynamics can be simulated and exploited in this model. Furthermore, the control variable in this model is the pump motor current instead of the pump speed, which so far has been used as the control variable in the currently existing model. This model is much more useful for optimally controlling the LVAD since it avoids solving the inverse problem for determining the pump motor current that produces an already determined optimized pump speed. The challenges in using this model to design a feedback controller for the LVAD motor current are discussed. The characteristics of the pump

speed and the pump flow signal, which are the variables that can be directly and accurately measured, when the pump is operating normally with no suction and when it is operating in suction, are also described based on results obtained from the model. This model can also be used to test the performance of a pump controller before the costly and time consuming animal experiments.

An effective LSVM-based suction detection algorithm that can be used as a part of a feedback controller for the LVAD was discussed. The algorithm was tested with in vivo LVAD data and compared to other existing algorithms. Initially, the pump flow signals from in vivo data were pre-processed, to remove the high frequency noise components, and then six features were extracted from the signals as suction indices based on time, frequency, and time-frequency domains. The LSVM algorithm, combined with the decision tree strategy was used to implement 2-state and 3-state suction classification tasks for two different pumps. Compared to three existing classification methods and the regular SVM algorithm, the proposed LSVM algorithm showed superior accuracy with high stability, short learning speed, and good robustness. The ability of this system to detect the onset of suction with such a high degree of performance allows this method to be used as part of a feedback control strategy to automatically adjust the pump speed in rotary LVADs.

The development of a control algorithm for an LVAD supporting a patient with heart failure is a challenging engineering problem in practical. In this dissertation, we investigated the control algorithm for improving the rotary blood pump performance for the congestive heart failure patients. A new patient-adaptive feedback controller for the rotary LVAD was proposed. The control system can respond to the instantaneous physiological change of the patient under different levels of the patient's activity by automatically regulating the pump motor current of the device without introducing suction ensured by the suction detector subsystem. In addition, once suction occurred, the suction detector subsystem can quickly detect this case and the control system immediately decreased the pump motor current in order to protect the muscles and tissues of the patient's failure heart. The proposed control system could be implemented in an animal experiment before applying it to the human patients in real time.

So far, the work has been done on the model simulation only. In the simulation, the heart rate is set as constant, and the patient's activity level (R_S) was estimated. In real life, there may be some complexity with the measurement of these variables. Especially, for the case of the heart rate, it is possible that there is an irregular cardiac rhythm or missing beats. Therefore, preprocessing or measurement condition needs to be considered for the application of this controller. In addition, ventricular suction is an extremely complicated case in real time. The patient implanted with an LVAD can be easily exposed to suction-critical conditions such as continuous coughing, Valsalva-Maneuver, sudden movement, and exercise starts and stops, making the suction

detection algorithm complicated and there may be some limitations regarding suction detection. Also, as to the selection of the pump current update gains in the controller, some more complicated algorithms based on a certain objective may be considered to enhance the performance of the controller. The future work includes further verification of both the proposed suction detection algorithm and the control strategy by using a mock loop or an animal experiment.

LIST OF REFERENCES

- [1] Gu, M. and Qin, Y., “Development of left ventricular assist devices,” *Int. J. Cardiovascular Disease*, vol. 36, no. 2, pp. 69-71, 2009.
- [2] Slaughter, M. S., Rogers, J. G., Milano, C. A., Russell, S. D., Conte, J. V., Feldman, D., et al, “Advanced heart failure treated with continuous-flow left ventricular assist device,” *The New England J. Med.*, vol. 361, no. 23, pp. 2241-2251, 2009.
- [3] Simaan, M.A., “Modeling and control of rotary left ventricular assist device,” *Handbook of Automation*, Ed S. Nof, Springer Verlag, 2009, pp. 1409-1422.
- [4] Simaan, M.A., Faragallah, G., Wang, Y., and Divo, E., “Left ventricular assist devices: Engineering design considerations,” Guillermo Reyes, Ed., *New Aspects of Ventricular Assist Devices*, Intech Publishers, 2011, ch. 2, pp. 21-42.
- [5] Wang, Y., Faragallah, G., Divo, E., and Simaan, M.A., “Feedback control of a rotary left ventricular assist device supporting a failing cardiovascular system,” in *Proc. 2012 American Control Conference*, Montréal, Canada, June 27-29, 2012, pp. 1137-1142.
- [6] Yuhki, A., Hatoh, E., Nogawa, M., Miura, M., Shimazaki, Y., and Takatani, S., “Detection of suction and regurgitation of the implantable centrifugal pump based on the motor current waveform analysis and its application to optimization of pump flow,” *Artif. Organs*, vol. 23, no. 6, pp. 532-537, 1999.

- [7] Oshikawa, M., Araki, K., Endo, G., Anai, H., and Sato, M., "Sensorless controlling method for a continuous flow left ventricular assist device," *Artif. Organs*, vol. 24, no. 8, pp. 600-605, 2000.
- [8] Tanaka, A., Yoshizawa, M., Olegario, P., Ogawa, D., Abe, K., Motomura, T., Igo, S., and Nose, Y., "Detection and avoiding ventricular suction of ventricular assist devices," in *Proc. 27th Annu. Int. Conf. IEEE Eng. Med. Biol.*, Shanghai, China, 2005, pp. 402-405.
- [9] Vollkron, M., Schima, H., Huber, L., Benkowski, R., Morello, G., and Wieselthaler, G., "Advanced suction detection for an axial flow pump," *Artif. Organs*, vol. 30, no. 9, pp. 665-670, Sep. 2006.
- [10] Karantonis, D.M, Lovell, N.H., Ayre, P.J., Mason, D.G. and Cloherty, S.L., "Identification and classification of physiologically significant pumping states in an implantable rotary blood pump," *Artif. Organs*, vol. 30, no. 9, pp. 671-679, 2006.
- [11] Ferreira, A., Chen, S., Simaan, M.A., Boston, J.R., and Antaki, J.F., "A discriminant-analysis-based suction detection system for rotary blood pumps," in *Proc. 28th Annu. Int. Conf. IEEE Eng. Med. Biol.*, New York, NY, 2006, pp. 5382-5385.
- [12] Karantonis, D.M, Cloherty, S.L., Lovell, N.H., Mason, D.G., Salamonsen, R.F., and Ayre, P.J., "Noninvasive detection of suction in an implantable rotary blood pump using neural networks," *Int. J. Computation Intelligence and Applications*, vol. 7, no. 3, pp. 237-247, 2008.

- [13] Wang, Y., Faragallah, G., Divo, E., and Simaan, M.A., "Detection of suction for rotary blood pumps using support vector machines," *Abstracts of 57th Annu. Conf. ASAIO*, Washington, DC, 2011. *ASAIO J.*, vol. 57, no. 2, March-April 2011, pp. 102.
- [14] Wang, Y., Faragallah, G., Divo, E., and Simaan, M.A., "Detection of ventricular suction in an implantable rotary blood pump using support vector machines," in *Proc. 33th Annu. Int. Conf. IEEE Eng. Med. Biol.*, Boston, MA, 2011, pp. 3318-3321.
- [15] Wang, Y. and Simaan, M.A., "A suction detection system for rotary blood pumps based on the lagrangian support vector machine algorithm," *IEEE J. Biomed. Health Inform.*, vol. 17, no. 3, pp. 654-663, May 2013.
- [16] Giridharan, G., Pantalos, G., Koenig, S., Gillars, K., and Skliar, M., "Achieving physiologic perfusion with ventricular assist devices: comparison of control strategies," in *Proc. American Control Conf.*, Portland, OR, 2005, pp. 3823-3828.
- [17] Chen, S., "Baroreflex-based physiological control of a left ventricular assist device," Ph.D. Dissertation, University of Pittsburgh, Pittsburgh, PA, 2006.
- [18] Ferreira, A., Boston, J.R., and Antaki, J.F., "A control system for rotary blood pumps based on suction detection," *IEEE Trans. Biomed. Eng.*, vol. 56, no. 3, pp. 656-665, 2009.
- [19] Simaan, M.A., Ferreira, A., Chen, S., Antaki, J.F., and Galati, D.G., "A Dynamical State Space Representation and Performance Analysis of a Feedback-Controlled Rotary Left

- Ventricular Assist Device,” *IEEE Trans. Contr. Syst. Technol.*, vol. 11, no. 7, pp. 15-28, 2009.
- [20] Faragallah, G., Wang, Y., Divo, E., and Simaan, M.A., “A new current-based control model of the combined cardiovascular and rotary left ventricular assist device,” in *Proc. American Control Conf.*, San Francisco, CA, 2011, pp. 4775-4780.
- [21] http://www.gzyld.org.cn/_medc/yxk/rjtp/0H5431H008.html
- [22] http://www.gzyld.org.cn/_medc/yxk/rjtp/050542152008.html
- [23] http://tupian.hudong.com/a3_52_13_01300000023544121285132410166_jpg.html
- [24] http://www.futura-sciences.com/fr/definition/t/medecine-2/d/systole_7317/
- [25] Guyton, C. and Hall, J.E., *Textbook of Medical Physiology*, 11th ed. Philadelphia, PA: Elsevier Saunders, 2006, ch. 9, pp. 103-115.
- [26] Wu, Y., Allaire, P., Tao, G., Wood, H., Olsen, D. and Tribble, C., “An advanced physiological controller design for a left ventricular assist device to prevent left ventricular collapse,” *Artif. Organs*, vol. 27, no. 10, pp. 926-930, 2003.
- [27] Suga, H. and Sagawa, K., “Instantaneous pressure-volume relationships and their ratio in the excised, supported canine left ventricle,” *Circulation Research*, vol. 35, no. 1, pp. 117-126, 1974.

- [28] Stergiopoulos, N., Meister, J. and Westerhof, N., “Determinants of stroke volume and systolic and diastolic aortic pressure,” *American J. Physiology*, vol. 270, no. 6, pp. 2050-2059, 1996.
- [29] Schima, H., Trubel, W., Moritz, A., et al, “Noninvasive monitoring of rotary blood pumps: necessity, possibilities, and limitations,” *Artif. Organs*, vol. 16, no. 2, pp. 195-202, 1992.
- [30] Mason, D.G., Hilton, A.K., and Salamonsen, R.F., “Reliable suction detection for patients with rotary blood pumps,” *ASIAO J.*, vol. 54, no. 4, pp. 359-366, 2008.
- [31] Ferreira, A., “A rule-based controller based on suction detection for rotary blood pumps,” Ph.D. Dissertation, University of Pittsburgh, Pittsburgh, PA, 2007.
- [32] Vollkron, M., Schima, H., Huber, L., Benkowski, R., Morello, G., and Wieselthaler, G., “Development of a suction detection system for axial blood pumps,” *Artif. Organs*, vol. 28, no. 8, pp. 709-716, 2004.
- [33] Ferreira, A., Simaan, M.A., Boston, J.R., and Antaki, J.F., “Frequency and time-frequency based indices for suction detection in rotary blood pumps,” in *Proc. 2006 IEEE Int. Conf. Acoustics Speech Signal Process*, Toulouse, France, 2006, pp. 1064-1067.
- [34] Cohen, L., *Time-Frequency Analysis*. Englewood Cliffs, NJ: Prentice-Hall, 1995.
- [35] Vapnik, V., *Statistical Learning Theory*. New York: Wiley, 1998.

- [36] Lu, C., Gestel, T.V., Suykens, J.A.K., Huffel, S.V., Vergoteb, I., and Timmerman, D., “Preoperative prediction of malignancy of ovarian tumors using least squares support vector machines,” *Artif. Intell. Med.*, vol. 28, pp. 281-306, 2003.
- [37] Melgani, F. and Bruzzone, L., “Classification of hyperspectral remote sensing images with support vector machines,” *IEEE Trans. Geoscience and Remote Sensing*, vol. 42, no. 8, pp. 1778-1790, 2004.
- [38] Song, M.H., Lee, J., Cho, S.P., Lee, K.J., and Yoo, S.K., “Support vector machine based arrhythmia classification using reduced features,” *Int. J. Contr. Autom. Sys.*, vol. 3, no. 4, pp. 571-579, 2005.
- [39] Liu, Y.H. and Chen, Y.T., “Face recognition using total margin-based adaptive fuzzy support vector machines,” *IEEE Trans. Neural Networks*, vol. 18, no. 1, pp. 178-192, 2007.
- [40] Scholkopf, B., Burges, C., and Smola, A., *Advances in Kernel Methods: Support Vector Learning*. Cambridge, MA: MIT Press, 1999.
- [41] Yang, B. and Lu, Y., “Classification method of support vector machine based on statistical learning theory,” *Computer Technology and Development*, vol. 16, no. 11, pp. 56-58, 2006.
- [42] Mangasarian, O.L. and Musicant D.R., “Lagrangian support vector machines,” *J. Machine Learning Res.*, vol. 1, pp. 161-177, 2001.

- [43] Mangasarian, O.L. and Solodov, M.V., “Nonlinear complementarity as unconstrained and constrained minimization,” *Mathematical Programming*, vol. 62, pp. 277-297, 1993.
- [44] Walker, H.K., Hall W.D., and Hurst J.W., *Clinical Methods: The History, Physical, and Laboratory Examinations*. 3rd ed. Boston, MA: Butterworths, 1990.
- [45] Fawcett, T., “An introduction to ROC analysis,” *Pattern Recogn. Lett.*, vol. 27, no. 8, pp. 861-874, 2006.
- [46] Killeen, P.R., “An Alternative to Null-Hypothesis Significance Tests,” *Psychological Science*, vol. 16, no. 5, pp. 345-353, May 2005.
- [47] Gabran, S.R.I., Moussa, W.W., Salama, M.M.A., and George, C., “Portable real-time support-vector-machine-based automated diagnosis and detection device of narcolepsy episodes,” in *Proc. 31st Annu. Int. Conf. IEEE Eng. Med. Biol.*, Minneapolis, MN, 2009, pp. 903-906.
- [48] Michel, P. and Kaliouby, R.E., “Real time facial expression recognition in video using support vector machines,” in *Proc. 5th Int. Conf. Multimodal Interfaces*, Vancouver, BC, Nov. 5-7, 2003, pp. 258-264.
- [49] Sitaram, R., Le, S., Ruiz, S., Rana, M., Veit, R., and Birbaumer, N., “Real-time support vector classification and feedback of multiple emotional brain states,” *J. NeuroImage*, vol. 56, no. 2, pp. 753-765, 2011.

- [50] Faragallah, G., Wang, Y., Divo, E., and Simaan, M.A., "A new control system for left ventricular assist device based on the physiological demand of the patient," in *Proc. 7th Int. Conf. Inverse Problem Eng.*, Orlando, FL, 2011, pp. 250-255.
- [51] Boston, J.R., Antaki, J.F., and Simaan, M.A., "Hierarchical control of heart-assist devices," *IEEE Robot. Autom. Mag.*, vol 10, no. 1, pp. 54-64, Mar. 2003.
- [52] Choi, S., Boston, J.R., and Antaki, J.F., "Hemodynamic controller for left ventricular assist device based on pulsatility ratio," *Artif. Organs*, vol. 31, no. 2, pp. 114-125, Feb. 2007.
- [53] Karantonis, D.M, Lim, E., Mason, D.G., Salamonsen, R.F., and Ayre, P.J., and Lovell, N.H., "Noninvasive activity-based control of an implantable rotary blood pump: comparative software simulation study," *Artif. Organs*, vol. 34, no. 2, pp. E34-E45, Feb. 2010.